MEASURMENT OF LOW-ENERGY NUCLEAR CROSS SECTIONS USING INERTIAL CONFINEMENT FUSION

By

Katelyn C. Cook

A thesis submitted in partial fulfillment of the
requirements for the degree of

Bachelor of Science

Houghton College

May 2019

Signature of Author……..
Department of Physics
May 11, 2019

……
Dr. Mark Yuly
Professor of Physics
Research Supervisor

……
Dr. Brandon Hoffman
Professor of Physics

MEASURMENT OF LOW-ENERGY NUCLEAR CROSS SECTIONS USING INERTIAL CONFINEMENT FUSION

By

Katelyn C. Cook

Submitted to the Department of Physics
on May 11, 2019 in partial fulfillment of the
requirement for the degree of
Bachelor of Science

Abstract

Inertial confinement fusion is a tool that may be used to for fundamental nuclear science measurements. In the method under consideration, nuclear reaction products in the expanding neutral gas following the target implosion will be collected and trapped using a turbomolecular pump. The beta-decay of reaction products with half-lives ranging between 20 ms and 10 s will be measured in-situ using a phoswich detector system starting within milliseconds after the implosion. Cross sections for several previously unmeasured low-energy deuterium and tritium reactions could be measured using this technique. To study the feasibility, several small-scale experiments are being carried out at Houghton College and SUNY Geneseo to simulate the rapid release of gas by the ICF target, its subsequent capture and decay counting.

Thesis Supervisor: Dr. Mark Yuly
Title: Professor of Physics

TABLE OF CONTENTS

Chapter 1 Introduction **7**
1.1. Overview **7**
1.2. Inertial Confinement Fusion as a Tool to Study Nuclear Science **7**
1.2.1. Particle Accelerator Experiments 7
1.2.2. Inertial Confinement Fusion 9
1.2.3. Advantages for Small, Low-Energy Cross Sections 12
1.2.3.1. Thermonuclear Reactions 12
1.2.3.2. Reaction Products with Sub-Second Half-Lives 13
1.2.3.3. Tritium and Deuterium 14
1.2.4. Motivation for using ICF to Study Nuclear Science 14
1.2.4.1. Never Previously Measured 14
1.2.4.2. Nucleosynthesis Models 16
1.2.4.3. Fusion Diagnostics 18
1.3. Previous Experiments to Study Nuclear Science Using ICF **18**
1.3.1. Earliest ICF measurements 18
1.3.2. Neutron Reactions 18
1.3.3. Thermonuclear Reactions 19
1.4. Proposed Experiment at OMEGA at LLE **19**
1.4.1. "Collection Tube" Approach 20
1.4.2. "Collect it All" Approach 20
1.4.3. "Getter" Approach 21
1.5. Small Scale Feasibility Study at Houghton College **21**

Chapter 2 Theory **26**
2.1. Introduction **26**
2.2. Thermonuclear Reaction Rate **26**
2.2.1. Reduced Mass, Relative Velocity and Relative Kinetic Energy 26
2.2.2. Nuclear Reaction Rate 29
2.2.3. Thermal (Maxwell) Velocity Distribution 31
2.3. Predicted Yields for Proposed Thermonuclear Reactions **33**
2.4. Reaction Pathways **34**
2.5. Background Reactions **34**
2.6. Expected Results **35**

Chapter 3 Experiment and Apparatus **38**
3.1. Introduction **38**
3.2. Vacuum Chamber **38**
3.3. Vacuum System **39**
3.3.1. Trap turbopump and detector system 39
3.3.2. Fast Valve and Introduction to Experiment 41
3.3.3. Fast Mini Ion Gauge 41
3.3.4. Fast Valve 46
3.3.5. Laser 48
3.4. Phoswich Detector **50**
3.4.1. Photomultiplier Tube and Base 51

3.4.2. dE/E histogram 54
3.5. Phoswich Detector Test Experiment at SUNY Geneseo 55
3.6. Argon Test Experiment 56
3.7. Conclusion 60

Chapter 4 Results and Analysis 62
4.1. Introduction 62
4.2. $^{9}Be(n,\alpha)^{6}He$ 62
4.2.1. dE/E Histograms and Decay Curve 62
4.2.2. Analysis and Conclusion of $^{9}Be(n,\alpha)^{6}He$ Experiment Results 63
4.3. $^{40}Ar(d,p)^{41}$ Experiment 64
4.3.1. ^{41}Ar Production at SUNY Geneseo 64
4.3.2. Growth Curves and Background-Subtracted Gamma Ray Spectrum 65
4.3.3. Analysis and Conclusion of $^{41}Ar(d,p)^{41}Ar$ Experiment Results 66
4.4. Pressure Front Across Chamber Experiment 67

Chapter 5 Conclusion 69
5.1. Summary 69
5.2. Summary of Preliminary Experiments 69
5.3. Future Experiments 71
5.4. Conclusion 73
Appendix A FEMTODAQ COMPUTER CODE 75
Appendix B VOLTAGE LEVEL TRANSLATOR CIRCUIT 80
Appendix C LATCH CIRCUIT 81
Appendix D ARDUINO CODE FOR THE FAST VALVE 82

TABLE OF FIGURES

Figure 1. The inertial confinement fusion process 10
Figure 2. OMEGA laser ICF implosion at LLE 10
Figure 3. OMEGA Laser Facility at the Laboratory for Laser Energetics. 11
Figure 4. OMEGA Laser bay at LLE and an ICF target 11
Figure 5. The time evolution of the experiment 13
Figure 6. Chart of nuclides 16
Figure 7. Cross sections at low incident energies for the $^{6}Li(t,p)^{8}Li$ reaction 17
Figure 8. The branching ratio of the $^{2}H(d,\gamma)^{4}He$ reaction 17
Figure 9. "Collection Tube" experimental design. 22
Figure 10. "Collect it All" experimental design 22
Figure 11. "Getter" experimental design. 23
Figure 12. Top view diagram of small-scale set up at Houghton College 24
Figure 13. Laboratory and center of mass coordinates. 27
Figure 14. Movement of the two nuclei species interacting during the nuclear reaction 29
Figure 15. Simplified diagram of the two nuclei species interacting in the plasma 30
Figure 16. Plots of cross section predictions for different proposed reactions 36
Figure 17. ^{6}He energy level diagram. 37
Figure 18. Vacuum chamber system at Houghton College. 40
Figure 19. Trap turbopump and detector system. 42
Figure 20. Custom-made fast mini ion gauge. 44
Figure 21. Fast mini ion gauge circuit 45
Figure 22. Fast mini ion gauge powered on. 45
Figure 23. A typical calibration curve using air for the fast mini ion gauge. 46
Figure 24. Output pulse from the fast ion gauge. 47
Figure 25. Fast valve attached to the vacuum chamber on a homemade conflat flange. 48
Figure 26. Fast valve power circuit. 49
Figure 27. 6 W 445 nm laser diode. 49
Figure 28. Microballoons. 51
Figure 29. Phoswich detector system 51
Figure 30. Plastic Scintillator Detectors. 52
Figure 31. Plastic scintillators optically coupled to PMT 52
Figure 32. Phoswich detector system 53
Figure 33. Pulses from a beta decay source into the phoswich detector system. 54
Figure 34. Circuit for separating phoswich detector pulses. 55
Figure 35. FemtoDAQ data acquisition system. 56
Figure 36. Histogram of the beta counts while testing the phoswich detector. 57
Figure 37. Plot of the method in which the data were collected in testing the phoswich 58
Figure 38. Target chamber at SUNY Geneseo on the Tandem Pelletron 59
Figure 39. Photographs from the ^{9}Be experiment at SUNY Geneseo. 60
Figure 40. Counting station to measure the ^{41}Ar after production at SUNY Geneseo 61
Figure 41. Tandem Pelletron setup at SUNY Geneseo 61
Figure 42. dE/E histogram from $^{9}Be(n,\alpha)^{6}He$ experiment 63
Figure 43. Decay curve of ^{6}He produced in the $^{9}Be(n,\alpha)^{6}He$ experiment 64
Figure 44. ^{41}Ar gamma ray energy spectrum. 65

Figure 45. Growth curve of ^{41}K during the ^{41}Ar experiment (HPGe detector) 66
Figure 46. Growth curve of ^{41}K during the ^{41}Ar experiment (SSB detector) 66
Figure 47. Testing pressure front across the vacuum chamber..... 67
Figure 48. Results from pressure front experiment..... 68
Figure 49. The 4π phoswich detector system 70
Figure 50. Preliminary laser test with a substrate 72
Figure 51. Future experiment: isotropic release of radioactive gas 74

Chapter 1

INTRODUCTION

1.1. Overview

A new technique is being investigated to allow fundamental nuclear science measurements using inertial confinement fusion (ICF). This chapter will introduce the research done over the past three years by a collaboration including scientists from Houghton College, the State University of New York at Geneseo and the Laboratory for Laser Energetics. First, ICF will be discussed; this includes a description of the ICF process, the proposed technique, measurements that can be made, and the advantages and disadvantages of this technique. Then, the motivation for the research will be outlined and the proposed experiment will be introduced. Finally, the small-scale feasibility study carried out at Houghton College will be presented.

1.2. Inertial Confinement Fusion as a Tool to Study Nuclear Science

The goal of the proposed research is to measure cross sections of low-energy nuclear fusion reactions. This is especially important in nuclear physics because cross sections measured at different laboratories using different methods can be compared to each other and used to test predictions of theory models. This is because the cross section is mostly independent of experimental design. That is, a cross section measured by a particle accelerator should be the same as the cross section measured using ICF for the same kinematics, since the cross section includes only the "physics" of the reaction.

1.2.1. Particle Accelerator Experiments

Nuclear cross sections are traditionally measured using particle accelerators. These machines accelerate charged particles to high energies to create a beam. This beam of charged particles then strikes a target and reaction products may be produced. These reactions are written in the general form of $A(a,b)B$ where A is the target nucleus, a represents the accelerated particles incident on the target, b denotes the detected particles

and *B* are the other undetected reaction products. Detected particles can be used to measure the probability, which is proportional to the cross section, for the reaction to occur under a set of conditions. Knowing the number of particles incident on the target and the cross section allows a calculation of the number of reaction products produced.

Using this method, measuring extremely small cross sections at low energies can be difficult because of the amount of time required to detect a statistically adequate number of reaction products. For example, the $^{7}Li(t,\alpha)^{6}He$ reaction at 25 keV yields 1,000 reactions in about a month using a particle accelerator with beam current of about 1 μA. Using ICF to measure the same reaction yields about 1,000,000 reactions in about 0.1 ns. The problem for accelerators is the amount of time it takes to get a large number of counts, which increases the background problem tremendously and is also very expensive. Using ICF is advantageous because the reactions all occur in a fraction of a nanosecond, but in that same interval about 10^{13} neutrons are also produced. This is also high background environment so finding the million reaction products that are detected will be like looking for a needle in a haystack. However, this problem can be bypassed because the reaction products are radioactive. Since the reaction products decay on the order of milliseconds, the detector system can be turned on to count decays in a quiet environment after the initial burst of radiation has passed (several milliseconds after the ICF shot).

Another disadvantage to using particle accelerators is the difficulty in producing, controlling and using the very low energy beams that would be needed. Finally, beams of some radioactive ions will contaminate the accelerator and laboratory. For example, many interesting reactions require a tritium (^{3}H) beam. Tritium, a radioactive isotope of hydrogen that emits beta radiation, can be inhaled and/or absorbed into the body. When accelerated, due to its long half-life of about 12 years, tritium contaminates the entire accelerator. Even during the low energy accelerator heydays of the 1950s and 1960s, there were not many laboratories willing to accelerate tritium. One of the last remaining tritium accelerators was the Los Alamos three-stage Van de Graaff Ion Beam Facility [1] which ended tritium beam production in 1994, was deactivated in 1999 [2] and decommissioned, decontaminated, and

demolished starting in 2005 [3]. Secondary tritium beams have also been produced in order to solve the safety problem of directly accelerating tritium [4]. These beams were successful in reaching an adequate beam intensity for certain types of experiments; however, they are still at high energies (≥ 65 MeV) [5]. For all the aforementioned reasons, very few tritium-initiated reactions have been studied.

1.2.2. Inertial Confinement Fusion

One way to overcome the disadvantages above is to use inertial confinement fusion (ICF) to produce these interesting reactions. ICF is a process in which thermonuclear reactions similar to those inside of stars can be triggered in earth-based laboratories. This is done by heating and compressing a small target filled with nuclear fuel, usually consisting of deuterium and tritium.

Laser-initiated ICF facilities consist of laser bays (with amplifiers), targets, target chamber, evacuation pumps and control rooms. The laser beams go through a series of stages where they are amplified, reflected and then focused down to a nuclear fuel filled target. As shown in Figure 1, the beams are incident from every direction on the target (stage 1), the outer layer of the target heats up to a point where it ablates or blows off like a rocket (stage 2), which creates shock waves moving towards the center of the target (stage 3). These shock waves result in compressing and heating the inner layer of the target to the point where nuclear reactions, including fusion, occur (stage 4). Figure 2 shows an ICF shot at the Laboratory for Laser Energetics.

The proposed experiment would be carried out at the Laboratory for Laser Energetics (LLE) at the University of Rochester. LLE has the second largest ICF facility in the nation and has been operational since 1970. LLE is a smaller facility and is known for being able to do a large number of shots in a day (up to one shot per hour repetition rate [6]) and the support for external users (60% of shots are allotted to outside users).

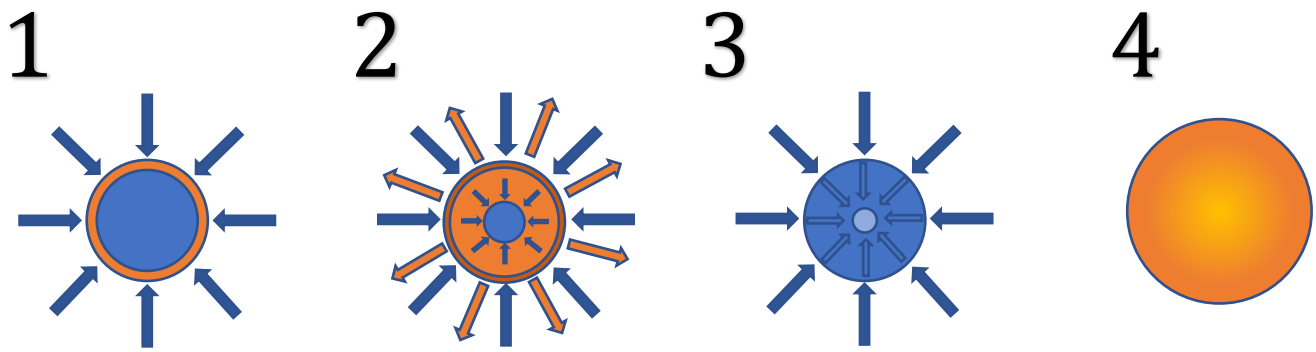

Figure 1. The inertial confinement fusion process. (1) The laser beams incident on the target. (2) The outer shell of the target heating to the point of ablation. (3) The compression of the nuclear fuel inside the target. (4) Fusion reactions occurring, similar to reactions inside a star.

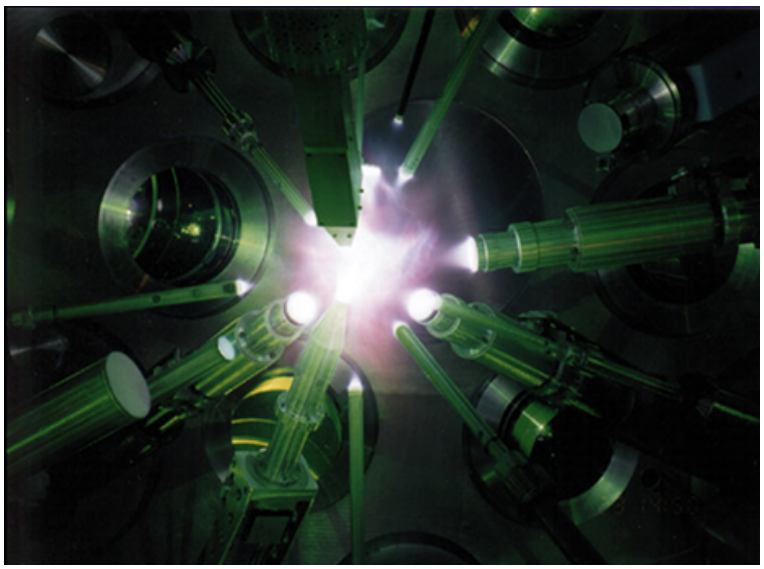

Figure 2. OMEGA laser ICF implosion at LLE. Detectors are close to the target chamber center. Lasers are incident on the nuclear fuel filled target to produce fusion reactions. Figure taken from Ref. [7].

LLE has two different laser systems that can be used in ICF experiments: OMEGA and OMEGA EP. The OMEGA facility [8], shown in Figure 3, has been functioning since 1995, and is housed in a building 10 meters tall and 100 meters in length. Three laser drivers are split and amplified to produce 60 UV laser beams (Figure 4). These beams are further amplified, reflected and then focused down to a nuclear fuel filled target. The total energy per shot on OMEGA is up to 30 MJ and the structure of the shots are mainly direct-drive, however they have done work for the National Ignition Campaign (NIC) in which the approach is indirect-drive.

The OMEGA EP facility [9], completed in 2005, is an extension of the OMEGA laser system. It has four beamlines that have short- and long-pulse capabilities. These systems can be used together to study plasma, high-field, high-pressure materials and high-energy-density physics.

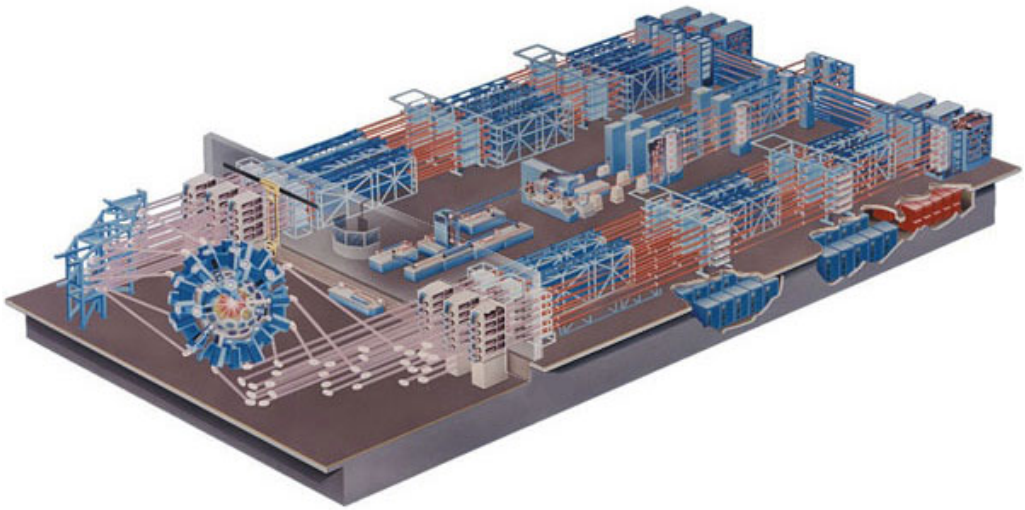

Figure 3. OMEGA Laser Facility at the Laboratory for Laser Energetics. This figure shows the entire layout of the facility with the target chamber on the left and the laser bay with amplifiers on the right. Lenses focus the lasers down to the target in the chamber. Figure taken from Ref. [7].

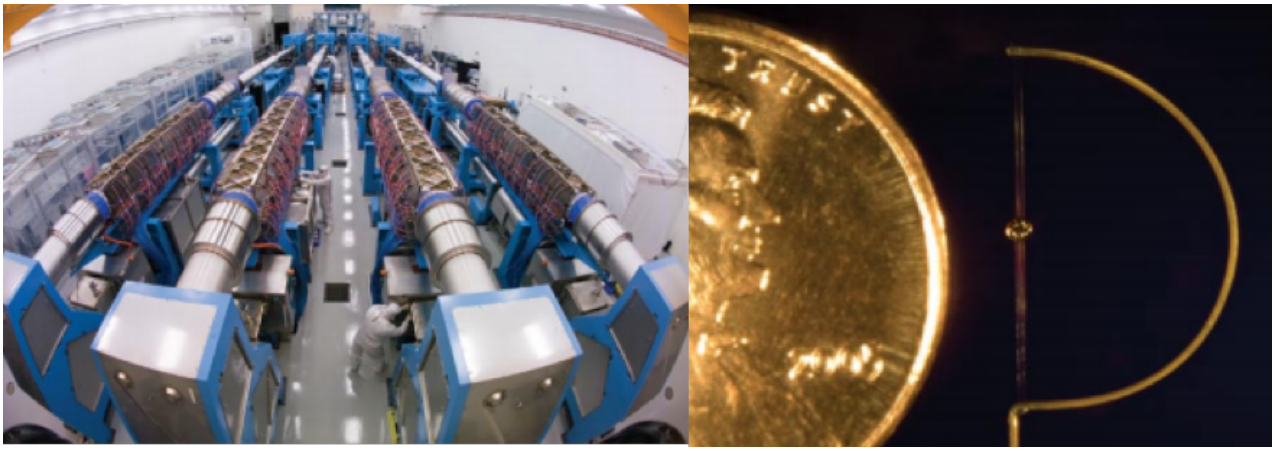

Figure 4. OMEGA Laser bay at LLE and an ICF target. The laser bay (left) consists of preamplifiers, amplifiers, calorimeters and spatial spacers to get the desired wavelength and energy of the laser beams to then focus on the target in the chamber. The ICF target (right) is compared to the size of a penny. This target is about 1 mm in diameter. Figure taken from Ref. [7].

Lawrence Livermore National Laboratory (LLNL) has the largest laser facility in the world, called the National Ignition Facility (NIF) which became operational in 2009. At the NIF, there are 192 lasers which produce a pulse of up to 1.8 MJ of ultraviolet light focused on a small target to induce nuclear fusion reactions. In 2010, the NIF launched the National Ignition Campaign (NIC), research focused on using the NIF to reach ignition, or the point where fusion reactions become self-sustaining. Ignition has still not been demonstrated and continues to be studied; however, if achieved it has the potential to be a source of clean energy for human use.

There is also a laser laboratory in France, called Laser Mégajoule (LMJ), with 176 lasers creating up to 1.5 MJ of ultraviolet light incident on a target to initiate ICF reactions [10]. Initial experiments were carried out in 2014. LMJ uses the indirect-drive approach to initiate nuclear fusion reactions. The LMJ has added the PETAL beam in which another high intensity and energy laser was added to the current set-up. This facility is used for academic research in high-energy density physics including plasma physics, material science, hydrodynamics, atomic and nuclear physics.

1.2.3. Advantages for Small, Low-Energy Cross Sections

ICF has many advantages when used to study fundamental nuclear science. Specifically, to measure small, low-energy cross sections, these advantages are the large number of interacting ions in a thermonuclear process, the short duration of the laser pulse and the facilities to handle deuterium and tritium as targets.

1.2.3.1. Thermonuclear Reactions

The first advantage to using ICF is the induced thermonuclear reaction in which the fuel in the target is heated to the point where nuclear reactions occur. Even though the cross section may be very small, the number of nuclei in the target is very large, making it possible to produce a measurable yield of reaction products for many of the proposed reactions. For example, consider the $^{3}H(t,\gamma)^{6}He$ reaction. In a recent measurement of the $^{3}H(t,2n)^{4}He$ reaction at OMEGA [11], shot numbers 55641-55647 using 12.1 atm of deuterium-tritium

(DT) mix with 38.7% tritium resulted in an average temperature of 8.0 keV, and therefore an average center-of-mass reactant energy of almost 29 keV. This can be seen in Table 1, for an OMEGA shot with the same yield, even with a $^{3}H(t,\gamma)$ to $^{3}H(t,2n)$ branching ratio of 10^{-7} about 80,000 ^{6}He nuclei would be produced in a fraction of a nanosecond. This is advantageous because in an accelerator experiment, it would take a very long time for this many reactions to occur.

Table 1. Projected ^{6}He yield based on an OMEGA shot.

DT neutron yield	25.5×10^{13}
Ratio of TT to DT neutrons	6.02×10^{-3}
TT neutron yield	1.6×10^{12}
$^{3}H(t,\gamma)$ to $^{3}H(t,2n)$ branching ratio	10^{-7}
^{6}He yield	8×10^{4}

1.2.3.2. Reaction Products with Sub-Second Half-Lives

Another advantage is that the reactions *all* occur in a fraction of a nanosecond. Since the proposed reaction products all have hundreds of milliseconds long half-lives, the measurement can be made "long after" the ICF shot but still in a period of only a few seconds.

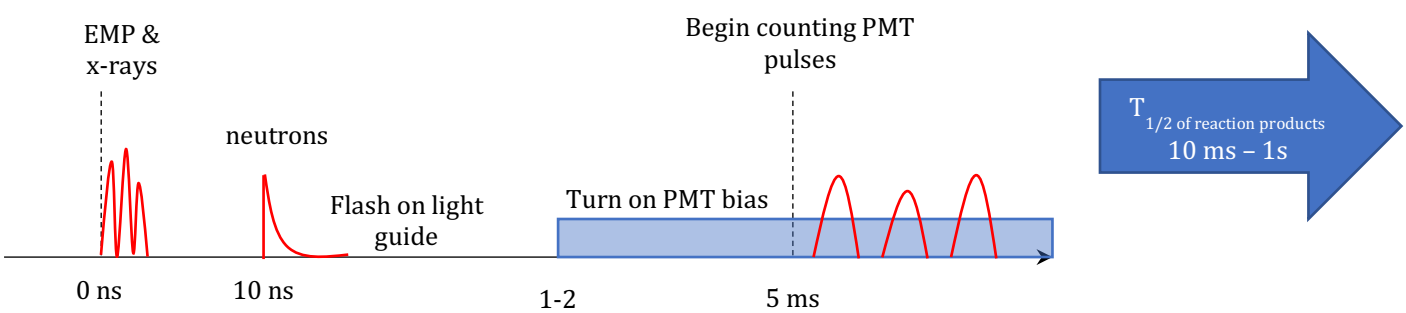

Figure 5. The time evolution of the experiment. The EMP, x-rays and neutrons are emitted within nanoseconds of the ICF shot. After milliseconds, the PMT is turned on to start detecting the beta particles up to seconds after the shot. This is feasible because the reaction products to be detected all have half-lives of 10 ms or longer, up to about 1 s.

This is because the initial electromagnetic (EMP) and DT neutron pulse occurs within nanoseconds of the laser shot (Figure 5). If the product is decaying on the order of milliseconds, counting can begin long after the gamma ray flash and associated background neutron and EMP pulse has passed. Measuring the cross section using ICF can therefore eliminate background noise and allow a very sensitive measurement if product nuclei are detected rather than the outgoing neutrons or gamma rays. Also, since the half-life is in milliseconds, the experiment is over in only a few seconds, there is very little background from the environment.

1.2.3.3. Tritium and Deuterium

Finally, the laboratories designed to study ICF are already prepared to deal with tritium filled targets. For the reactions with tritium targets or incident particles, ICF provides a safe way to work with this isotope, opposed to accelerator labs which become unusable after becoming contaminated with tritium. ICF facilities are prepared to work with a small amount of tritium as most of the shots are deuterium-tritium (DT).

1.2.4. Motivation for using ICF to Study Nuclear Science

There are several other motivating factors that make studying fundamental nuclear science using ICF favorable. Overall, the nuclear measurements can be made at energies and densities useful for astrophysical studies of stellar nucleosynthesis.

1.2.4.1. Never Previously Measured

Most tritium induced nuclear reactions have never been measured at low thermonuclear energies that are important for astrophysics and fusion research. Moreover, to fully understand stellar objects, these reactions need to be measured at high-energy-density, similar to the plasma produced in the ICF shot. Figure 6 shows part of the chart of nuclides that includes the reaction products for several proposed reactions under consideration outlined in red. These nuclei beta decay in the range of 20 ms to 10 s half-life. These products can be reached by the following reactions: $^{3}H(t,\gamma)^{6}He$, $^{6}Li(t,p)^{8}Li$, $^{7}Li(t,\alpha)^{6}He$, $^{9}Be(t,\alpha)^{8}Li$, and $^{11}B(d,p)^{12}B$. There are many more reactions that can get to the desired products, however,

these reactions were selected based on the target and incident particle being deuterium or tritium, the reaction products having sub-second half-lives and a reaction threshold of 0 MeV.

There are many different types of reactions that do not have measured low-energy cross sections. Radiative capture, stripping and (t,α) reactions have the possibility of being measured using ICF. Radiative capture reactions occur when incident nuclei are captured to make a compound nucleus while emitting a gamma ray in the process. For example, $^{3}H(t,\gamma)^{6}He$ is a radiative capture reaction that has not been measured at any energy or any laboratory. This cross section is predicted to be very small but was the original motivation for this research.

These cross sections have not been measured at thermonuclear energies. Figure 7 shows an example of one of the proposed reactions, $^{3}Li(t,p)^{8}Li$, that has been measured in the 2-10 MeV range, but not at lower energy. For astrophysical applications, the reaction needs to be measured in the keV range. Extrapolations of the cross section to the lower energies have large uncertainties and experimentally measuring these values would provide a test of theoretical calculations. Now that the high-energy-density plasma inside of stars is achievable in the laboratory setting, these cross sections should be studied to understand nucleosynthesis.

There are examples of theoretically predicted cross sections that have turned out to be wrong. For example, in the 1980s, physicists predicted [12] the branching ratio of the $^{2}H(d,\gamma)^{4}He$ to $^{2}H(d,n)$ reaction (Figure 8) to be very low (about 10^{-14}) at low energies (keV). However, the branching ratio was later measured to be about 10^{-7}, which is a difference of *seven* orders of magnitude. The discrepancy was explained by a previously unknown admixture in the ground state of ^{4}He that caused the increase in the branching ratio. This emphasizes the importance of making experimental measurements to test theory predictions for low energy light ion reactions.

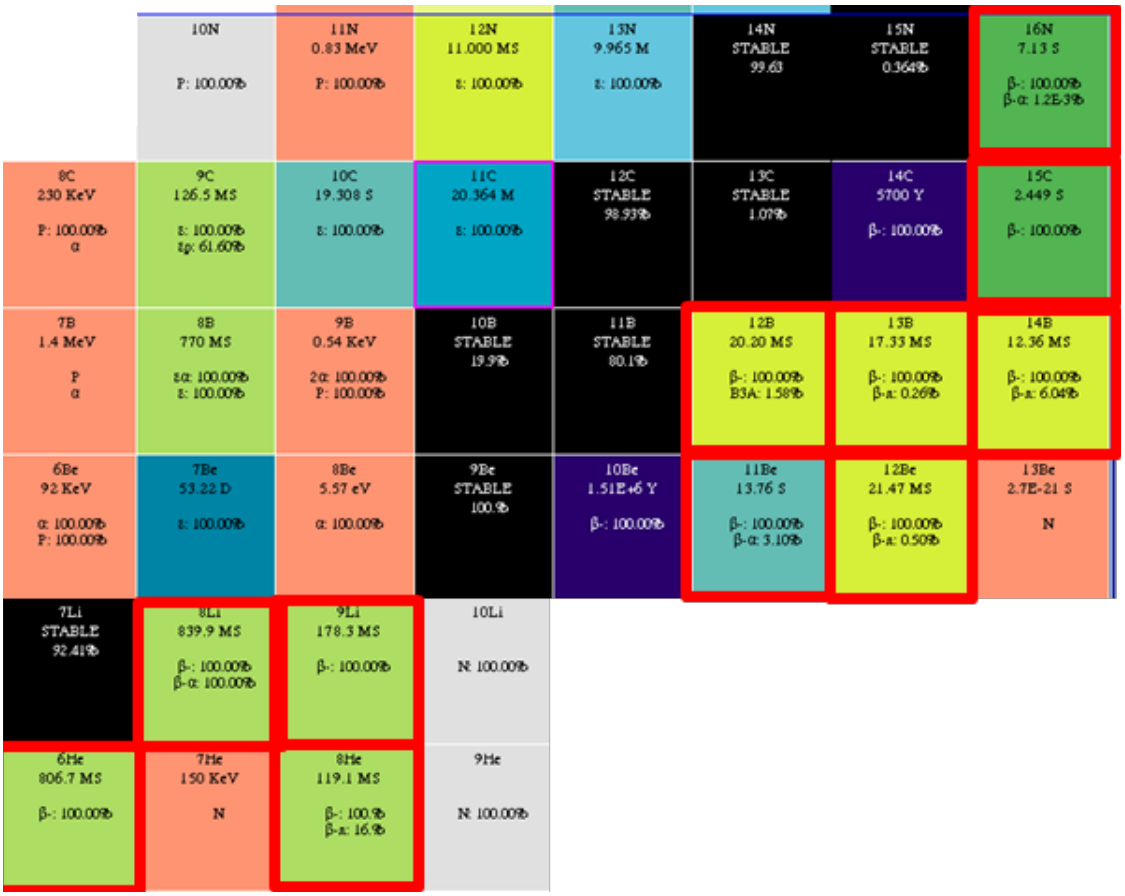

Figure 6. Chart of nuclides. Number of protons is increasing on the vertical axis and number of neutrons increases on the horizontal. The nuclei boxed in red are the desired reaction products with half-lives from 20 ms to 10 s that may be reached by the reactions described in the text. Figure taken from Ref [13].

1.2.4.2. Nucleosynthesis Models

All of these light ion reactions are important for nucleosynthesis models. For example, for $^{3}H(t,\gamma)^{6}He$, the reaction product ^{6}He decays into ^{6}Li. Currently, big-bang nucleosynthesis models overpredict the abundance of ^{7}Li while underpredicting the abundance of ^{6}Li [14, 15]. The cross section measurement for the $^{3}H(t,\gamma)^{6}He$ radiative capture reaction could increase the accuracy of this prediction because it is not currently included in the model and creates ^{6}Li via the beta decay of ^{6}He: $^{6}He \rightarrow {}^{6}Li + e^{-} + \bar{\nu}$. Other proposed reactions also occur in stars and in big-bang models.

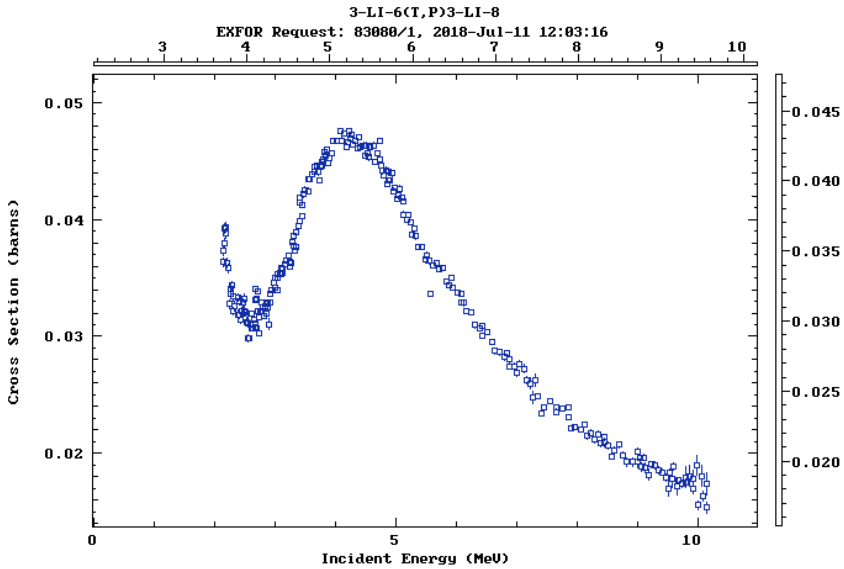

Figure 7. Cross sections at low incident energies for the $^{6}Li(t,p)^{8}Li$ reaction. There are currently no measurements of the $^{3}Li(t,p)^{8}Li$ stripping reaction below 2 MeV incident energy. For nucleosynthesis studies, energies on the order of keV are desired. Figure taken from Ref [16].

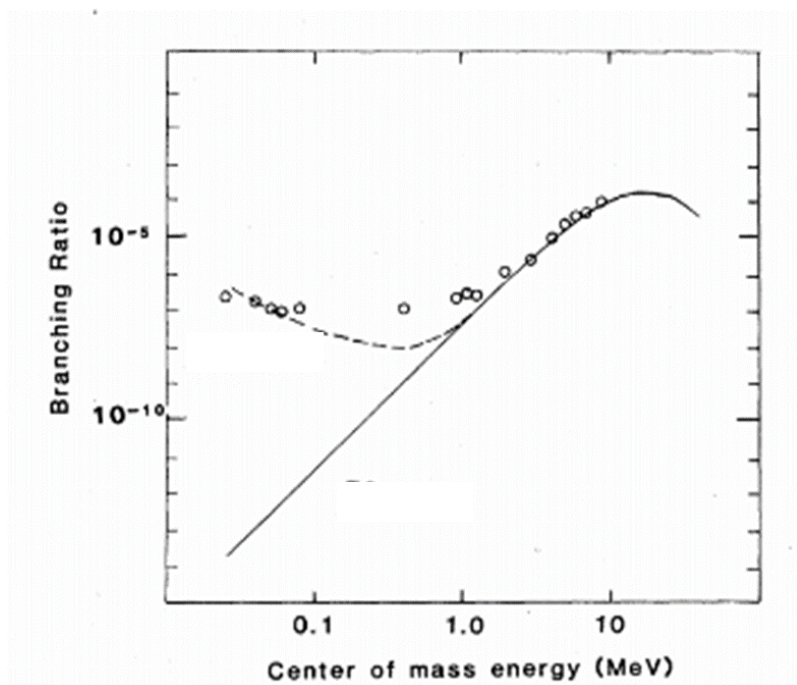

Figure 8. The branching ratio of the $^{2}H(d,\gamma)^{4}He$ reaction. Note the seven orders of magnitude difference in the theoretical prediction of the branching ratio (solid line) compared to the data points. Figure taken from Ref [12].

1.2.4.3. Fusion Diagnostics

Some of the proposed reactions can be used as diagnostics [17] for high temperature DT plasmas or may be unwanted background in other diagnostic measurements. Measuring the cross sections of these reactions could help fully characterize what is occurring inside the ICF chamber during a shot. Learning about the background reactions can aide in the sensitivity of the reaction being measured.

1.3. Previous Experiments to Study Nuclear Science Using ICF

There have been several nuclear science experiments using ICF [18] at LLE and other facilities. However, they have mainly done work in the field of high-energy-density and plasma physics, so fundamental nuclear science using ICF is a growing field.

1.3.1. Earliest ICF measurements

In 2011, the first measurements of the differential cross section of elastically scattered ^{3}H and ^{2}H ions from neutrons at 14.1 MeV using ICF were published. This was an important first step for the study of fundamental nuclear physics using inertial confinement fusion and reproduced what had previously been measured using accelerators. This experiment used DT gas-filled thin-glass targets with diameters of about 850 μm. The gas was at about 20 atm and was composed of about 48.2% deuterium and 48.8% tritium. The OMEGA lasers produced 30 kJ to the target in a 1 ns pulse. The burn-averaged ion temperature was about 8.5 keV and about $4x10^{13}$ neutrons were produced and measured using a magnet-based charged-particle spectrometer. The resulting cross section measurements had less uncertainty than previously measured using accelerator-based methods. Results agreed with previous measurements and theoretical predictions.

1.3.2. Neutron Reactions

Neutron time-of-flight (TOF) spectra have also been measured using ICF [19] at LLE the $^{3}H(t,2n)\alpha$ reaction using the NIF. The target at the NIF was made up of 99.9% tritium. When the target imploded, 16 keV center of mass energy was achieved and the 14 keV neutrons were measured using neutron TOF detectors (about 10^{13}). These types of reactions continue

to be studied as there is potential to learn about the different interactions between neutrons and other particles in the thermonuclear environment.

1.3.3. Thermonuclear Reactions

Measurements with conditions similar to the inside of stars have made at the National Ignition Facility. Specifically, astrophysical measurements of $^{2}H(d,n)^{3}He$ and $^{3}H(t,2n)^{4}He$ were made [18]. The 192 lasers at the NIF with 0.8-1.5 MJ of energy were incident on the TT and DT gas-filled targets. Using neutron and x-ray diagnostics, the resulting plasma was observed. The TT reactions were within the 2-5 keV range and the DT reactions were within the 2.5-5.5 keV range. This showed that conditions similar to those inside stellar objects (specifically stars) are achievable in the laboratory.

1.4. Proposed Experiment at OMEGA at LLE

In order to measure the cross sections of nuclear reactions, the reaction product nuclei or outgoing gamma rays, neutrons, or alpha particles must be detected. One way to detect and count the reaction products is to measure their decays. Measuring the decay curve of the product nuclei allows the initial number of product nuclei to be determined.

For the proposed experiments, the target capsule will be filled with tritium, deuterium or doped with other nuclei based on the intended reaction. The laser shot causes the outer shell to ablate, then the nuclei inside the target capsule are to be compressed and heated to the point where nuclear fusion reactions can occur. The reaction products will lose energy as they travel through the resulting plasma. Most reaction product ions will not have enough energy to escape the plasma so they will thermalize and recombine to create a neutral gas that expands outward in the target chamber.

To make a cross section measurement at the OMEGA facility, reaction products can be detected either as energetic ions or in the expanding neutral gas. Since most product ions cannot escape and recombine, the proposed experiments collect the neutral gas and count the decays of the radioactive product.

To detect the reaction products from the expanding radioactive gas, a trap such as a turbopump and detector system needs to be developed to collect, trap and then detect the gas. Another approach is to detect reaction products from the neutral gas using a getter. The getter needs to be placed close to the target so the neutral gas can react chemically and be detected.

The three experimental designs that are under consideration for measuring these small, low-energy nuclear cross sections using the OMEGA facility at LLE will be discussed below.

1.4.1. "Collection Tube" Approach

The "Collection Tube" approach consists of a long gas collection tube attached to a turbopump that extends as close as possible to the target chamber center to collect reaction product nuclei as shown in Figure 9. These reaction product gas molecules will travel down the tube and become trapped by the turbopump (in about 1.5 ms). The detector system will be attached to the foreline of the turbopump where the nuclei will be trapped. Once trapped in the foreline, the nuclei will decay by beta emission and the electrons will be detected. Only a small fraction of the total number of product nuclei will be counted. However, the fraction collected should be approximately proportional to the solid angle subtended by the opening of the tube, simplifying the cross section calculation. This is expected to be a good approximation because the rest of the target chamber will be quickly evacuated by large pumps and the products therefore will not enter the collection tube after the initial burst. The advantages of this method include collecting the gas quickly, and a known efficiency based on the assumption that the gas is expanding isotropically. The major disadvantage to this method is the reduced fraction of reaction products collected, and therefore worse statistical uncertainty. Also, the possibility of the gas escaping back down the tube or additional gas being collected later may cause problems with this approach.

1.4.2. "Collect it All" Approach

The "Collect it All" approach is shown in Figure 10. A large turbopump attached to the target chamber will collect all the gas released by the ICF implosion as long as none stick to the target chamber walls. A small turbopump mounted to a large turbopump will capture the

gas. Just like in the "Collection Tube" approach, the gas containing the reaction products is trapped so the decays can be counted using the phoswich detector system. This method is most advantageous for reactions that have longer half-lives closer because it is expected to take about 90 s to completely evacuate the target chamber [20] so the half-lives on the order of hundreds of milliseconds would be difficult to measure using this method. In some ways it is preferable, however, because it would collect a large fraction of the gas in the chamber. For low yields, collecting all the reaction products may be the only way to detect anything.

1.4.3. "Getter" Approach

The "Getter" approach (Figure 11) may be preferable for reactions that have non-inert gases as products. These reaction products will expand isotropically in the neutral gas and stick to a getter (could be made of graphite, titanium or other material) placed in front of the detector as close as possible to the target chamber center. The atoms would become chemically bound to the getter material, where their nuclei would decay by beta emission. A phoswich detector system would produce light pulses that travel through a long light guide to a photomultiplier tube, which will be placed far away from the implosion. The signals could then be read out through the electronics system. This method is advantageous for non-inert gases that are capable of sticking to a getter, such as Lithium, because the detector is close to the implosion with a large, well defined solid angle. However, a disadvantage is that this approach cannot be used for all of the proposed reactions, but only those that result in chemically active products.

1.5. Small Scale Feasibility Study at Houghton College

A small scale apparatus at Houghton College, shown in Figure 12, has been assembled to determine the feasibility of the three different methods for measuring cross sections using ICF. The goal of this study is to simulate the expanding neutral radioactive gas after a shot at LLE in a small-scale table top laboratory setting. The vacuum chamber is analogous to the OMEGA target chamber and the preliminary experiments involve of the rapid release of stable and radioactive gas (both inert and non-inert), fast pressure measurement and subsequent detection of the beta particles emitted over several half-lives.

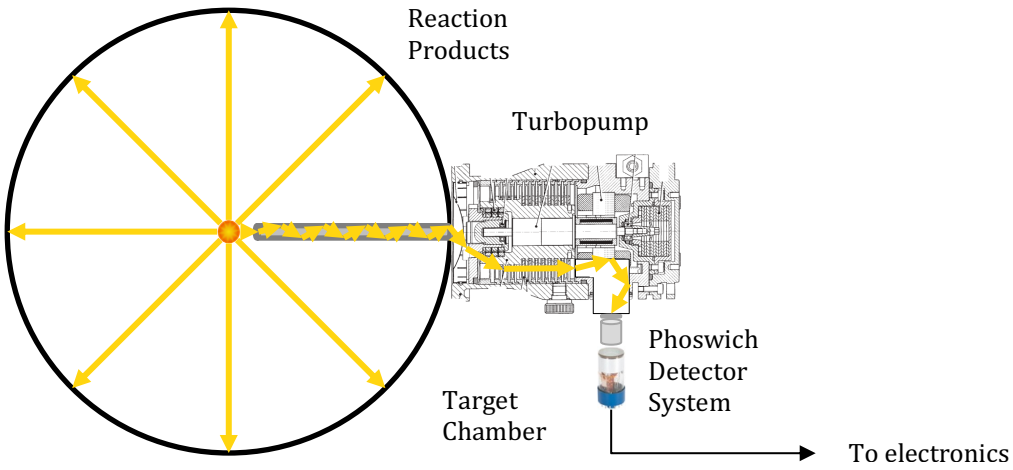

Figure 9. "Collection Tube" experimental design. Neutral gas would bounce through the collection tube, be trapped by the turbopump and the beta particles released from the decay would be counted using the phoswich detector system.

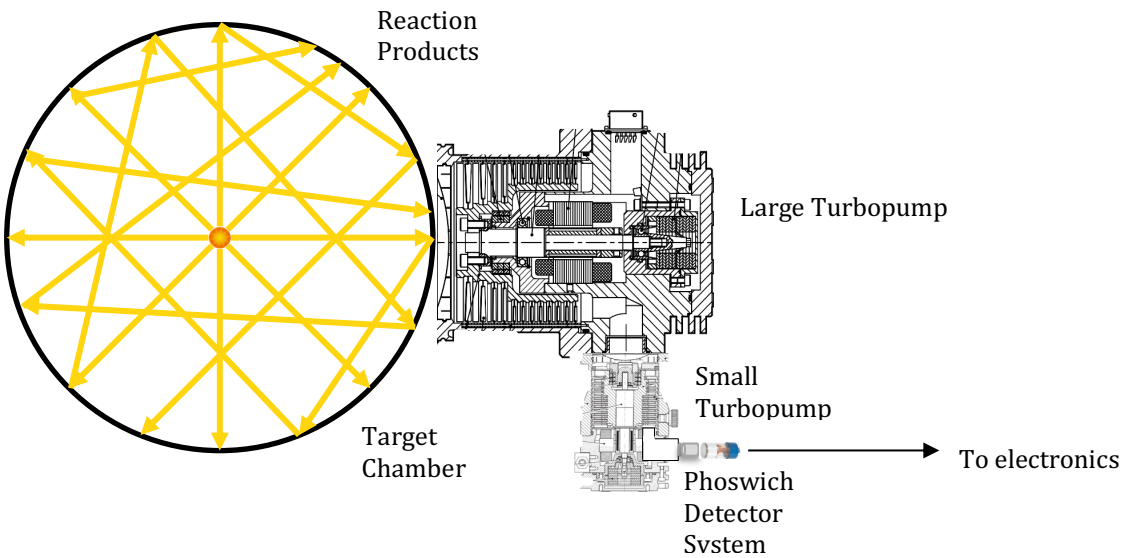

Figure 10. "Collect it All" experimental design. All reaction products will be trapped in a turbopump system. As the chamber is evacuated after the shot, a small turbopump attached to the large turbopump would trap the reaction product nuclei and the resulting beta decays would be counted by the phoswich detector system.

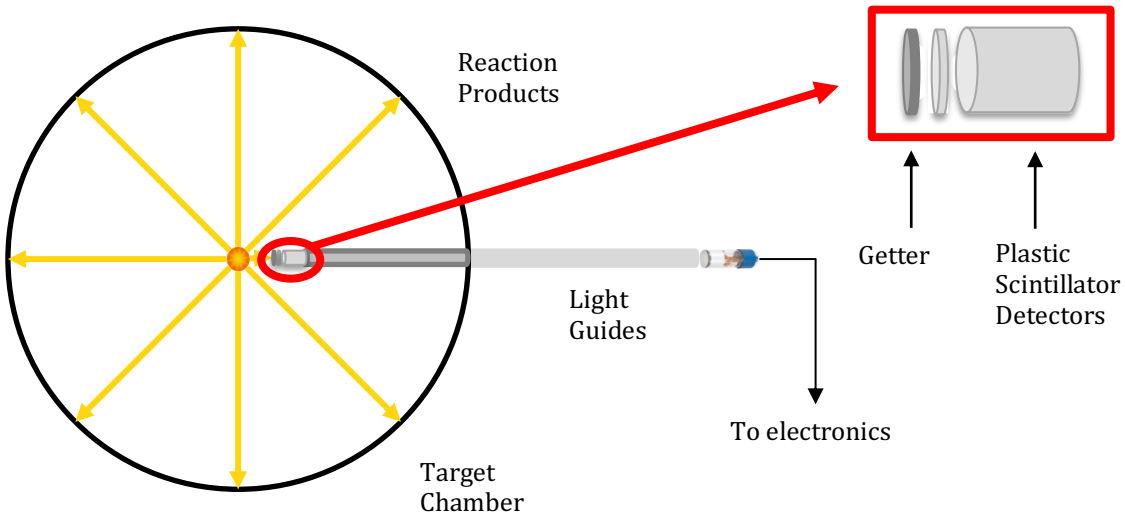

Figure 11. "Getter" experimental design. After the ICF implosion, products would stick to a getter. A phoswich detector system attached to the getter would count beta decays. The light pulses would travel through a long light guide to keep the PMT and electronics far away from the EMP pulse.

Before an ICF measurement can be made, many questions need to be answered. It is important to understand how the trap turbopump detection system works and how the gas behaves in the evacuated chamber.

The first preliminary experiment was to demonstrate that radioactive gas can be created, trapped in the turbopump and then detected by its beta decay using the phoswich detector system. This preliminary experiment was done during the summer of 2018.

As later described in more detail, the ^{40}Ar(d,p)^{41}Ar reaction produced ^{41}Ar using the SUNY Geneseo Tandem Pelletron Accelerator. Then the ^{40}Ar-^{41}Ar gas mixture (with half-life of 109 minutes) was transported to Houghton College and released into the chamber by a fast valve, in pulses as short as 300 μs. The fast valve rapidly released ^{41}Ar gas into the target chamber and the "Collection Tube" approach was used to determine if a turbopump and detector system could successfully trap and detect ^{41}Ar. The long collection tube was extended various lengths across the target chamber. When gas was released through the fast valve, a fraction of it traveled down the collection tube and was trapped by the trap turbopump. A silicon surface barrier detector was attached to the trap turbopump through the foreline.

Thus, when the gas was stuck in the back of the trap turbopump, it decayed, and the betas were detected.

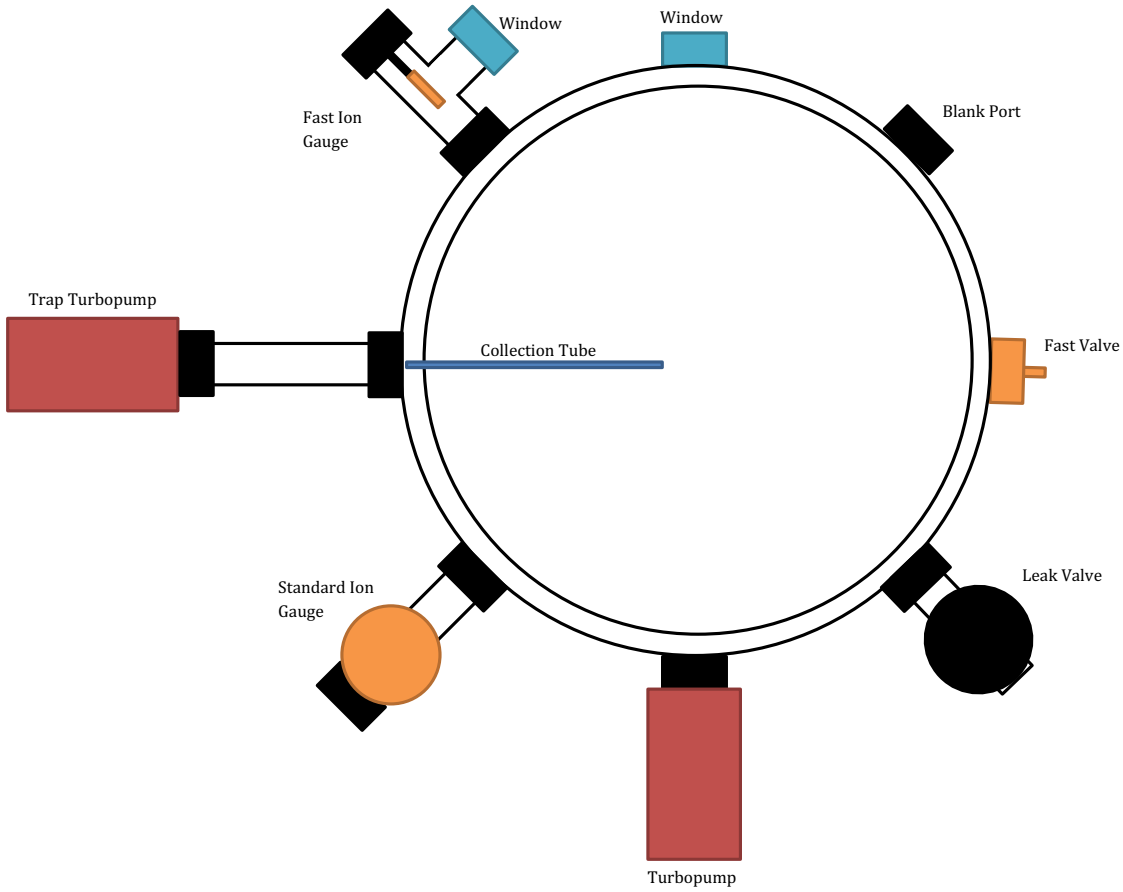

Figure 12. Top view diagram of small-scale set up at Houghton College. The main turbopump brings the pressure down to about 10^{-6} Torr. The fast valve allows short gas pulses into the vacuum chamber, the collection tube collects the gas and is attached to the trap turbopump which traps the nuclei in its sealed exit port. The standard ion gauge and leak valve are in place to control the conditions in the chamber. Other experiments use the laser and the multiple fast mini ion gauges inserted in the lid.

The laser is also an important component of the small-scale study as it can be used to release gas from target cells similar to the ones used at LLE or NIF, microballons or radioactive materials on substrates. This will produce an expanding radioactive gas similar to that present in the OMEGA chamber after an ICF implosion. Using a $^{137}Cs/^{137m}Ba$ isotope generator, ^{137m}Ba solution (with a 2.6-minute half-life) may be produced and put on a substrate. The substrate would then be placed into the target chamber center. A laser beam

passing through a vacuum window would then pulse and hit the substrate releasing a radioactive gas that can be detected.

Experiments with microballoons (or ICF target capsules) could be done by filling the chamber with gas, placing the target inside the chamber and letting the gas permeate the walls. After re-evacuating the chamber, the laser could then pulse and strike the target hopefully creating an isotropic release (and subsequent detection) of the radioactive gas. This would be closer to what is occurring in the OMEGA target chamber. It is important to know how the gas expands in the chamber so mini fast ion gauges will be placed across the lid of the target chamber to quantify the behavior of the gas.

Special fast mini ion gauges were constructed that can respond to pressure changes much quicker than commercial ion gauges. A fast mini ion gauge can also be placed in the foreline trap to determine the fraction of the released gas that is trapped and detected.

Other possible questions would be about the non-inert gas reaction products. The laser could be incident on lithium or boron or compounds that when vaporized might stick to a getter.

Chapter 2

THEORY

2.1. Introduction

In this chapter, cross section will be defined, and an explanation given of how it has been calculated for several reactions of interest. There will also be a discussion of possible background neutron reactions and the expected results of the proposed experiments.

2.2. Thermonuclear Reaction Rate

Thermonuclear reactions occur between the charged nuclei in a high-temperature plasma, and the rate at which the nuclei interact is the thermonuclear reaction rate. As the nuclei approach each other, there is an increase in electrostatic repulsion that has to be overcome for fusion to occur. The Coulomb barrier is the energy required to overcome this electrostatic force [21]. Based on classical theory, high temperature/energies are required to allow fusion reactions. However, when incident energies are below the Coulomb barrier, the reactions are still possible because of quantum mechanical effects. This why some reactions have no threshold energy and why they can occur even at the low energies available using ICF. The probability that the reaction will occur if the energy is lower than the Coulomb barrier is proportional to the nuclear cross section. Generally, the cross section will be small for charged particles at low energies; however, because of the huge numbers of ions available in a thermonuclear reaction, they will still occur in measurable numbers.

2.2.1. Reduced Mass, Relative Velocity and Relative Kinetic Energy

Figure 13 shows the laboratory and center of mass coordinates for a system in three dimensions. Reduced mass, relative velocity and relative kinetic energy need to be used in the explanation how the nuclei in the fusion reactions interact. In the following discussion, the mass number of the interacting nuclei is given by A and CM denotes the center of mass.

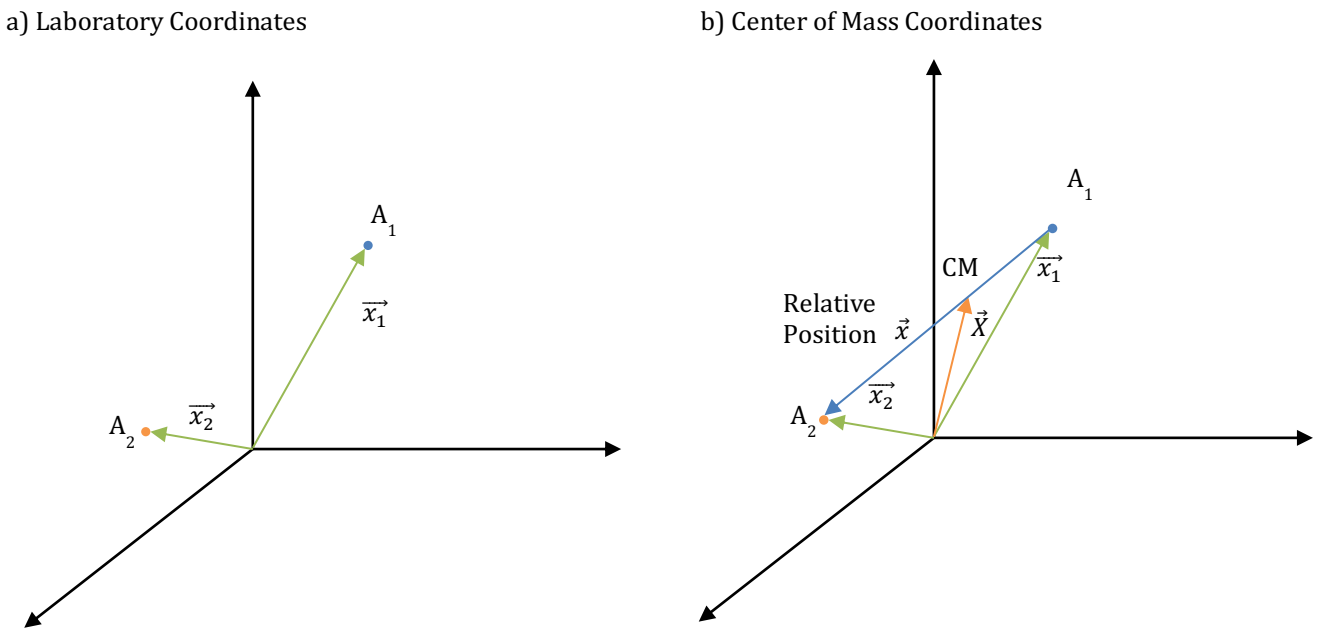

Figure 13. Laboratory (a) and center of mass coordinates (b) for two interaction nuclei A_1 at $\vec{x_1}$ and A_2 at $\vec{x_2}$. A is the mass number of the interacting nuclei and CM denotes the center of mass.

The position of the center of mass (CM) X is

$$\vec{X} \equiv \frac{MA_1\vec{x_1} + MA_2\vec{x_2}}{M(A_1 + A_2)}, \tag{1}$$

and the relative position x is

$$\vec{x} = \vec{x_2} - \vec{x_1} \tag{2}$$

where M is the nucleon mass. These equations can be solved for x_1 and x_2:

$$\vec{x_1} = \vec{X} - \frac{MA_2\vec{x}}{M(A_1 + A_2)} \tag{3}$$

and

$$\vec{x_2} = \vec{X} + \frac{MA_1\vec{x}}{M(A_1 + A_2)}. \tag{4}$$

The derivatives of the positions can be taken to find the velocities of the nuclei:

$$\overrightarrow{v_1} = \dot{\vec{X}} - \frac{MA_2\dot{\vec{x}}}{M(A_1 + A_2)} \tag{5}$$

and

$$\overrightarrow{v_2} = \dot{\vec{X}} + \frac{MA_1\dot{\vec{x}}}{M(A_1 + A_2)}. \tag{6}$$

The total relative kinetic energy of the system is

$$E = \frac{1}{2}MA_1v_1^2 + \frac{1}{2}MA_2v_2^2. \tag{7}$$

Using the velocities from Equations (5) and (6) above, it can be shown that

$$E = \frac{1}{2}\mathcal{M}\dot{X}^2 + \frac{1}{2}\mu\dot{x}^2. \tag{8}$$

where $\mathcal{M} = M(A_1 + A_2)$ is the total mass and $\dot{\overrightarrow{X}}$ is the velocity in the center of mass frame and the reduced mass $\mu = M\frac{A_1A_2}{A_1+A_2} \equiv MA$ (where A_1 and A_2 are the mass numbers of the interacting nuclei) and $\dot{\overrightarrow{x}}$ is the relative speed of the two interacting nuclei. Therefore, the first term in the energy equation is the center of mass energy and the second term is the relative energy E_{rel},

$$\begin{aligned} E_{rel} &= \frac{1}{2}\mu v_{rel}^2 \\ &= \frac{1}{2}MAv_{rel}^2, \end{aligned} \tag{9}$$

which implies

$$v_{rel} = \left(\frac{2E_{rel}}{MA}\right)^{\frac{1}{2}}. \tag{10}$$

This value will be used in the rest of the derivation of the nuclear reaction cross section.

2.2.2. Nuclear Reaction Rate

Figure 14 shows what is occurring when the nuclei in a plasma interact. Note that n is number density of the nuclei in a volume modeled as a cylinder. In the laboratory frame, particles from both A_1 and A_2 are traveling at velocities v_1 and v_2 respectively towards each other. Consider, however, the rest frame of the A_2 particles. In this frame, A_1 particles travel towards the A_2 particles with the relative speed of the two nuclei, v_{rel}.

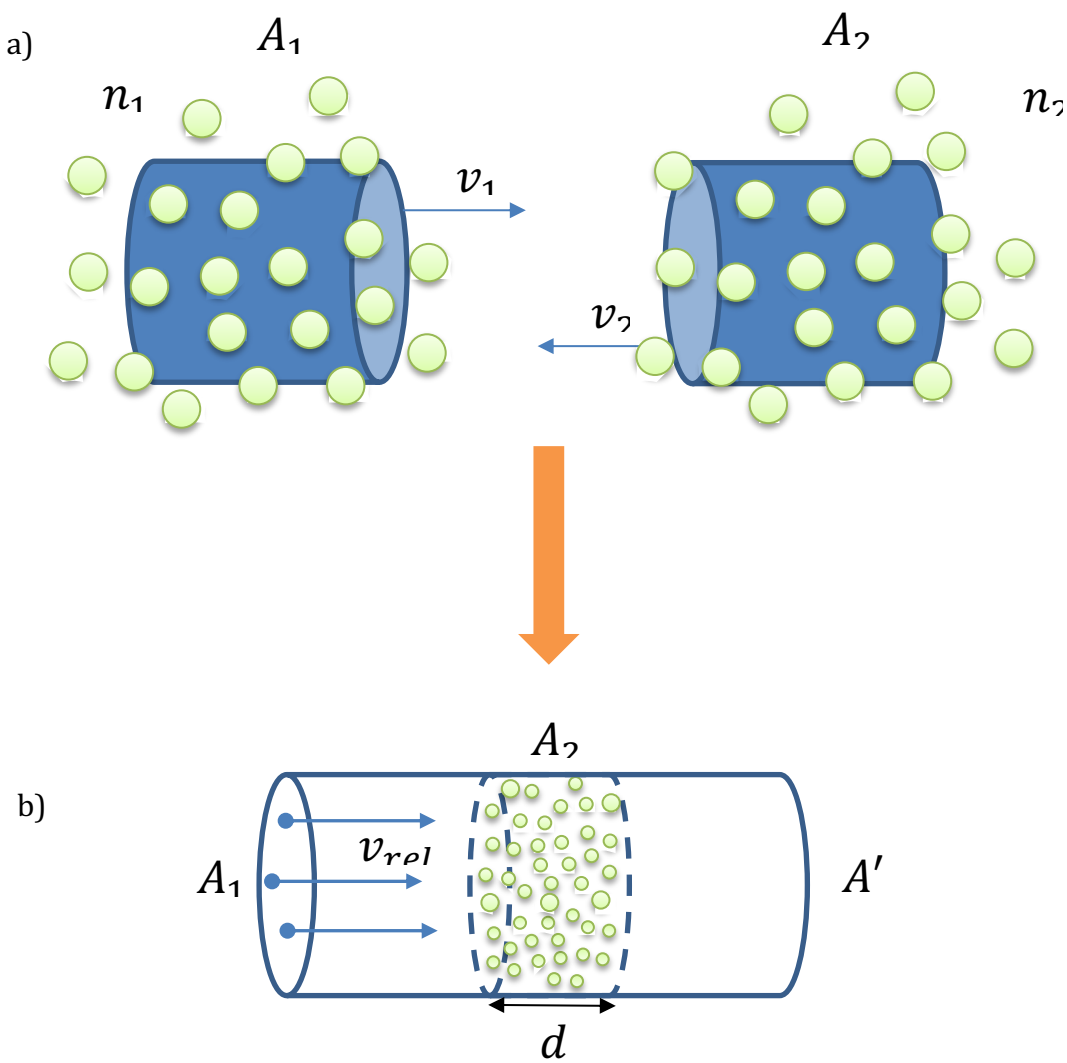

Figure 14. Movement of the two nuclei species interacting during the nuclear reaction. (a) Lab frame: A_1 particles are traveling $\overrightarrow{v_1}$towards A_2 particles and A_2 particles traveling at v_2. Note that n is the particle number density. (b) In the rest frame of A_2, the A_1 particles are moving at $\overrightarrow{v_{rel}}$. A' is the cross-sectional area of the cylinder; d is the thickness A_2 particles span and $v_{rel}$is the relative velocity.

The time it takes for A_1 particles to travel the thickness, d, through the A_2 nuclei, is $t = \frac{d}{v_{rel}}$. Thus, the description can be simplified to Figure 15 where all the A_1 particles travel at velocity $\vec{v}_{rel}$, through the "target" of A_2 nuclei with thickness d in a time t. The derivation for the cross section and yield of reaction products assumes this is the way the nuclei interact in the plasma after the ICF laser shot. The cross-sectional area, A', of the cylindrical volume can be considered infinitesimal and integrated over for non-uniform particle fields. The A_1 particles are traveling at the relative velocity given in Equation (10) above.

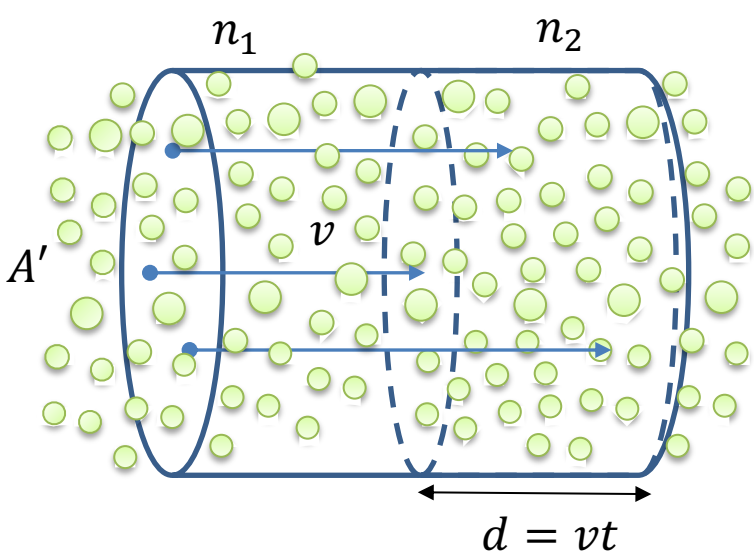

Figure 15. Simplified diagram of the two nuclei species interacting in the plasma. Nuclei A_1 with number density n_1 travel through the volume, $V = Ad = Avt$ which holds A_2 nuclei with number density n_2.

The total number of reactions, N, can now be written in terms of the cross section

$$N = \sigma N_1 \frac{N_2}{A'} = \sigma(n_1 A' d)(n_2 d) \tag{11}$$

where σ is the total cross section at the incident energy of the A_1 nuclei given by $E_1 = \frac{1}{2} m_1 v_1^2$ which assumes non-relativistic energies. The number of A_1 and A_2 nuclei that interact in the volume $A'd$, are $N_1 = n_1 A' d$ and $N_2 = n_2 A' d$, respectively. The number that pass through the "target," or the space where the other nuclei are located with areal density, $n_2 d$, can be represented by $n_1 A d$.

Equation 11 can be rewritten as

$$N = \sigma n_1 n_2 v^2 t^2 A' q. \tag{12}$$

This implies that the reaction rate (number of reactions per unit volume per unit time), R, is given by

$$R = \frac{N}{(Ad)t} = \sigma n_1 n_2 v. \tag{13}$$

2.2.3. Thermal (Maxwell) Velocity Distribution

So far it has been assumed that A_1 particles all have the same velocity, v. This is not a valid assumption. The particles have a thermal (Maxwellian) distribution for a thermonuclear reaction. The thermal velocity distribution [21] is

$$dn = 4\pi n \left[\frac{m}{2\pi kT}\right]^{\frac{3}{2}} e^{-\frac{mv^2}{kT}} v^2 dv \tag{14}$$

where dn is the number of particles with velocity between v and $v + dv$, n is the number of particles per unit volume, m is the mass of the particle, and T is the absolute temperature. To write this distribution in terms of energy,

$$dE = \frac{1}{2} MA(2v)dv \tag{15}$$

and therefore, combining Equations (10) and (14),

$$dn = 4\pi n \left[\frac{MA}{2\pi kT}\right]^{\frac{3}{2}} e^{-\frac{E}{kT}} \left[\frac{2E}{MA}\right] \left[\frac{2}{2MAv}\right] \tag{16}$$

which implies,

$$dn = \frac{4n}{(2\pi M)^{\frac{1}{2}}(kT)^{\frac{3}{2}}} e^{-\frac{E}{T}} \left[\frac{E}{v}\right] dE. \tag{17}$$

Referring back to Equation (13), the reaction rate produced by the velocity distribution of A_1 nuclei interacting with A_2 nuclei in the A_2 rest frame is given by

$$\begin{aligned} R &= \int_0^\infty \sigma(E)\, n_2 [v\, dn_1] \\ &= \int_0^\infty \sigma(E) n_2 \frac{4n_1}{(2\pi MA)^{\frac{1}{2}}(kT)^{\frac{3}{2}}} e^{-\frac{E}{kT}} E\, dE \\ &= \frac{4n_1 n_2}{(2\pi MA)^{\frac{1}{2}}(kT)^{\frac{3}{2}}} \int_0^\infty \sigma(E) e^{-\frac{E}{kT}} E\, dE = n_1 n_2 \langle \sigma v \rangle \end{aligned} \tag{18}$$

where

$$\langle \sigma v \rangle = \frac{4}{(2\pi MA)^{\frac{1}{2}}(kT)^{\frac{3}{2}}} \int_0^\infty \sigma(E) e^{-\frac{E}{kT}} E\, dE \tag{19}$$

and $\sigma(E)$ is the laboratory frame cross section at incident laboratory energy E.

The number of reactions in a given volume, called the yield (Y), is proportional to the reaction rate assuming the reaction rate stays relatively constant. The relationship is given by

$$Y_{12} \propto R_{12} = f_1 f_2 \left(\frac{\rho}{\bar{m}}\right)^2 \langle \sigma v \rangle_{12}, \tag{20}$$

where $f_1 = \frac{n_1}{n}, f_2 = \frac{n_2}{n}$ with $n = \frac{\rho}{\bar{m}}$ representing the total number density with the total mass density ρ and $\bar{m} = \frac{m_1+m_2}{2}$, the average mass of the interacting nuclei. Under the assumption that the nuclei are mixed evenly and $\langle \sigma v \rangle$ changes relatively slowly throughout the range of temperatures of the fuel. the ratio of the yields becomes

$$\frac{Y_{12}}{Y_{34}} \cong \frac{f_1 f_2}{f_3 f_4} \frac{\langle \sigma v \rangle_{12}}{\langle \sigma v \rangle_{34}} \tag{21}$$

where 1,2,3 and 4 can denote different species of nuclei interacting and undergoing nuclear fusion via a thermonuclear reaction.

Equation (21) was used to calculate Table 2 as follows

$$\frac{Y_{TT}}{Y_{DT}} \cong \frac{f_T f_T}{f_D f_T} \frac{\langle \sigma v \rangle_{TT}}{\langle \sigma v \rangle_{DT}} \tag{22}$$

where D denotes deuterium and T denotes tritium but can be replaced with different nuclei. The $\langle \sigma v \rangle$ are predicted cross sections and the f_T and f_D are the ratio of the tritium and deuterium nuclei to the overall number of nuclei produced, respectively.

2.3. Predicted Yields for Proposed Thermonuclear Reactions

In the last section, the calculation for the yield of a thermonuclear reaction is given based on the nuclear reaction rate. However, at the desired low energies, the cross sections of these reactions have never been measured and were therefore calculated using the code TALYS-1.9 [22]. TALYS can be applied to calculate cross sections for reactions that contain neutrons, protons, deuterons, tritons, ^{3}He and alpha particles (targets Z≥3 and N≥5) occurring in the 1 keV-200 MeV range.

As shown in Figure 16, measurements at higher energies for many of these reactions gave much higher cross sections than TALYS, by as much as three orders of magnitude. Also, an increase in DT yield in the ICF shot would dramatically these predicted yields. Referencing Table 3, DT yield may be expected to reach 10^{16} in the future which would be advantageous for measuring small cross sections. Table 3 shows the parameters from OMEGA shots 39794 and 77951 used to make estimates found in Table 2. The yield increases like the number of neutrons squared, thus there would be an increase by a factor of 10,000 in the yields relative to those quoted in Table 2.

2.4. Reaction Pathways

Many different reaction pathways can occur that lead to the desired product. Since the cross section is expected to be small, the desired reaction pathway may not be the most likely pathway for the reaction to take. For example, for the $^{3}H(t,\gamma)^{6}He$ radiative capture reaction, based on Figure 17, the $^{3}H+^{3}H$ system occurs at 12.305 MeV above the ground state of ^{6}He and the reaction may pass through different reaction pathways. It might be expected that the highest yielding path would be straight to the ground state of ^{6}He, however, this is forbidden for orbital angular momentum $\ell = 0$. Another possible pathway is through the first excited state of ^{6}He at 1.797 MeV and then to the ground state, however the first excited state decays by neutron emission, $^{4}He+2n$, and therefore typically does not produce ^{6}He in the ground state. The reaction could pass through a higher energy resonance, then to the ground state; however, it might also then pass through the first excited state and out the neutron channel. There is also a chance that there is a small angular momentum admixture in the ground state of ^{6}He. This could create a channel directly from the tritium-tritium system to the ground state of ^{6}He that conserves angular momentum for $\ell = 0$. Finally, non-head-on collisions with $\ell > 0$ are possible but have reduced probability.

2.5. Background Reactions

During the ICF implosion, there is a large neutron flux that can interact with the reactants and reaction products to produce unwanted background events. For most of the proposed reactions, this is not a problem. However, for certain B and Li reactions, the neutrons will create unwanted background and increase the uncertainty in the cross section measurement.

For example, in the $^{6}Li(t,p)^{8}Li$ reaction, $^{6}Li(n,p)^{6}He$ would be occurring in the background. The half-lives of these reaction products are very similar: ^{6}He has a half-life of 807 ms and ^{8}Li has an 840 ms half-life; therefore, it could be difficult to discern between the two reactions by these reaction products. For the $^{7}Li(t,\alpha)^{6}He$ reaction, $^{6}Li(n,p)^{6}He$ could also be background since it would be hard to get completely pure ^{7}Li without any ^{6}Li. Finally, for $^{9}Be(t,\alpha)^{8}Li$ there would also be $^{9}Be(n,\alpha)^{6}He$. The ^{10}B and ^{11}B reactions along with the

$^{3}H(t,\gamma)^{6}He$ radiative capture reaction do not have the problem with the neutron flux creating background reactions, making these reactions more favorable.

2.6. Expected Results

Based on the research done for the proposed reactions, the $^{6}Li(t,p)^{8}Li$ reaction has the highest predicted yield at 2,000-9,000 nuclei captured. Therefore, this reaction would theoretically be the most feasible cross section to measure. For this reaction, we would need the capability to dope the tritium-filled ICF target with ^{6}Li.

Table 2. Reactions that might possibly be measured using ICF. The half-life and reactant abundance are listed as well as the predicted yields using the yields obtained in two different OMEGA laser shots. In all reactions listed below, except $^{3}H(t,\gamma)^{6}He$, the targets are assumed to be doped to 1%. The yellow highlighted rows indicate the reactions with the greatest predicted yields that may be feasible to measure at OMEGA.

			Shot 39794 (50-50 DT, 11.8 keV)		Shot 77951 (1.5-98.5 DT, 18.3 keV)	
Reaction	Product Half-life	Reactant Abund.	Predicted Yield	Captured	Predicted Yield	Captured
$^{3}H(t,\gamma)^{6}He$	807 ms	^{3}H fill	Branching ratio of ~10^{-7}		8×10^{4}	200
$^{6}Li(t,p)^{8}Li$	840 ms	7.6%	$2\text{-}10\times10^{5}$	1000-6000	$4\text{-}16\times10^{5}$	2000-9000
$^{7}Li(t,\alpha)^{6}He$	807 ms	92.4%	$1\text{-}3\times10^{5}$	500-1500	$1\text{-}4\times10^{5}$	700-2300
$^{9}Be(t,\alpha)^{8}Li$	840 ms	100%	2.3×10^{4}	130	8×10^{4}	460
$^{9}Be(t,\gamma)^{12}B$	20.2 ms	100%	2.8	0.02	3.0	0.02
$^{10}B(t,p)^{12}B$	20.2 ms	19.9%	78.3	0.44	923	5.2
$^{11}B(d,p)^{12}B$	20.2 ms	80.1%	372	2.09	1735	9.8
$^{13}C(t,\gamma)^{16}N$	7.1 s	1.1%	0.05	0.0003	0.1	0.001
$^{13}C(t,\alpha)^{12}B$	20.2 ms	1.1%	8.2	0.05	108	0.6
$^{13}C(t,p)^{15}C$	2.45 s	1.1%	1.2	0.01	17.7	0.10
$^{14}N(t,p)^{16}N$	7.1 s	99.6%	0.06	0.0003	2.5	0.01
$^{15}N(d,p)^{16}N$	7.1 s	0.4%	0.10	0.0006	2.0	0.01

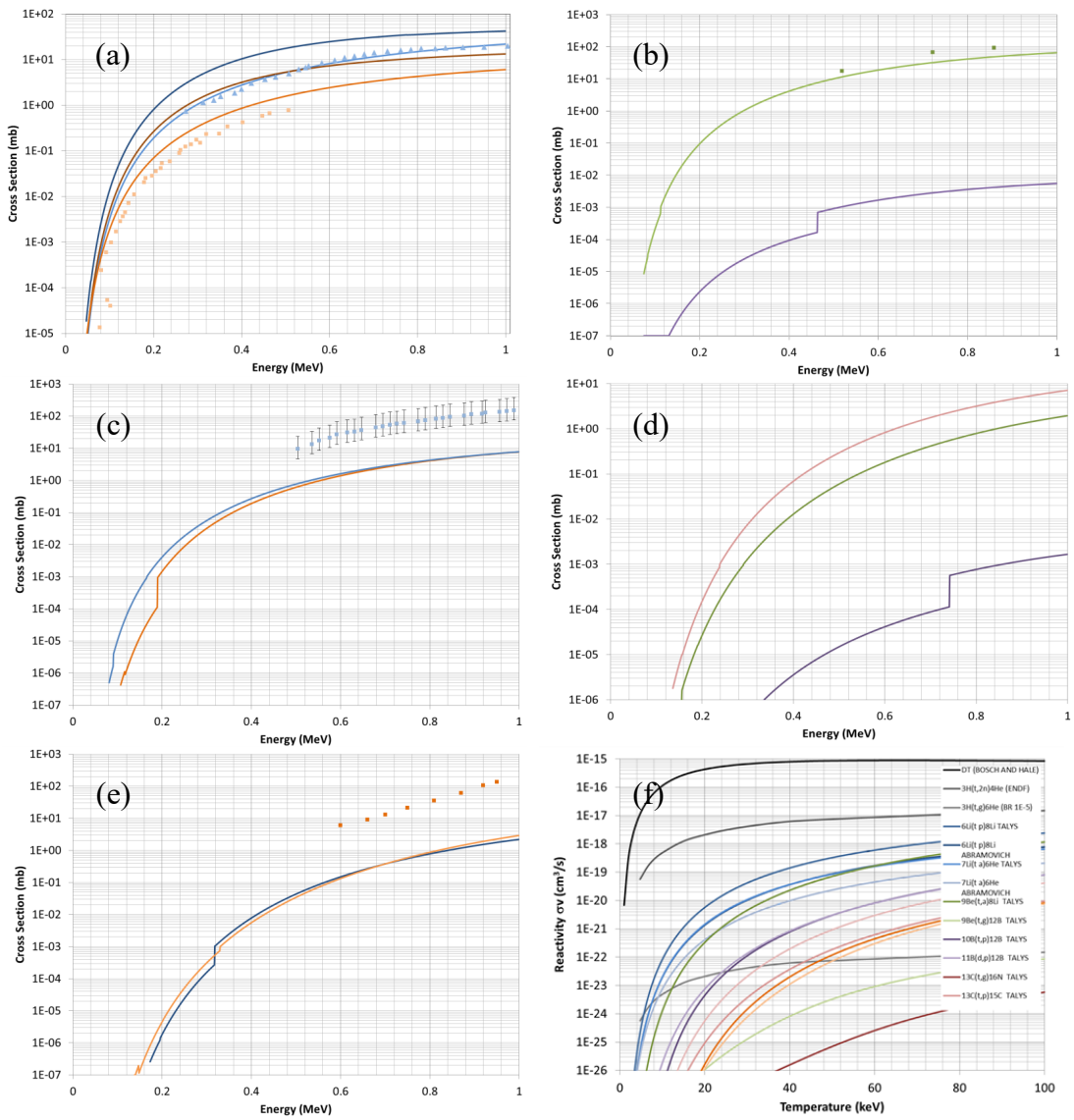

Figure 16. Plots of cross section predictions for different proposed reactions. (a) Cross sections for 6Li(t,p)8Li predicted by TALYS (dark blue curve), S-factor (light blue curve) and measured (light blue triangles), and for 7Li(t,α0)6He predicted by TALYS (dark brown curve), S-factor (orange curve) and measured (orange squares). (b) Cross sections for 9Be(t,α)8Li predicted by TALYS (green curve), and measured (green squares), and for 9Be(t,γ)12B predicted by TALYS (purple curve). (c) Cross sections for 10B(t,p)12B predicted by TALYS (orange curve), and for 11B(d,p)12B predicted by TALYS (blue curve) and measured (blue squares). (d) Cross sections for 13C(t,p)15C (green), 13C(t,γ)16N (purple) and 13C(t,α)12B (pink) predicted by TALYS. (e) Cross sections for 14N(t,p)16N predicted by TALYS (blue curve), and for 15N(d,p)16N predicted by TALYS (orange curve) and measured (orange squares). Reactivities calculated by integrating Equation (19) for each of the predicted cross sections.

Table 3. Parameters from OMEGA shots 39794 and 77951 used to make estimates found in Table 2.

	Shot 39794	**Shot 77951**
DT Yield	3.8×10^{13}	2.6×10^{11}
f_D	56%	1.5%
f_T	39%	98.5%
kT	11.8 keV	18.3 keV
Dopant	1%	1%

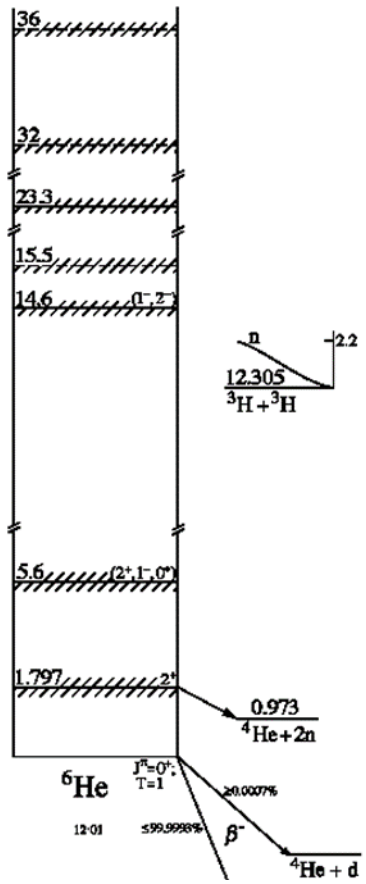

Figure 17. ^{6}He energy level diagram. Figure taken from Ref. [23].

Chapter 3

EXPERIMENT AND APPARATUS

3.1. Introduction

The main goal of the experiments outlined in this chapter is to answer questions about the proposed experiment at LLE and optimize the experimental design. The method for measuring the cross section is to detect the beta particles from the decay of the trapped reaction products. Some of the proposed reaction cross sections would typically be measured using the prompt neutrons or gamma rays. It is not conventional to measure the product by the beta decay because of the "short" half-lives; however, doing so could decrease the background that results from the prompt neutrons, gamma rays and EMP pulse. This could allow measurements that could not otherwise be made.

The apparatus described in this chapter allows a number of experiments to be performed to determine the best method to trap and count the decaying reaction products. The main parts of the apparatus are the vacuum chamber and vacuum system (analogous to the target chamber at LLE), phoswich detector system (with trap turbopump) and the detector electronics. Radioactive or non-radioactive gas may be released by various methods into the vacuum chamber and trapped by the turbopump. The radioactive nuclei can then be detected by the phoswich detector system and the number of counts is read out by the electronics. The phoswich detector needs to survive in the radiation environment near or in the ICF chamber.

3.2. Vacuum Chamber

Figure 18 shows the small-scale vacuum chamber setup at Houghton College. The stainless-steel vacuum chamber is 50.8 cm in inner diameter and 15.24 cm in inner height. It has eight 2.75 in. conflat ports uniformly distributed around the body of the chamber. The top and bottom lids of the chamber are 1.27 cm thick aluminum lids that seal the chamber with about 20 cm radius rubber o-rings in the grooves about 5 cm in from the outer radius of the lids. There is an additional steel lid with five ports (two 2.75 in. and three 1.33 in. conflat) linearly

arranged across the top (as shown in Figure 47) to allow pressure measurements at different points in the chamber.

3.3. Vacuum System

The white plastic tubing with 9.5 mm outer diameter is part of the water-cooling system for the two Edwards EXT70H turbopumps that evacuate the chamber. The water-cooling system starts with the Haskris Co. Refrigeration and Air Conditioning Controlled Temperature System model A5H chiller containing distilled water treated with Algae Destroyer Advanced algaecide. The water flows through a filtration system to protect the turbopumps from dirt and any particulates. It flows through the white tubing to the turbopumps and returns to the chiller. The flow rate of this system is about 2.5 lpm through both pumps measured by a standard flow meter.

An Alcatel Pascal 2005 SD rotary forepump pumps the foreline of the turbopumps through plastic tubing seen in the top right of Figure 18. The tubing has a wire inserted through it in a coil to strengthen it against compression. One forepump pumps both the turbopumps.

The Duniway T-075-N ionization gauge with a Granville-Phillips Convectron GP 275 controller reads out the pressure of the chamber while in the range of mTorr. Once the turbopumps are on, the Duniway T-075-N ionization gauge with Varian multigauge controller read out the pressure of the chamber ($\sim 10^{-6}$ Torr). This ion gauge takes about 15 minutes to output an accurate pressure reading. The Edwards EXT70H turbopumps reach chamber pressures of about 10^{-6} Torr in about 3 hours depending on the condition of the vacuum chamber.

3.3.1. Trap turbopump and detector system

A long stainless-steel collection tube extends various lengths across the target chamber. This tube is 4.1 mm in inner diameter and 22 cm long from the conflat flange port towards the center of the chamber. An attachment can be added to the collection tube to extend it towards the opposite end of the chamber. The tube is supported in the chamber by a conflat flange (which centers the tube) and o-ring then the trap turbopump is attached to the same port

with long bolts. The trap turbopump is where the nuclei will be trapped behind the turbine blades. This pump will be evacuating less gas than the main turbopump because it has a smaller cross-sectional inlet area. The trap turbopump collects a fraction of the gas, determined by the solid angle.

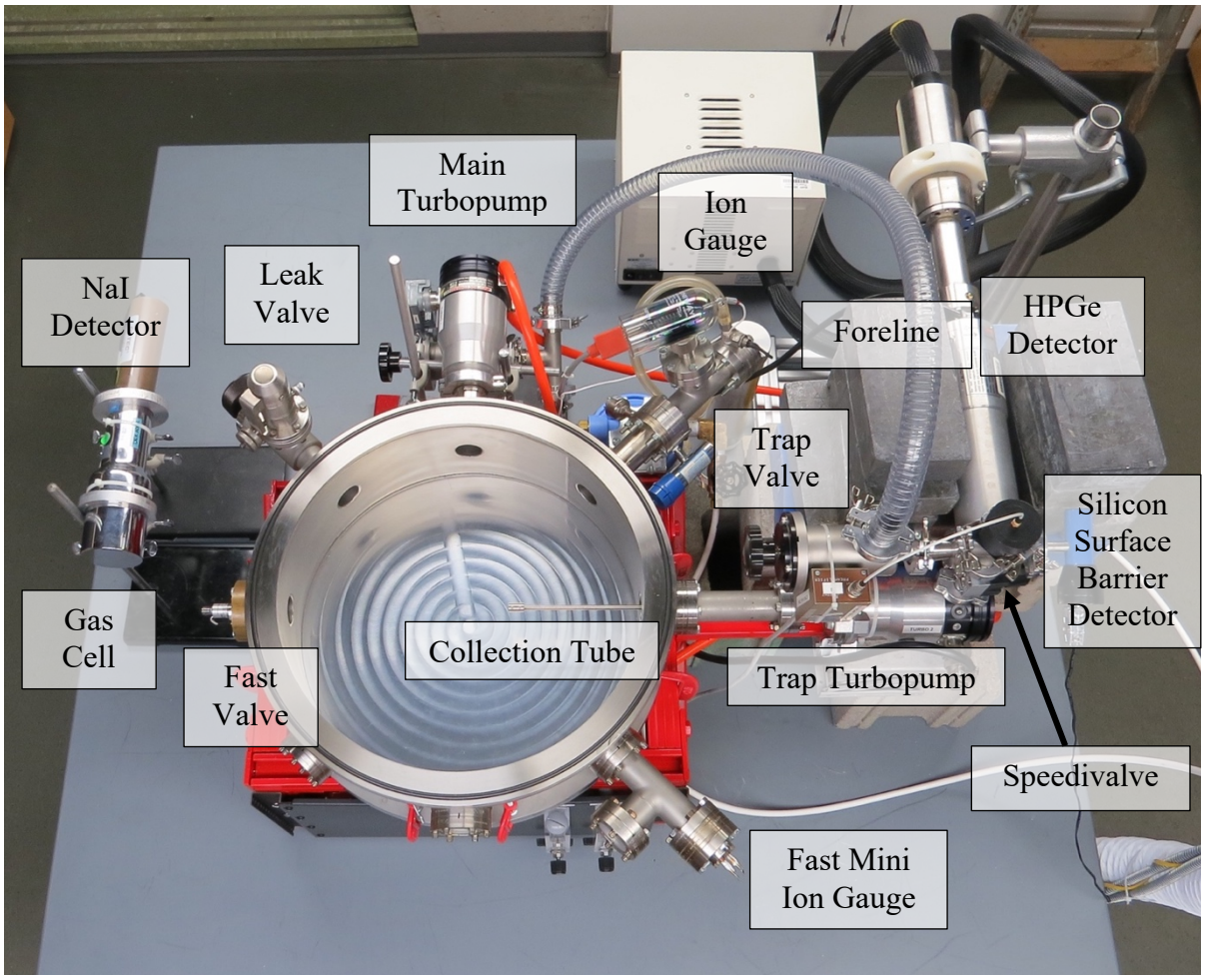

Figure 18. Vacuum chamber system at Houghton College. This top view shows the chamber along with the various attachments for the preliminary experiments. The main turbopump keeps the chamber evacuated. The trap turbopump collects and traps radioactive gas to be counted by the detector system. The leak valve calibrates the ionization gauges. The ion gauges read out the pressure of the chamber. The foreline to the trap turbopump is shut off by the trap valve to trap the nuclei. The speedivalve is then shut to keep the nuclei contained to be detected so the foreline can be opened back up to the trap turbopump to keep it from breaking. The detectors count the radioactive gas that was trapped. The NaI detector was used to monitor the radioactive gas in the gas cell before it was released through the fast valve.

Attached to the foreline of the trap turbopump will be the phoswich detector system. This detector system (described later) will be capable of identifying beta particles. In the preliminary experiments described here, a silicon surface barrier detector was used to detect the beta particles. There was also a high-purity Germanium (HPGe) gamma detector close to the "cross" area in the foreline (see Figure 19) where the radioactive nuclei are trapped. The detector systems count the beta decays and emitted gamma rays once the gas is trapped in the turbopump and foreline.

3.3.2. Fast Valve and Introduction to Experiment

On the other end of the vacuum chamber, a fast valve is attached. This valve is capable of opening in about 300 μs. It simulates the rapid release of the neutral radioactive gas following the ICF shot.

The first preliminary experiment to be conducted using this apparatus was to determine the fraction of radioactive nuclei trapped compared to the initial number. Radioactive gas was released through the fast valve. The foreline was quickly shut off by the trap valve (Figure 18) allowing a fraction of the gas to travel down the collection tube and instead of being evacuated, become trapped by the trap turbopump. Then the gas traveled up to the "cross" and was trapped there by the speedivalve. When the gas was trapped in the "cross," it began to decay. The beta particles and gamma rays were detected over about one half-life of the radioactive nuclei.

3.3.3. Fast Mini Ion Gauge

A custom-made fast ion gauge was constructed to read out faster pressure changes than is possible with commercial gauges. This gauge should be able to measure a leading-edge pressure rise time as fast as 200 μs. These ion gauges were made according to the design by T.E. Weber and T.P. Intrator [24].

Ion gauges have three main components: a filament, a high voltage grid and a collector as shown in Figure 20. The filament releases electrons when it is heated by current flowing

through it. These electrons are attracted to and pass through the positive high voltage grid. These electrons ionize the gas inside the grid; the resulting ions are then attracted to the grounded collector. The ions produce a current that depends on the pressure.

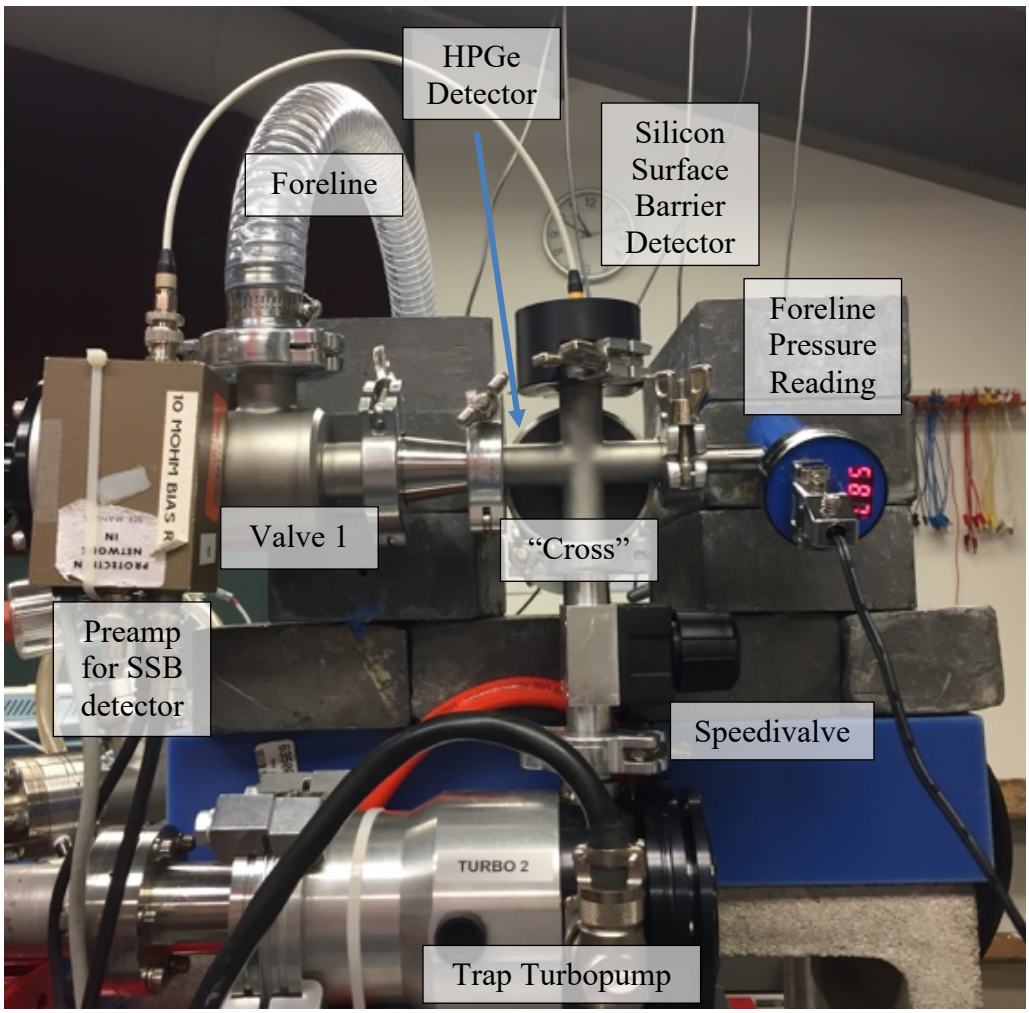

Figure 19. Trap turbopump and detector system. The foreline to the trap turbopump was shut off by the trap valve to trap the nuclei. The speedivalve was shut to keep the nuclei contained. A silicon surface barrier (SSB) detector identified beta decays (used for the same purpose as the phoswich detector system). The preamplifier for the SSB detector was connected to electronics behind the vacuum chamber. Behind the "cross" was the high purity Ge detector which counts the emitted gamma rays. The lead bricks eliminate background radiation. The pressure gauge in the foreline confirms the gas made it to the foreline to be detected.

The filament in Figure 20 was made of 0.05 mm diameter thoriated tungsten wire and was wrapped 22 times around a #73 drill bit with diameter of 0.6 mm. The HV grid in Figure 20

is made of 0.25 mm diameter stainless steel lock wire, wrapped 6 times around a #44 drill bit with diameter of 2.2 mm. Both grid and filament coils are approximately 6.4 mm long.

Stainless steel support wires and ceramic insulators were assembled to hold the ion gauge together. In Figure 20, the support wires are the furthest left and right wires holding up both the grid and filament coils, respectively. The support wires were spot welded to the filament coil by stainless-steel foil tabs to keep it in place. The foil tabs are used because spot welding directly to the thin filament and grid wires would destroy them. These support wires are then glued with Hysol epoxy into the ceramic insulators which were 2.32 mm by 3.62 mm by about 3 cm in length with two holes to insert the wires. This is to keep all the wires electrically isolated from each other. The ceramic insulators were glued together far from the filament with Hysol epoxy to secure all the components. Near the flament, the ceramic insulators were also wrapped with 0.27 mm diameter stainless steel wire to keep them bundled and in place because the glue was breaking down because of the high temperature near the filament. The geometry of these fast mini ion gauges is important to the operation of the gauge. This is because the gauges read out pressures on the order of 100 μs and amount of ionization depends on the number of electrons passing through the grid. The filament and grid should be parallel and very close together, so all the electrons released make it to the grid. However, they cannot be touching. The gauges were then spot welded at 20 J energy to feedthroughs attached to flanges to insert them in the chamber through the vacuum chamber ports.

Figure 21 shows the circuit used to power the gauge. The floating supply gives the 1 A to the filament that releases the electrons. A heated filament is shown in Figure 22. The electron current leaving the filament is read out on the oscilloscope that is attached to ground through a 100-ohm resistor. When powering the gauge, the filament needs to be turned up slowly to condition it. The ion gauges need to be running for a while to read out accurate changes in pressure, thus conditioning the gauges increases the reliability of the measurement. For all experiments, the filament current was about 1 A. The HV supply is used to power the grid. A positive 100 V was applied to the grid throughout the multiple experiments. Finally, the

collector current is read out by the oscilloscope across a 100 kΩ resistor. The voltage across the collector resistor indicates the pressure in the chamber.

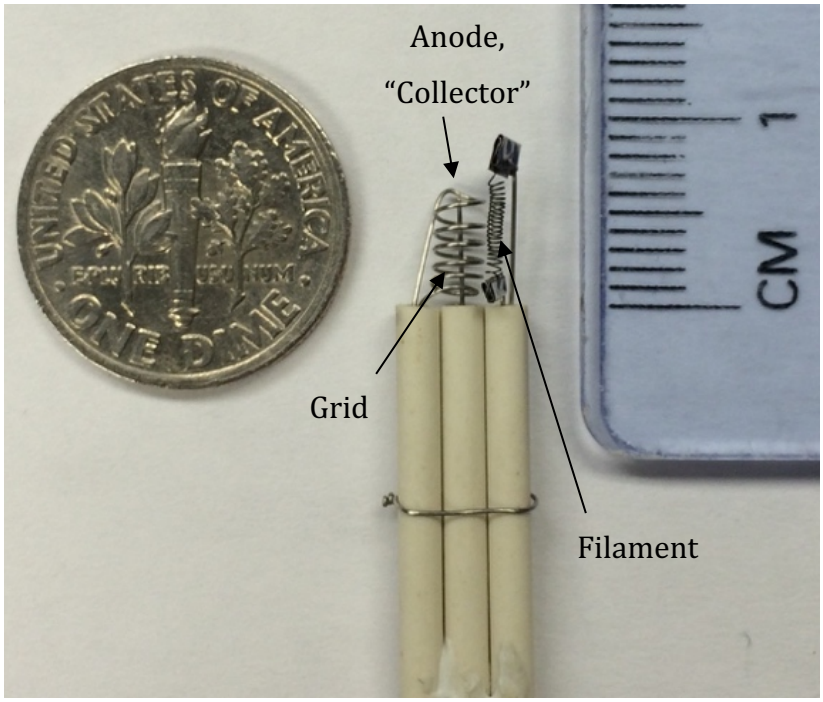

Figure 20. Custom-made fast mini ion gauge. The ion gauge is about 1 cm in length. The grid is the coil of larger radius with fewer turns, the filament is the thin wire with many turns and the collector passes through the grid. The filament releases electrons when it is heated by current flowing through it. These electrons are attracted to and pass through the positive high voltage grid. These electrons ionize the gas inside the grid; the resulting ions are then attracted to the grounded collector. The ions produce a current that depends on the pressure. This is much smaller than the conventional industrial ion gauge and is used to measure changes in pressure on a faster time scale.

The fast mini ion gauges were tested and calibrated by evacuating a small test chamber then turning off the turbopump to allow the pressure to rise slowly. The ratio between the collection and emission current was then measured as a function of pressure, which was measured using a calibrated commercial ion gauge. Figure 24 shows the calibration curve for a typical fast mini ionization gauge. As the pressure in the chamber slowly rises from 0 to 300 μTorr, the ratio between collection and emission current increases linearly.

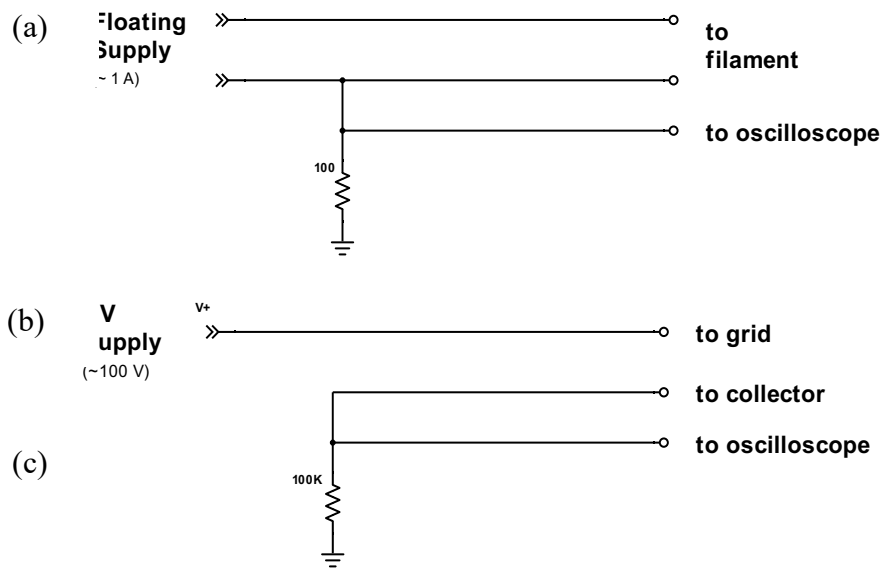

Figure 21. Fast mini ion gauge circuit. a) Current (1 A) travels through the filament to power it as shown below. The electron current leaving the filament can be read out by an oscilloscope or multimeter. b) The high voltage power supply gives a positive 100 V to the grid. This creates an attractive force for the electrons released by the filament. c) The ion current on the collector is read out by the voltage drop across a resistor via an oscilloscope. An example of a signal from the collector is shown in Figure 24.

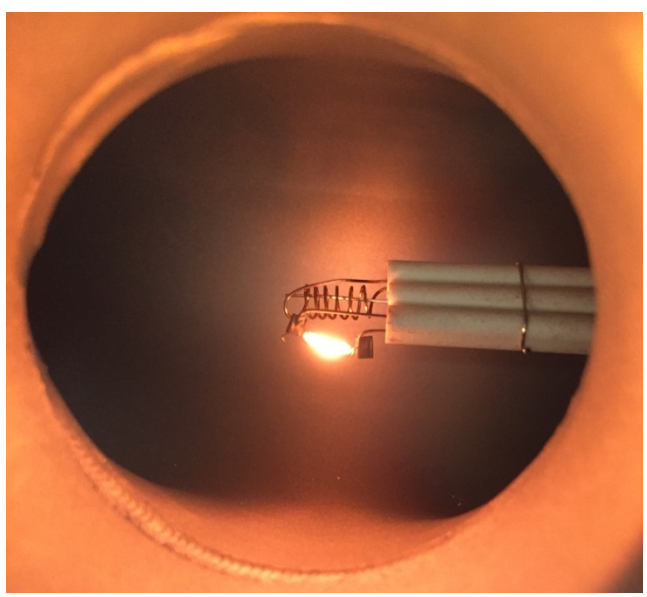

Figure 22. Fast mini ion gauge powered on. The filament requires 1 A to reach the brightness shown here.

Figure 25 shows the signal from the collector of a typical fast mini ion gauge. The blue curve indicates the TTL pulse that is used to trigger the opening of the fast valve. Once the valve was open, it took about 1.2 ms for the ion gauge to register a rise in the current. The calculated time required for N_2 to cross the chamber (50.8 cm), based on its rms speed at room temperature (about 478 $^{m}/_{s}$), should be about 1.06 ms, therefore this signal is in rough agreement with the theoretical time required for air to travel the distance from the valve to the ion gauge.

The signal shows an 8 ms rise time. This is much longer than the reported [24] 200 μs rise time.

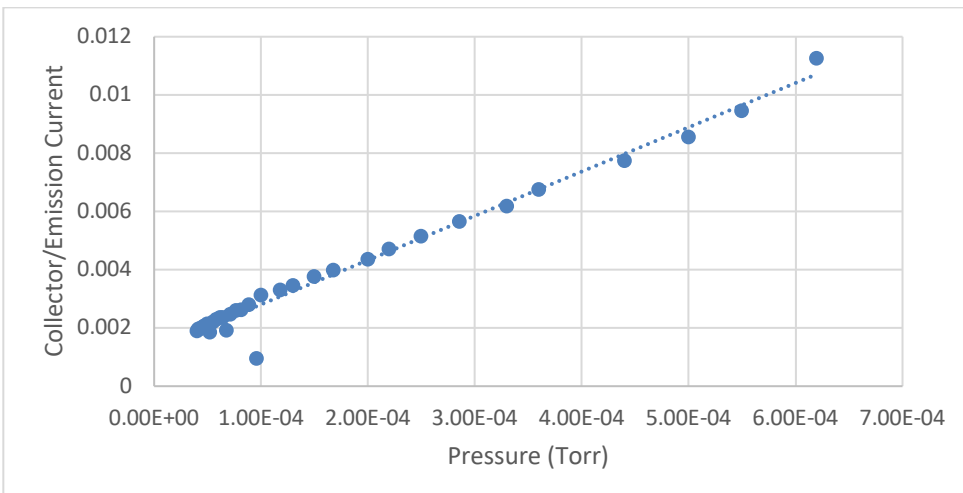

Figure 23. A typical calibration curve using air for the fast mini ion gauge. This was measured by slowly allowing the pressure to rise from 0 to 300 μTorr in the small test chamber.

3.3.4. Fast Valve

The fast valve simulates the rapid release of gas that occurs after the ICF shot. It is used in the small scale test experiments to test how the gas behaves in the target chamber and the efficiency of the trap turbopump and detector system. Figure 25 is an image of a Parker Precision Fluidics 009-0181-900 Ultra Low Leak Extreme Performance Valve. The fast valve is attached to the chamber via a homemade 2.75 inch conflat flange. The flange is custom-made for the fast valve because of the non-standard flange on the valve. The conflat flange has a small hole to direct the gas flow directly into the chamber. According to the

manufacturer, this fast valve can create pulses as short as 300 μs into the vacuum chamber, where the pressure can then be read by the ion gauges.

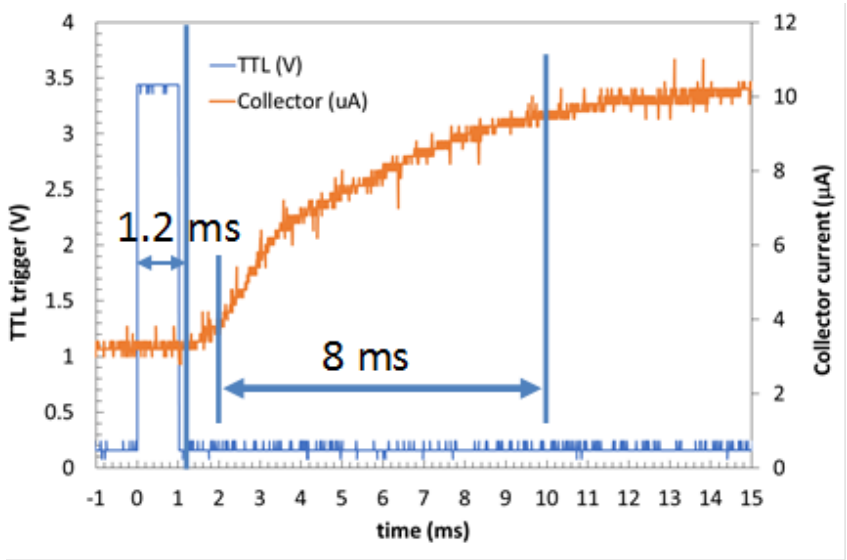

Figure 24. Output pulse from the fast ion gauge when a pulse of air is released from the fast valve. The TTL trigger was used to open the fast valve. The approximate time required for N_2 to cross the chamber, based on its rms speed at room temperature, should be about 1.2 ms. The measured 8 ms rise time is much longer than the expected 200 μs due, perhaps to a large resistor in the circuit connecting the collector to ground.

A high voltage pulse is needed to trigger the fast valve to open and close. The circuit in Figure 26 receives an input TTL pulse from an Arduino Uno. Two bipolar transistors raise the voltage to 7V to power the high voltage MOSFET so the valve solenoid can open and close as fast as possible. The valve requires only 28 V to open (and be held open); however, to open faster, it needs up to 600 V [24]. Figure 26 shows the circuit for opening the fast valve. Two power supplies were connected in series to apply up to 628 V to the fast valve. The valve can be held open using only 28 V; however, to get it open on the order of μs it needs a higher voltage. This voltage is only needed for a very short time once it is open on 28 V is needed to hold it. Higher voltage for a long period would cause the valve coil to overheat. During some of the small scale experiments, the valve was powered by about 200 V to open it for about 1 ms. The circuit begins with a TTL pulse supplied by an Arduino Uno. It passed through a resistor and then switches a 3N3904 NPN transistor attached to +7 V to create a 7 V inverted pulse. This pulse switches a 2N3904 NPN transistor to get a 7 V non-inverted pulse. The STF3NK80Z MOSFET used is rated for up to 800 V on the valve solenoid and it requires 7 V

to turn on. This circuit allows a button to be pushed which outputs the TTL pulse that triggers the circuit and opens the valve for a set amount of time (indicated in the Arduino code).

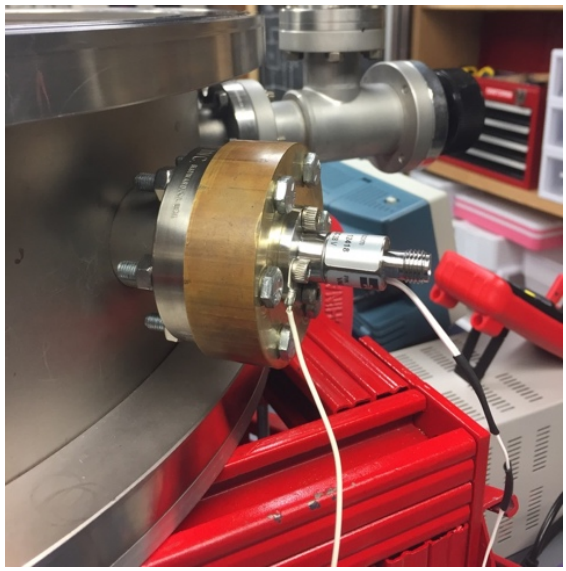

Figure 25. Fast valve attached to the vacuum chamber on a homemade conflat flange. A gas cell can be bolted to the flange. The circuit in Figure 26 is attached to the two wires coming from the valve. The valve is essentially a solenoid that quickly opens and closes via a small hole to let in gas to the chamber.

3.3.5. Laser

A 6 W 445 nm Nichia NUBM 44 laser diode shown in Figure 27 is available to use for small-scale experiments where radioactive samples are vaporized in the chamber. The laser will enter the chamber through a viewport attached to the vacuum chamber and strike the target. This will allow the study of the behavior of the expanding gas in the chamber, simulating more closely the isotropic nature of the gas from the ICF shot.

The laser is controlled by a circuit similar to the fast valve circuit. An Arduino produces a 5 V pulse to the laser board to turn the laser on, and the duration of the pulse determines how long the laser is on. A buzzer was inserted into the circuit to increase safety and awareness of when the laser *could* be on, by buzzing power is available, because the laser beam cannot be seen.

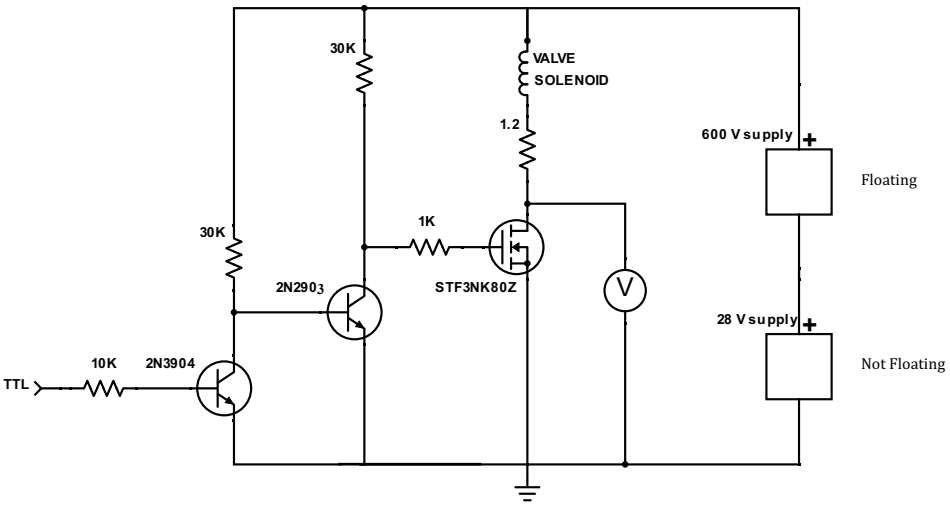

Figure 26. Fast valve power circuit. The TTL pulse is supplied by an Arduino Uno. It passes through a resistor turning on a 2N2904 NPN transistor attached to +7 V to create a 7 V pulse. At this point, the square pulse is inverted so that when it continues to a 2N2903 NPN transistor it is back to the original pulse. This square pulse is used to turn on the STF3NK80Z MOSFET. This is required because up to 600 V may be used to open the fast valve. The MOSFET used here is rated for up to 800 V on the valve solenoid and it requires 7 V. This circuit allows a button to be pushed which outputs a pulse that opens the valve for a set amount of time (indicated in the Arduino code).

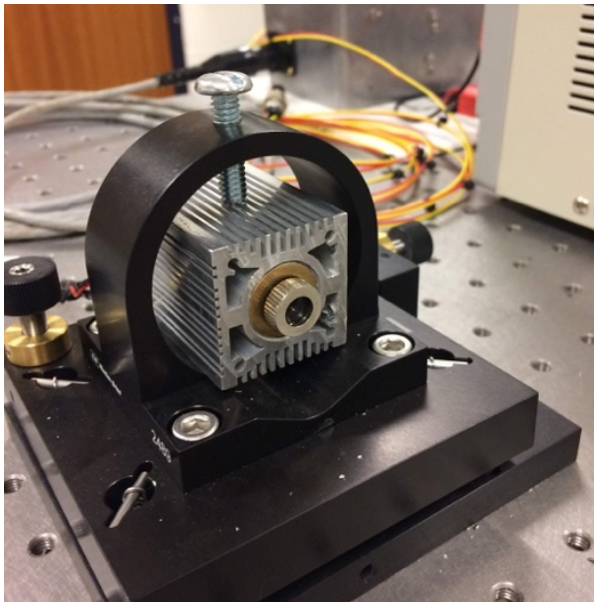

Figure 27. 6 W 445 nm laser diode. The laser is used for small scale experiments in which radioactive material is vaporized so the neutral radioactive gas behavior can be observed.

This laser can be used to "pop" target capsules (any type of opaque shell that can be filled with radioactive material or gas) similar to the ones used in ICF shots. It would be ideal to get actual ICF target capsules from LLE that have been rejected in order to test this idea.

Microballoons can also be used as the target for these experiments. Microballoons are hollow spheres with shells made of glass, acrylic or phenolic resin with diameters between about 10 μm and 80 μm and they are shown in Figure 28. The microballoons used can be purchased commercially since they are used as a lightweight epoxy filler. Approximately 4 W of laser power was used for a few seconds to see if these microballoons could be vaporized or melted. Observations showed no effect on the transparent glass or acrylic microballoons, although an ink line on the microscope slide behind them was scorched, indicating the laser was incident on the microballoons and microscope slides. These microballoons are so transparent they did not absorb very much laser power. However, when they were dyed and able to absorb more laser power, they melted because the melting point of acrylic is only about 130 °C. The phenolic microballoons are opaque, but unfortunately phenolic resins are used commercially for their fire-resistant properties therefore they have no melting point, and do not decompose until temperatures over about 500 °C, and this only results in charring. Figure 28 shows before and after photographs of charred phenolic microballoons.

Other radioactive materials, like a substrate coated with ^{137}Ba from a radioisotope generator, could also be hit by the laser releasing radioactive gas in the vacuum chamber.

The different sources will all simulate the expanding radioactive gas that will be present in the OMEGA chamber after an ICF implosion. While small scale, test experiments with this laser could be beneficial in determining the feasibility of measuring the beta decays from the different radioactive gases.

3.4. Phoswich Detector

Measuring the beta decay of the reaction products requires a detector system with maximum efficiency for detection of beta particles, while being able to survive the electromagnetic

pulse, gamma rays and neutrons produced during ICF. The beta particles will be measured in-situ using a dE-E phoswich detector system (Figure 29) milliseconds after the implosion.

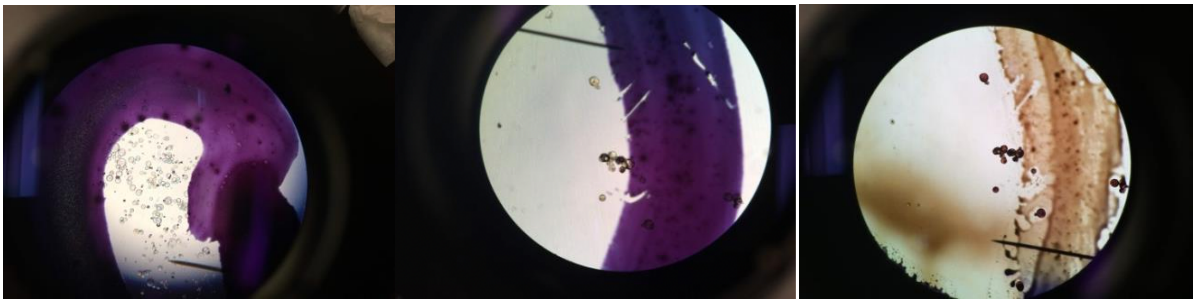

Figure 28. Microballoons. (Left) Acrylic microballoons about 10 μm to 80 μm in diameter at 100x. (Middle) Phenolic microballoons before being hit by the laser. (Right) Phenolic microballoons after being hit with the laser. The brown spot on the left shows the burn mark from the laser. Purple marks are from permanent markers to make the microballoons visible.

The test phoswich detector system is composed of a 1 mm thick, 2.1 ns decay time Eljen EJ-200 dE plastic scintillator attached to a 18 mm thick, 285 ns decay time Eljen EJ-240 E plastic scintillator and ET Enterprises XP2262 photomultiplier tube optically coupled with iRad silicone coupling compound optical grease.

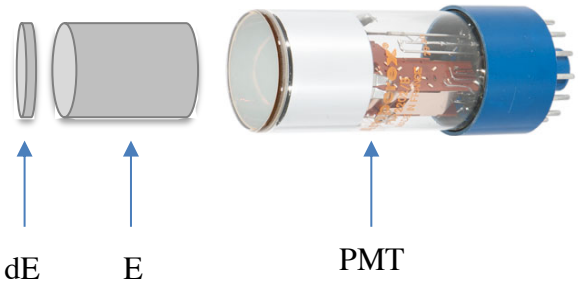

Figure 29. Phoswich detector system. The dE and E scintillator detectors are optically coupled (using optical grease) to each other and the PMT. This is a test detector for the experiments while a 4π phoswich detector is being developed. This detector system was used in the Tandem Pelletron experiment to demonstrate that ^{6}He can be created and detected. In this experiment, electrons enter the detector, deposit a small amount of energy in the thin dE detector and then deposit the rest in the thick E detector. The light pulses are then converted to current pulses to be read out by the electronics.

3.4.1. Photomultiplier Tube and Base

Various photomultiplier tubes (PMTs) and bases were tested to determine the combination that would output the best pulse with the least amount of noise and ringing. The best PMTs

were both 2-in, 12-stage photomultiplier tubes: Photonis XP 2262B PMT and RCA 8575. These tubes require -1800 V and -2000 V respectively. The bases are Ortec 269 (20 pins) and 265 (21 pins), respectively. A BURLE 8575 phototube and Ortec 265 base were used in the test experiment at SUNY Geneseo.

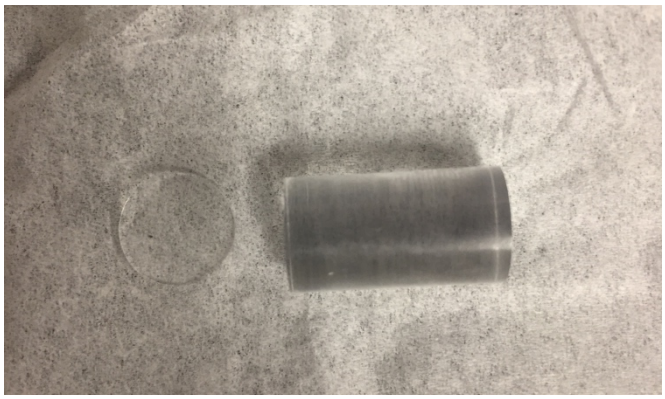

Figure 30. Plastic Scintillator Detectors. (Left) dE detector Eljen EJ-200 1 mm thick with 2.1 ns decay time. (Right) E detector Eljen EJ-204 18 mm thick with 285 ns decay time.

Figure 31. Plastic scintillators optically coupled to PMT. Pictured is a ET Enterprises XP2262 photomultiplier tube with the plastic scintillators shown in Figure 30.

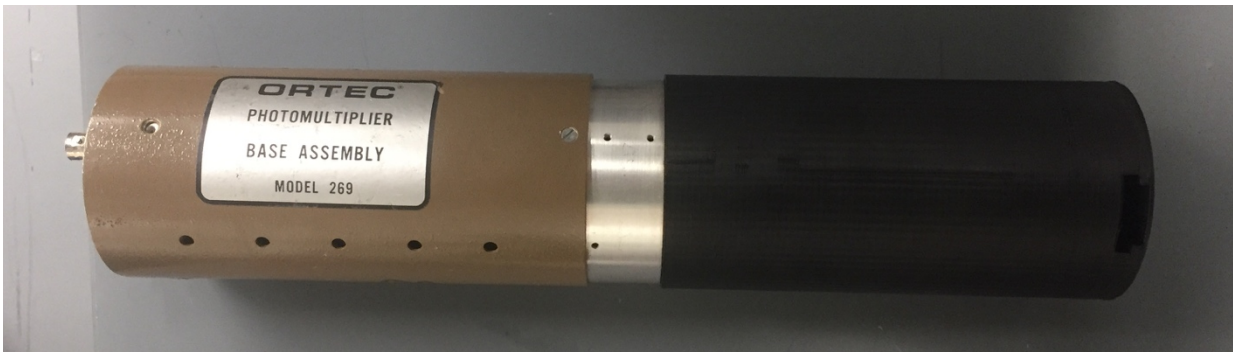

Figure 32. Phoswich detector system. In this picture, the PMT is attached to an ORTEC base and is covered by a 3D printed black light-tight cap.

Figure 33 shows a typical pulse from the phoswich detector system. The first oscilloscope screenshot shows a pulse from a ^{207}Bi monoenergetic beta source through only the dE thin plastic scintillator detector. The second oscilloscope screenshot is a pulse from the same source with only the E thick plastic scintillator detector optically coupled to the PMT. The last screenshot shows a pulse from the same source with both the dE and E plastic scintillator detectors optically coupled to the PMT.

The phoswich detector system is advantageous because only one PMT is used to measure both the dE and E signals. To do this, it requires electronics to separate the pulses. Figure 34 shows the circuit for the phoswich detector system to analyze the pulses from the PMT. This pulse first enters the fanout which splits it between the trigger electronics and the analog dE and E signal circuit.

A constant fraction discriminator (CFD) is the first step of the trigger circuit that makes a logic pulse if the input is above a certain voltage. The gate generator delays the logic pulse to trigger the FemtoDAQ. The FemtoDAQ is a two-channel data acquisition system [25]. The voltage of the gate pulse is then brought down to 3.3 V so it can be input to trigger the FemtoDAQ. The imput pulse is put through another fanout. It takes the linear gate some time to process the signal, so the E detector is delayed 128 ns so that both the dE and E tail are entering the FemtoDAQ at the same time as the trigger pulse. The dE then passes through a linear gate to split it from the E detector.

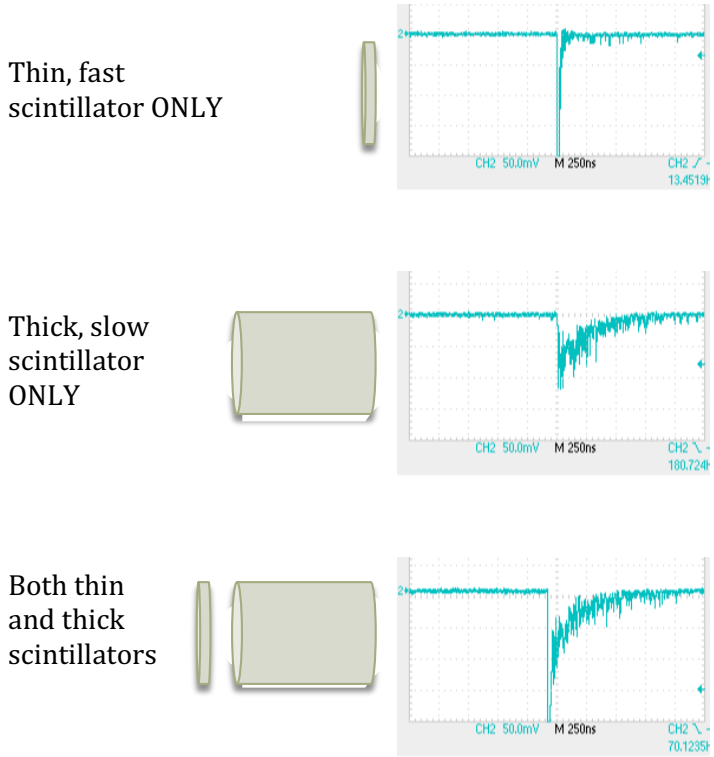

Figure 33. Pulses from a beta decay source into the phoswich detector system. The top pulse is from only the dE plastic scintillator detector, it is quick and intense. The middle pulse shows just the E detector pulse which is long with a tail. The final pulse is the combination of the dE and E detectors that gets split by the electronics to create the dE/E histogram.

3.4.2. dE/E histogram

As beta particles travel through the phoswich plastic scintillator detectors, they deposit a small amount of energy in the dE detector giving a short, intense light pulse. The beta particle deposits the rest of its energy in the E detector giving a longer, less intense light pulse. This light travels through light guides to the photo-multiplier tube and the resulting current pulse to the electronics. As seen in Figure 34, a linear gate circuit separates the short dE pulse from the longer E tail and then a femtoDAQ data acquisition system selects counts that are in the energy range of beta decay particles and plots the counts as a function of time. This should give the decay curve which will be used to measure the cross section.

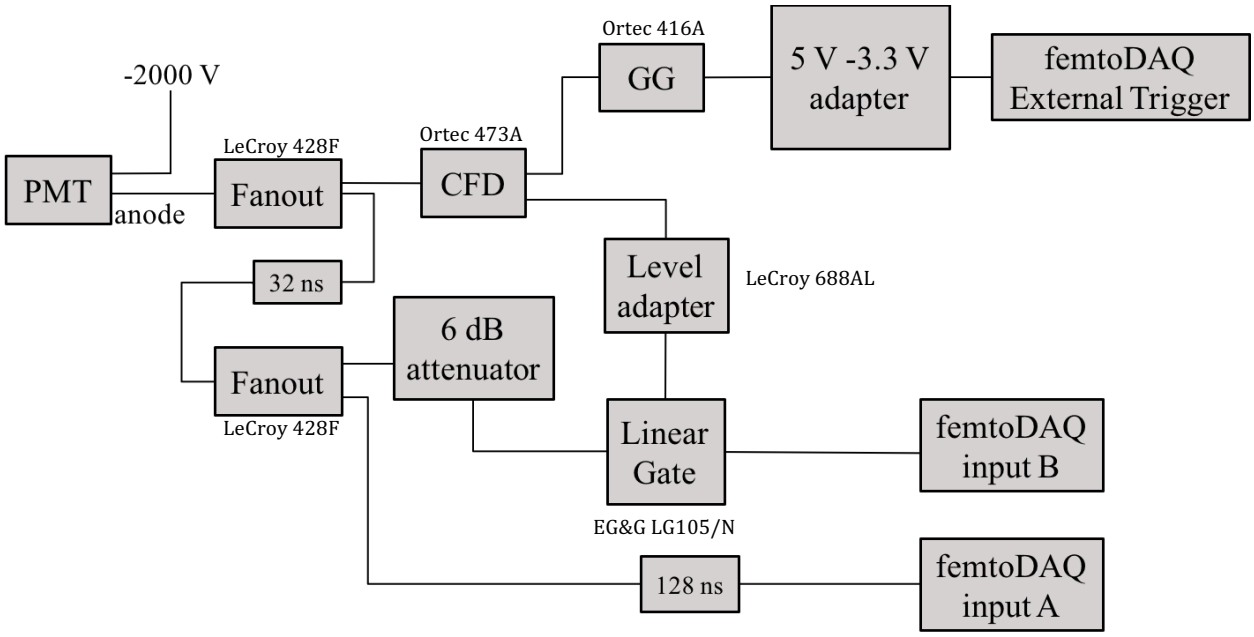

Figure 34. Circuit for separating phoswich detector pulses. The beta particle travels through the scintillator detectors. The pulse then goes through a fanout. This splits the pulse between the trigger circuit and the analog pulse circuits.

Figure 36 shows 2D histograms of the dE and E pulses from a beta source. The vertical axis is counts from the dE detector and the horizontal axis is counts from the E detector. The data shows a signature band for collimated (top) and uncollimated (bottom) monoenergetic 947 keV betas from ^{207}Bi, and background (middle).

3.5. Phoswich Detector Test Experiment at SUNY Geneseo

The phoswich dE-E detector system was also tested using the Tandem Pelletron accelerator at SUNY Geneseo. An approximately 100 nA beam of 2.19 MeV deuterons struck a 0.36 mm thick deuterated polyethylene target which emitted neutrons via the ^{2}H(d,n)^{3}He reaction. These neutrons traveled through a vacuum window and then hit a 19.5 mm by 26 mm by 6.5 mm ^{9}Be target to create ^{6}He nuclei via the ^{9}Be(n,α)^{6}He reaction. As shown in Figure 37, the beam was on for five seconds so the ^{6}He particles could build up in the ^{9}Be. The beam was then quickly blocked by a Faraday cup to measure the ^{6}He beta decay curve. A latch circuit (Appendix D) started the data collection when the count rate from a NaI detector located beside the phoswich detector fell below a fixed value. When the beam was shut off, the latch circuit signaled the femtoDAQ acquisition system to begin collecting data for ten seconds.

This process was repeated 160 times to collect better statistics. The python code for data collection can be found in Appendix A.

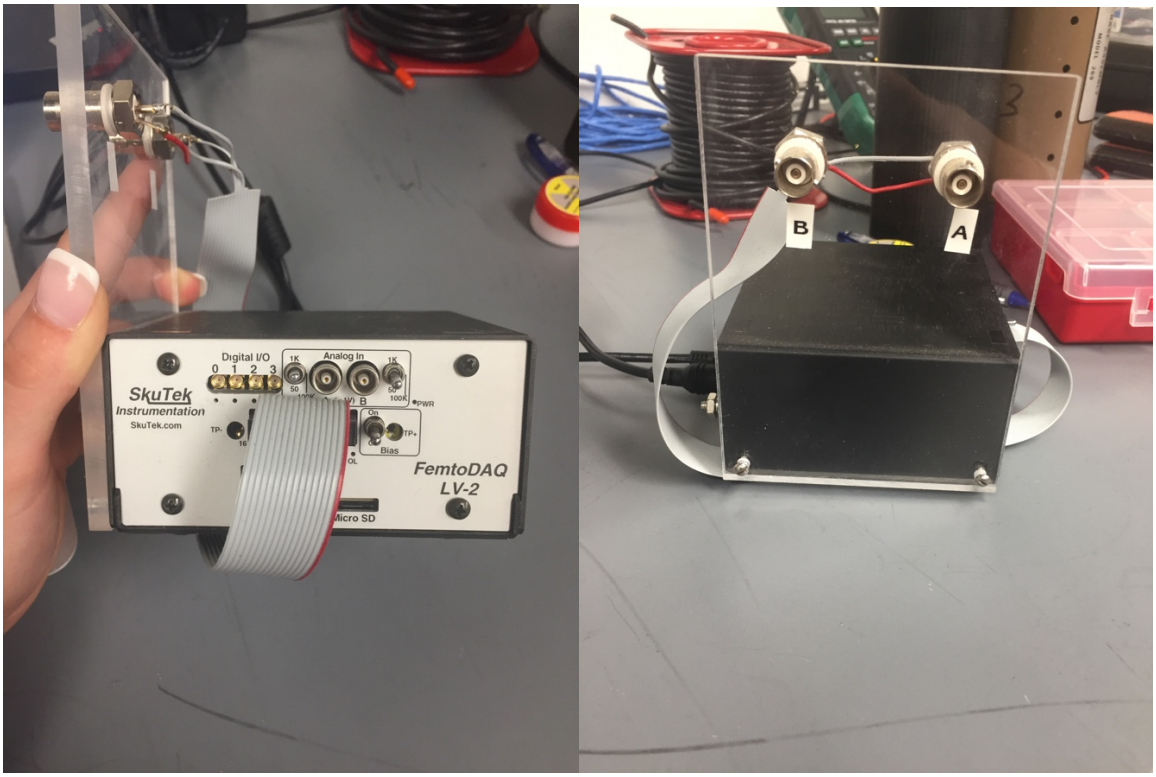

Figure 35. FemtoDAQ data acquisition system. (Left) Front panel for inputs. (Right) BNC ports for the dE and E detector signals.

3.6. Argon Test Experiment

Once the phoswich detector system was working, an experimental design needed to be developed to complete the experiment to measure the cross sections of the considered reactions. The next experiment was done to observe how the gas expands in the chamber and what fraction of the gas can be collected. In the ICF experiment at LLE, the gas will be coming after the shot and formation of the plasma. In this small scale experiment, radioactive gas was pulsed into the vacuum chamber to simulate the rapid release of the gas from the plasma in an ICF shot.

SUNY Geneseo collaborators worked to make the radioactive gas to attach to the vacuum chamber at Houghton College. At SUNY Geneseo, the Tandem Pelletron accelerator was produced a 3.0 MeV, 30 nA deuteron beam [26]. At the end of the target chamber, a Kapton

window allowed the beam to leave and enter the argon gas cell (made of PVC). There was a metal cap with a gas valve that was used to fill the cell with ^{40}Ar.

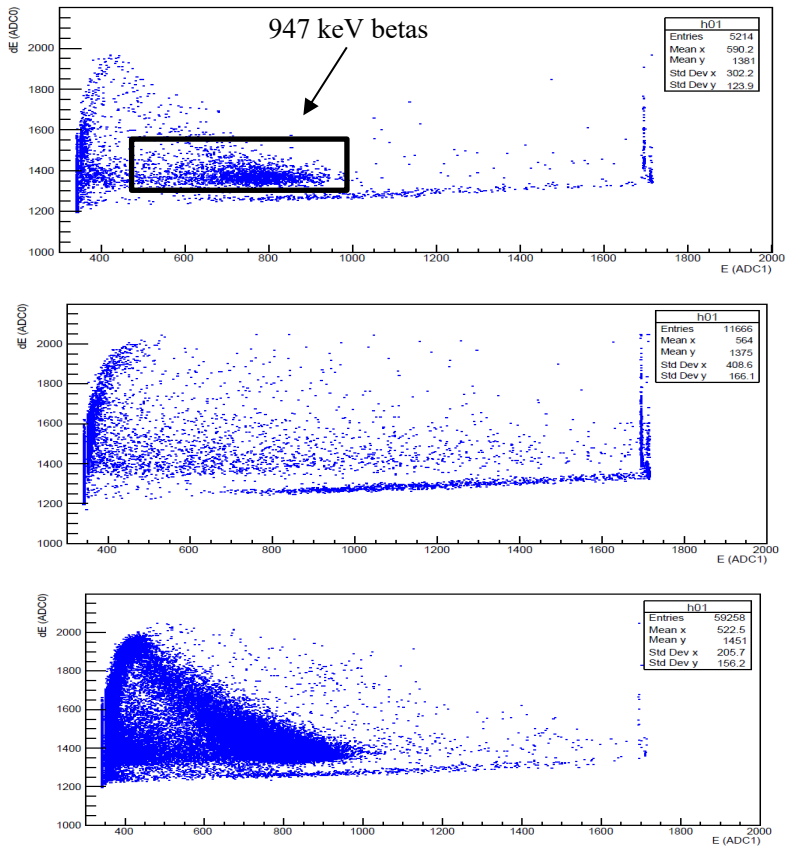

Figure 36. Histogram of the beta counts while testing the phoswich detector. The vertical axis is the pulse height in the dE detector while the horizontal axis is the pulse height in the E detector. The band represents the beta counts while the line of counts at the bottom and up the right-hand side is background. The data is from a monoenergetic ^{207}Bi source which emits 947 keV electrons. The top histogram shows the collimated source, this means that all the electrons are entering the detectors perpendicularly. The middle plot is the background radiation (no source close to the detector system). The bottom histogram shows the uncollimated source. When the source is uncollimated the beta particles can enter the detector at all angles, so the distribution is scattered on the histogram outside of the beta band because when entering the detector at different angles, different amounts of energy are deposited so it is as if it was not a beta particle entering the detector.

The argon gas cell consisted of two PVC valves (red, as seen in Figure 41) and an end-cap pushed against the Kapton window. When filling the cell with ^{40}Ar, both red valves were open, and the end cap was off so it could be flushed out as much as possible. The PVC and gas

line valves were then shut while the first PVC valve remained open. This was done quickly and at roughly the same time, so the cell stayed at a pressure of roughly 1 atm.

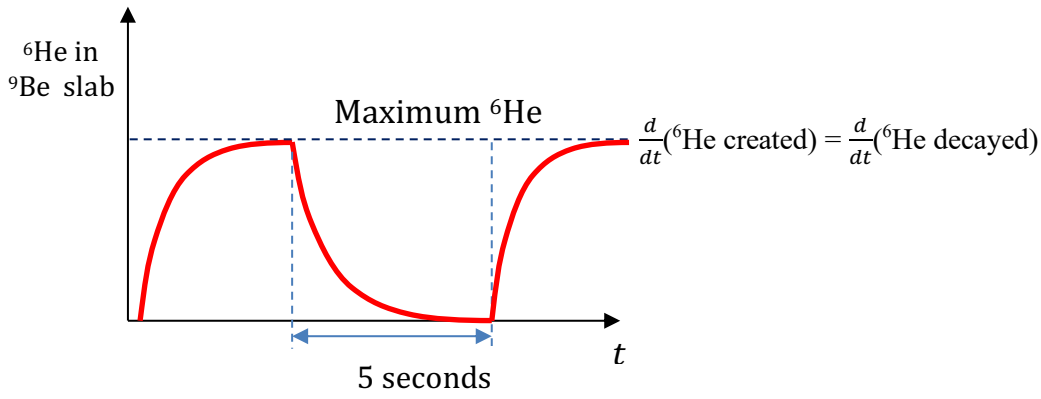

Figure 37. Plot of the method in which the data were collected in testing the phoswich. The vertical axis is the number of ^{6}He nuclei in the ^{9}Be slab. The horizontal axis indicates time. This showing the experimental procedure of turning the beam on and off. The beam was on for 5 s and then off for 10 s to observe the decay of the ^{6}He. The half-life of ^{6}He is 807 ms so in 5 s the maximum number of ^{6}He nuclei should be created. The top dashed horizontal line indicates where the rate that ^{6}He are created is the same as the rate that the ^{6}He are decaying. Thus, at this point, the maximum number of ^{6}He nuclei are in the ^{9}Be slab.

Then the beam was turned on and it entered into the cell initiating the neutron transfer reaction: ^{40}Ar(d,p)^{41}Ar. After running for about an hour, the first PVC valve was closed which effectively trapped a large volume of the gas between the PVC valves. The cell was then detached from the end of the chamber.

Next, the gas cell was inserted in a counting station (Figure 40) with a high purity germanium detector (diameter of 3 in) set up in a lead house to reduce the background. The gamma rays emitted were counted over several half-lives (about 4.5 hours). The 1293 keV gamma rays from ^{41}Ar decays were counted and used to generate the decay curve.

The gas cell was filled again, and bombarded with deuterons, then the gas cell filled with ^{40}Ar and ^{41}Ar was transported from SUNY Geneseo to Houghton College, a trip taking about 45 minutes. The gamma rays were monitored throughout the trip to confirm there was still ^{41}Ar

contained in the gas cell. Since the half-life of ^{41}Ar is 109 minutes, it was expected that there would be enough ^{41}Ar nuclei after the trip to conduct the experiment.

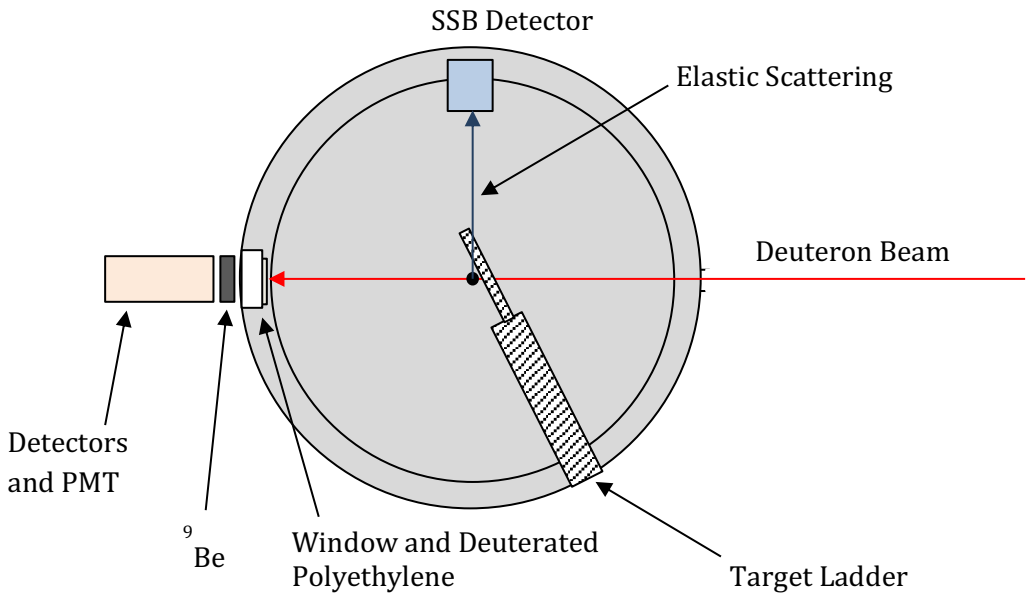

Figure 38. Target chamber at SUNY Geneseo on the Tandem Pelletron to test the phoswich detector. A 100 nA, 2 V deuteron beam hit a sheet of deuterated polyethylene and neutrons produced via the $^{2}H(d,n)^{3}He$ reaction passed through the vacuum window to the ^{9}Be slab. ^{6}He nuclei were then created by the $^{9}Be(n,\alpha)^{6}He$ reaction and were detected by the phoswich detector based on their beta decay into ^{6}Li.

Upon arrival to Houghton College, the gas cell was attached to the vacuum chamber by the fast valve (Figure 25). The first step in the experimental procedure was to shut off the foreline to the trap turbopump. This is so when a pulse of ^{41}Ar gas was released into the chamber, it would not be evacuated out the turbopump through the foreline, instead be trapped. Once the foreline was closed, the transfer line was evacuated, the Ar gas was released into the transfer line. Once Ar gas is in the transfer line, a 1 ms pulse was released into the vacuum chamber.

The collection tube was pushed about 2 cm from the opening of the fast valve and as the gas was released, a fraction went through the collection tube. The other end of the collection tube was attached to the turbopump at the opposite end of the chamber. At this point, the

gas was in the back of the trap turbopump and traveled to the "cross" section where the beta decays and gamma rays could be detected. The betas were detected by an ORTEC LEC 500-3000 2.5 cm diameter, 2 cm thick silicon surface barrier detector placed above the cross and a 7.6 cm diameter, about 15 cm long HPGe detector counted the gamma rays from the ^{41}Ar decay. Data were collected over one half-life of ^{41}Ar (109 minutes). This experiment was the first step to determining if radioactive gas could be trapped and detected using the beta detector system. A top view of the small-scale vacuum system set up for the Argon test experiment can be seen in Section 3.3, Figure 18.

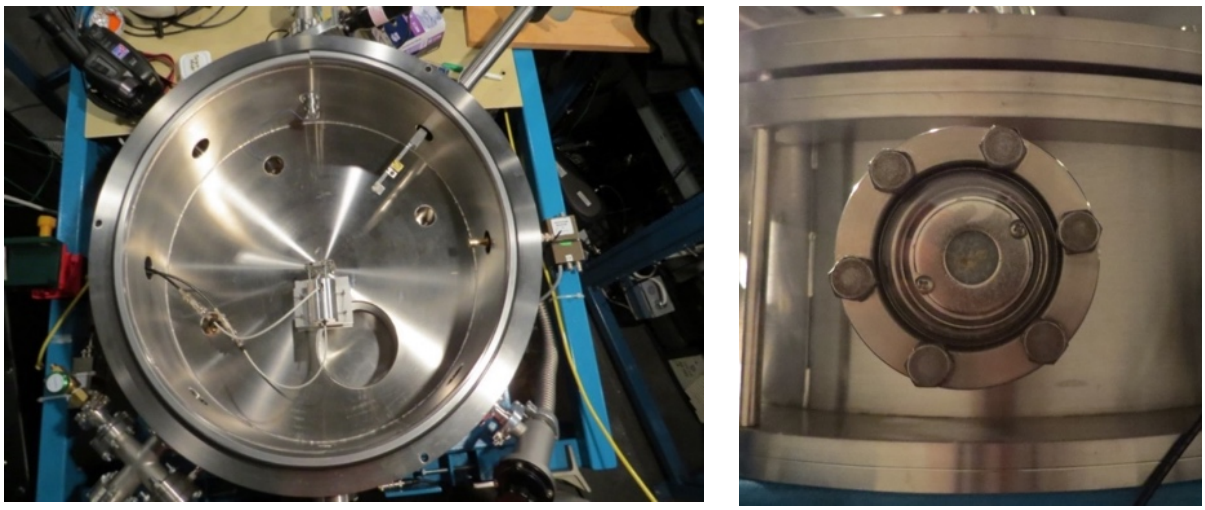

Figure 39. Photographs from the ^{9}Be experiment at SUNY Geneseo. (Left) The top view of the target chamber with the detector placed behind the chamber center (from the test experiment that shows ^{6}He can be created and detected). In this experiment, the detector was placed just outside the chamber against the window in the right photograph. This shows the deuterated polyethylene sheet inside the vacuum window.

3.7. Conclusion

The small-scale test apparatus has been assembled at Houghton College to determine which measurement method is most feasible. The goal of the series of experiments is to understand the behavior of the gas and the trapping system, in particular, to determine what fraction of the neutral radioactive gas can be collected with the trap turbopump system. There are still many more questions to ask in order to discern which method will result in the highest yield.

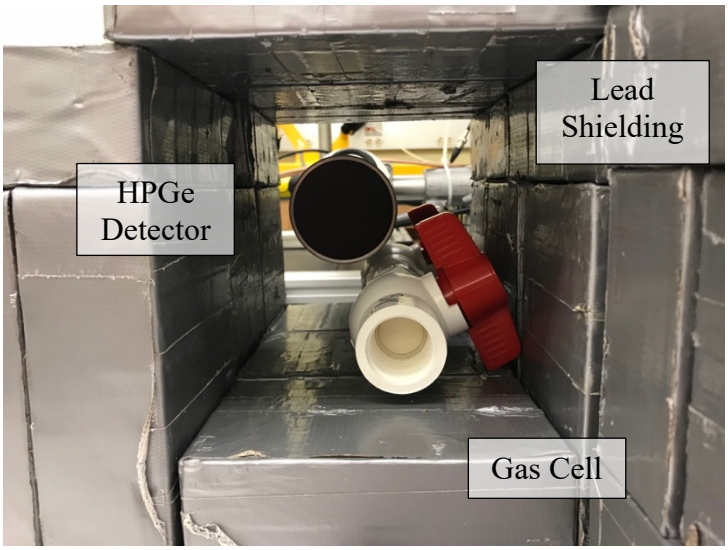

Figure 40. Counting station to measure the ^{41}Ar after production at SUNY Geneseo. The HPGe detector counted the gamma rays produced by the decay of ^{41}Ar. The lead brick house reduced background counts.

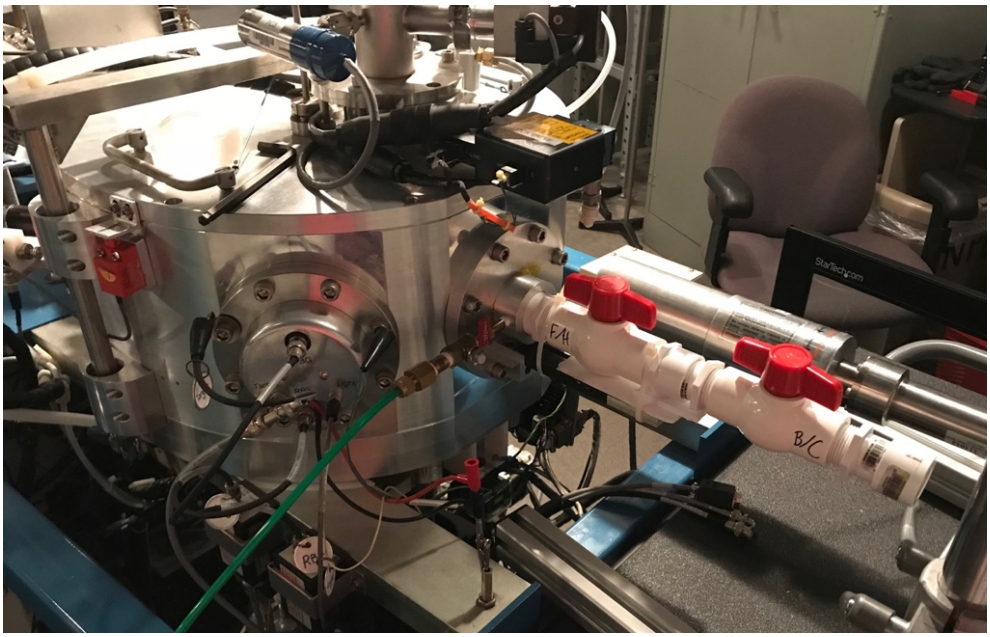

Figure 41. Tandem Pelletron setup at SUNY Geneseo. ^{41}Ar gas was created and trapped in the gas cell for transport to Houghton College. The gas cell was aligned with Kapton window at SUNY Geneseo's Tandem Pelletron Accelerator end chamber.

Chapter 4

RESULTS AND ANALYSIS

4.1. Introduction

The two main experiments described in Chapter 3 were the $^{9}Be(n,\alpha)^{6}He$ to test the phoswich detector and the $^{40}Ar(d,p)^{41}Ar$ experiment to test the trap turbopump system. These have been the first preliminary experiments for the feasibility study. The results suggest that the phoswich detector system can be used to detect these short-half-life beta decay products, and that radioactive gas can be trapped, and the decays can be detected by a silicon surface barrier detector and high-purity Germanium (HPGe) detector.

4.2. $^{9}Be(n,\alpha)^{6}He$ Experiment Results

The purpose of this experiment, and the apparatus for which is described in Section 3.5, was to demonstrate the creation and detection of ^{6}He. This was done using the Tandem Pelletron accelerator at SUNY Geneseo. This accelerator produced a 3.0 MeV and 100 nA deuteron beam that hit a deuterated polyethylene target, generating neutrons by the $^{2}H(d,n)^{3}He$ reaction. The neutrons were then incident on the ^{9}Be slab and via the $^{9}Be(n,\alpha)^{6}He$ reaction, ^{6}He was produced and then detected using the dE/E phoswich detector system method.

4.2.1. dE/E Histograms and Decay Curve

Figure 42 shows a dE/E histogram of the beta-decay events for 160 cycles. The vertical axis is the energy deposited in the dE detector and the horizontal axis is the rest of the beta energy deposited in the E detector. This plot allows the beta particles to be identified by the expected dE/E band as indicated by the red points. These points indicate the projected electron range as a function of energy for collimated electrons perpendicular to the detector. For example, an electron with 1.2 MeV energy is expected to be located on that specific red circle. Because they do not all strike the detector perpendicular to the surface, all of the events within the green boundary were counted as beta particles and used to measure the

half-life of ^{6}He. The counts outside the green box are excluded from the final number of counts in the decay curve of the ^{6}He.

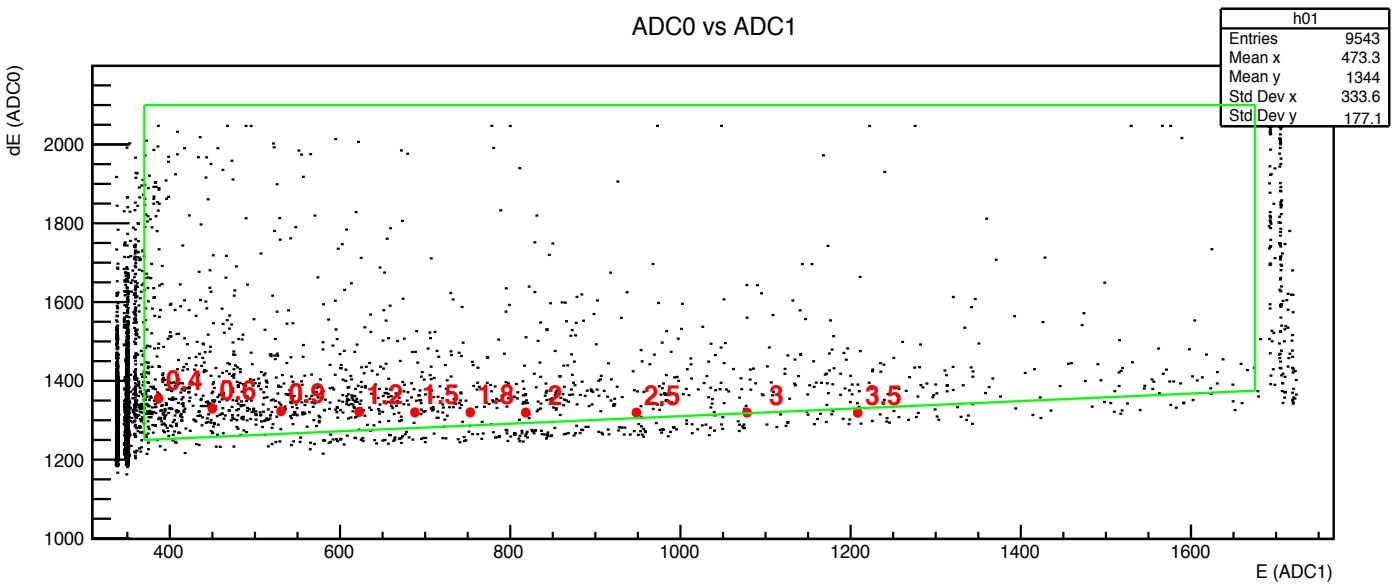

Figure 42. dE/E histogram from ^{9}Be(n,α)^{6}He experiment. The vertical axis is the energy deposited in the dE detector as a function of the horizontal axis displaying the energy deposited in the E detector. The red points show the projected electron range as a function of energy. The green box indicates the identified beta events from the decay of ^{6}He. The counts inside the green box were used to generate the decay curve of the ^{6}He.

Figure 43 shows the decay curve of the ^{6}He produced in the ^{9}Be(n,α)^{6}He experiment. The plot is the beta decay count rate as a function of time. The best-fit decay curve, indicated by the red line, measured the half-life of ^{6}He to be 789.2 ± 37.8 ms. This result is in agreement with the previously measured 807 ms half-life of ^{6}He [27]. This suggests that ^{6}He was created and detected by the phoswich detector system. The data was analyzed, and the plot was generated using the C code found in Appendix A.

4.2.2. Analysis and Conclusion of ^{9}Be(n,α)^{6}He Experiment Results

This experiment demonstrated that the phoswich detector system is capable of measuring the beta decay of ^{6}He, which was created through the ^{9}Be(n,α)^{6}He reaction. The next step is to build and test a 4π phoswich detector system that can be used with the trap turbopump.

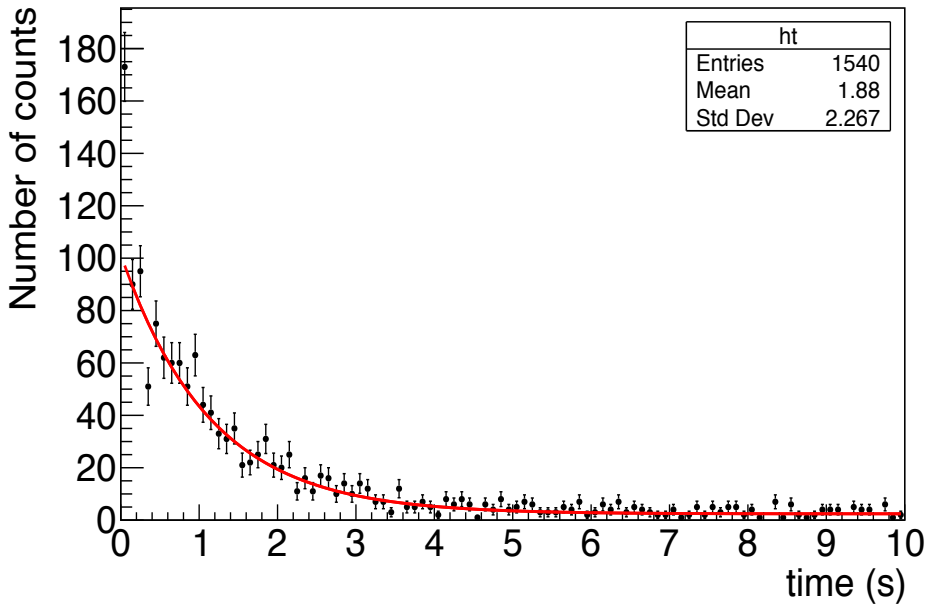

Figure 43. Decay curve of ^{6}He produced in the ^{9}Be(n,α)^{6}He experiment. The half-life was measured to be 789.2 ± 37.8 ms. This demonstrates that ^{6}He can be created and detected with the phoswich detector system.

4.3. ^{40}Ar(d,p)^{41}Ar Experiment Results

The next experiment was to test the "collection tube" method. The ultimate goal is to determine the fraction of the neutral radioactive gas that is collected following its release from the fast valve. First as described in Section 3.6, ^{41}Ar was created at SUNY Geneseo using the Tandem Pelletron Accelerator. The gas cell containing the neutral radioactive gas was transported and attached to the Houghton College vacuum system. The fast valve let in a pulse of the gas, which was trapped by the turbopump and counted by the detector system.

4.3.1. ^{41}Ar Production at SUNY Geneseo

Figure 44 below shows the energy spectrum of ^{41}Ar gamma rays that were counted by the HPGe detector. The large peak represents the excited ^{41}K promptly emitting a 1.293 MeV gamma ray. The small peak at 511 keV is ^{13}N positron decay from the positron annihilation of the ^{12}C(d,n)^{13}N reaction occurring in the background.

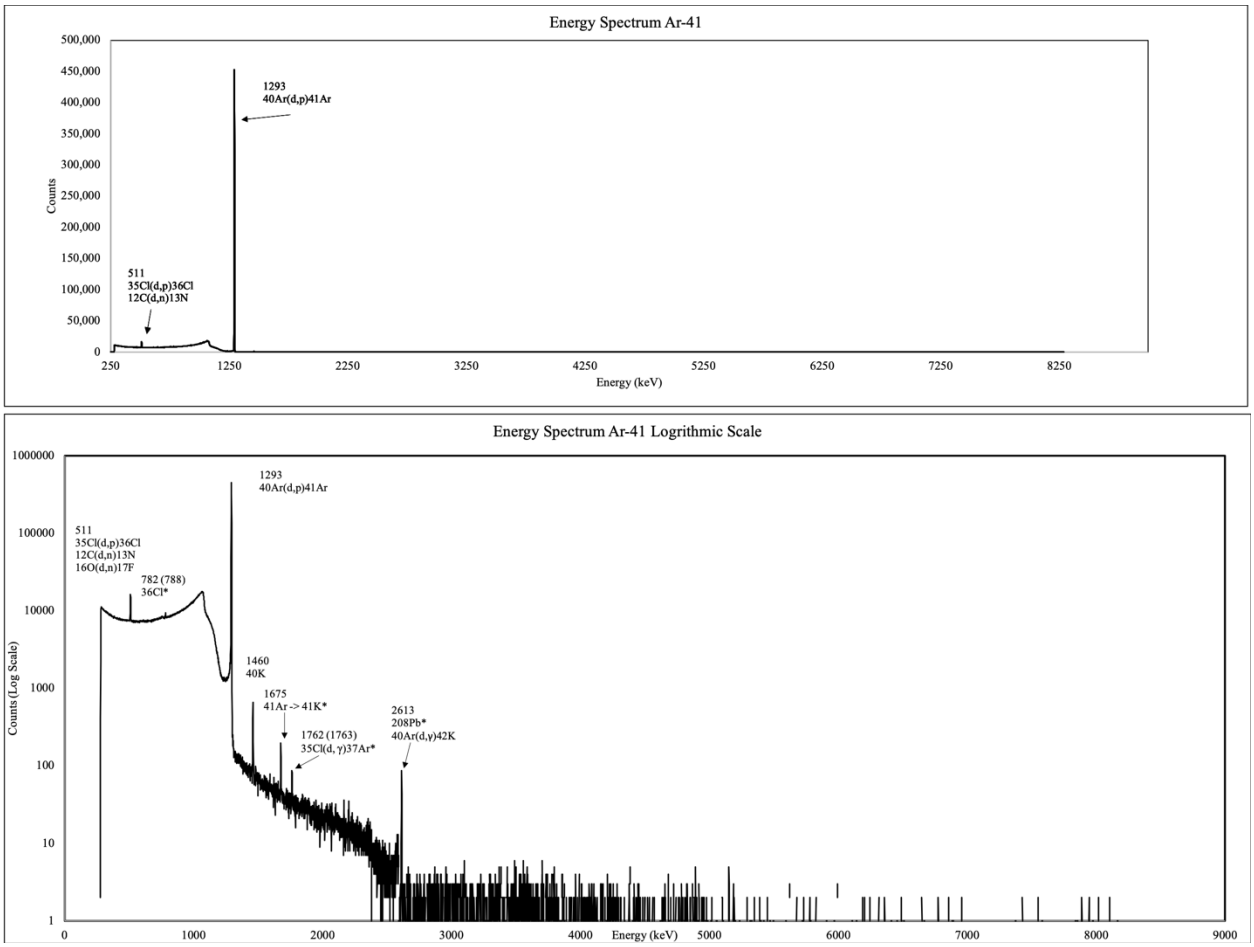

Figure 44. ^{41}Ar gamma ray energy spectrum. These plots were generated from the decay of ^{41}Ar as detected by the HPGe detector over 4.5 hours.

4.3.2. Growth Curves and Background-Subtracted Gamma Ray Spectrum

The HPGe detector and a silicon surface barrier detector counted the beta decay and gamma ray emission of the ^{41}Ar, and the following plots and measurements were made. For gamma rays, the number of counts added to the 1.293 MeV peak per second was plotted. Figure 45 and Figure 46 show the growth curve fits of ^{41}Kr as ^{41}Ar decays by beta and gamma emission. The trapped ^{41}Ar gas was counted for one half-life of about 109 minutes. The HPGe detector measured a half-life of 119 ± 12 minutes and the silicon surface barrier detector measured a half-life of 110 ± 7 minutes. These results agree with the previously measured half-life of ^{41}Ar [27].

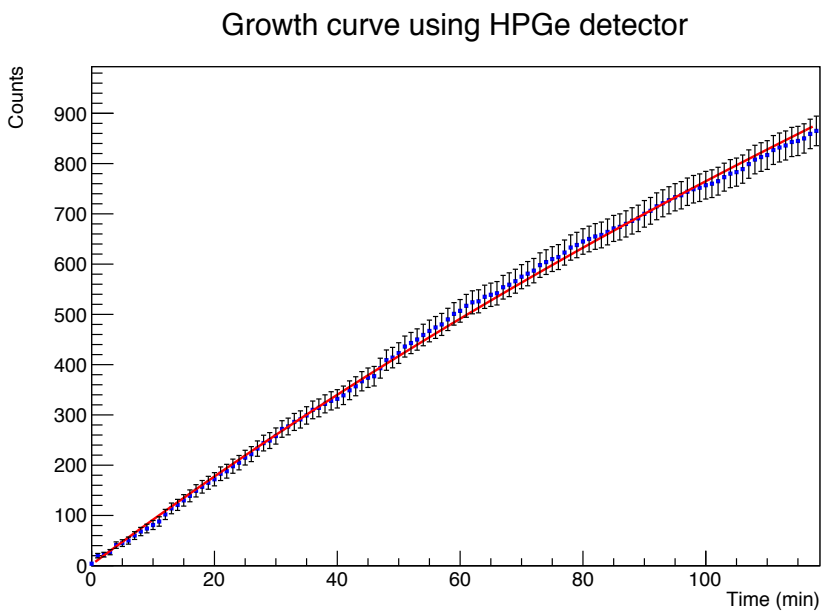

Figure 45. Growth curve of ^{41}K during the ^{41}Ar experiment using data from the HPGe detector.

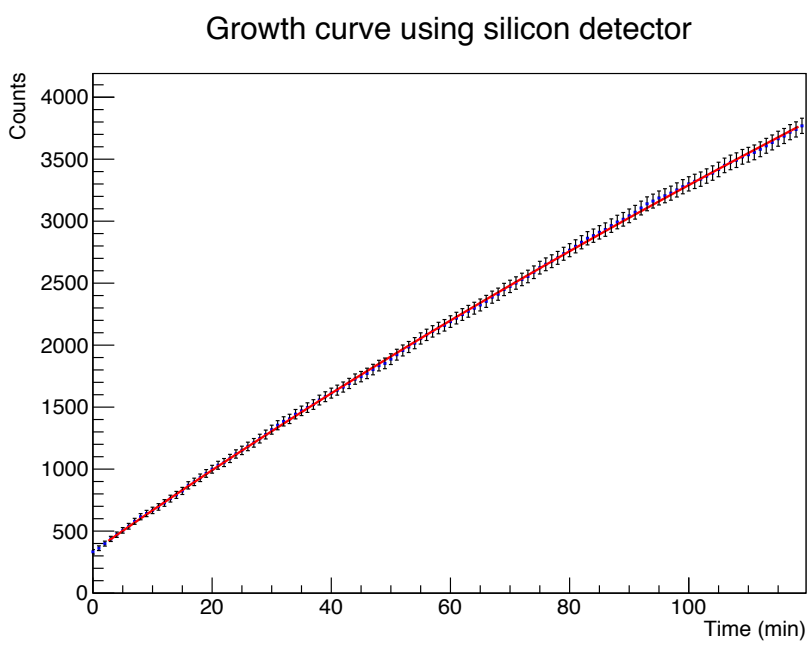

Figure 46. Growth curve of ^{41}K during the ^{41}Ar experiment using data from the silicon surface barrier detector.

4.3.3. Analysis and Conclusion of ^{41}Ar(d,p)^{41}Ar Experiment Results

While this experiment did not allow the fraction of the gas collected and detected by the trap turbopump and detection system to be determined, it did show that ^{41}Ar travelled through the vacuum chamber, was trapped, and could be detected. In future experiments,

determining the fraction of the gas collected will be crucial for analyzing the results of any low-energy nuclear cross section measurements at LLE using ICF.

4.4. Pressure Front Across Chamber Experiment

The goal of this experiment was to measure the pressure front as it moved across the chamber. A 1 ms pulse of air was released into the chamber by the fast valve and three of the fast mini ion gauges described in Section 3.3.2 were attached to feedthroughs in the chamber lid to study the behavior of the gas inside the vacuum chamber. Figure 47 shows the new lid with five ports to insert ion gauges.

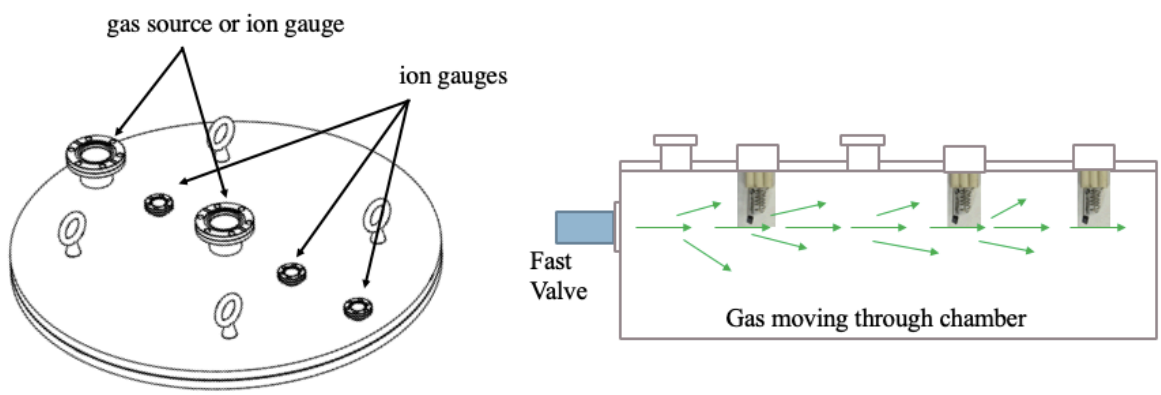

Figure 47. Testing pressure front across the vacuum chamber. (Left) The new lid for the target chamber. It has five ports to insert either gas sources (for future experiments) or ion gauges. (Right) Cartoon diagram of the pressure front experiment. Fast valve lets in air (or other gas) which travels across the chamber, triggering the fast mini ion gauges.

The results of the pressure front experiment are shown in Figure 48. The green signal indicates the TTL pulse that opened the fast valve. The yellow signal is from the first ion gauge, blue is the second and purple is an ion gauge off to the right, away from the direct path of the valve orifice. The rise time for the ion gauges (about 500 μs) is about five times longer than expected, possibly due to the large resistor necessary to obtain a clean signal from the collector of the ion gauge (see section 3.3.2 and Figure 21). The time delay seems reasonable, but the rise time is still too long to analyze the results.

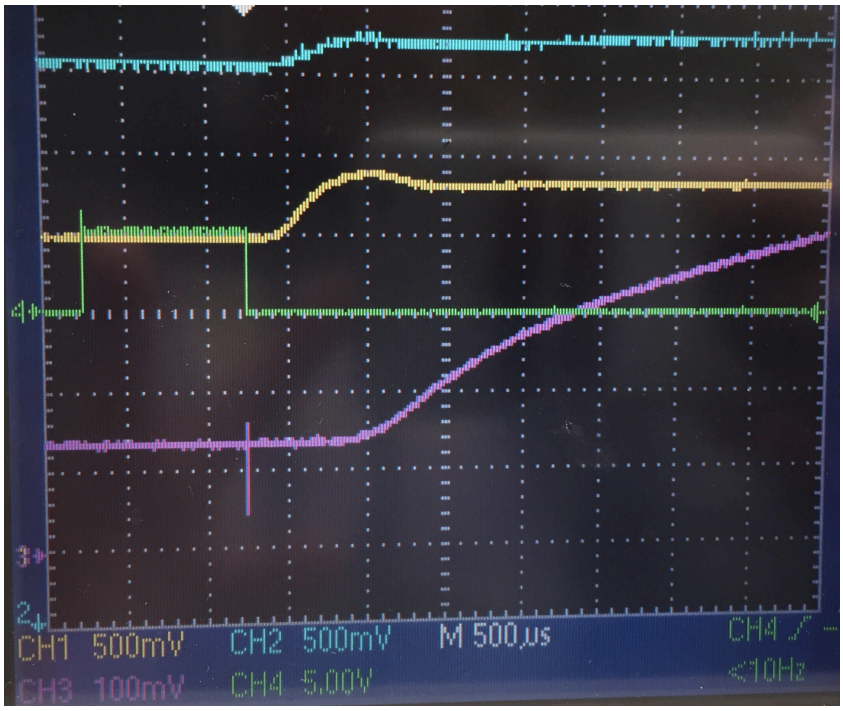

Figure 48. Results from pressure front experiment. The green signal indicates the TTL pulse that opens the fast valve. The yellow signal is from the first ion gauge, blue is the second and purple is an ion gauge off to the right of the direct path of the valve opening. The rise time for the ion gauges is longer than expected due to a large resistor necessary to limit the noisiness of the signal from the collector of the ion gauge.

Chapter 5

CONCLUSION AND FUTURE PLANS

5.1. Summary

The goal of this research is to use inertial confinement fusion as a tool to study fundamental nuclear physics. In particular, the cross sections of low-energy nuclear reactions with sub-second half-life reaction products could be measured by collecting the neutral reaction products in the expanding gas after the ICF shot and plasma formation. Prior to attempting the measurement using ICF at LLE, a series of preliminary experiments are being undertaken to show that these cross sections are capable of being measured. A small-scale feasibility study at Houghton College is being used to determine the practicality of the trap turbopump and detection system.

5.2. Summary of Preliminary Experiments

The ^{9}Be(n,α)^{6}He experiment was done at SUNY Geneseo using the Tandem Pelletron Accelerator. A 3 MeV, 100 nA deuteron beam hit a deuterated polyethylene target creating neutrons via the ^{2}H(d,n)^{3}He reaction. These neutrons then hit a ^{9}Be slab and ^{6}He was created via the ^{9}Be(n,α)^{6}He reaction. A phoswich detector system counted the beta particles from the decay of ^{6}He into ^{6}Li to confirm that the reaction took place. In conclusion, this experiment showed that ^{6}He can be created and detected using the phoswich detector system. The result was a 789.2 $\pm$ 37.8 ms half-life of ^{6}He which is in agreement with the previously measured value.

The ^{40}Ar(d,p) ^{41}Ar experiment started at SUNY Geneseo's Tandem Pelletron Accelerator. A gas cell filled with ^{40}Ar was placed against a Kapton window at the end chamber. The deuteron beam passed through the Kapton window, deuterons interacted with the ^{40}Ar creating ^{41}Ar via the ^{40}Ar(d,p)^{41}Ar reaction. Then the gas cell full of a mixture of ^{40}Ar and ^{41}Ar was transported to the small scale setup at Houghton College. The gas cell was attached to the fast valve, a short pulse of ^{41}Ar gas was released into the chamber, trapped in the back of

the turbopump and detected using a silicon surface barrier detector and a HPGe detector (to count betas and gammas, respectively). This experiment showed that the trap turbopump and detector system are capable of collecting the neutral radioactive gas and detecting the decaying nuclei. However, the fraction of the gas collected is still unknown.

Figure 49 shows a new 4π phoswich detector design. This detector is currently being constructed. The 4π phoswich detector system will maximize the number of beta particles that could be counted in the foreline trap of the turbopump. This will be tested on the small scale setup at Houghton College with the same experimental procedure as the ^{41}Ar experiment. The new detector will be in place of the silicon surface barrier detector and should greatly increase the count rate for this test experiment.

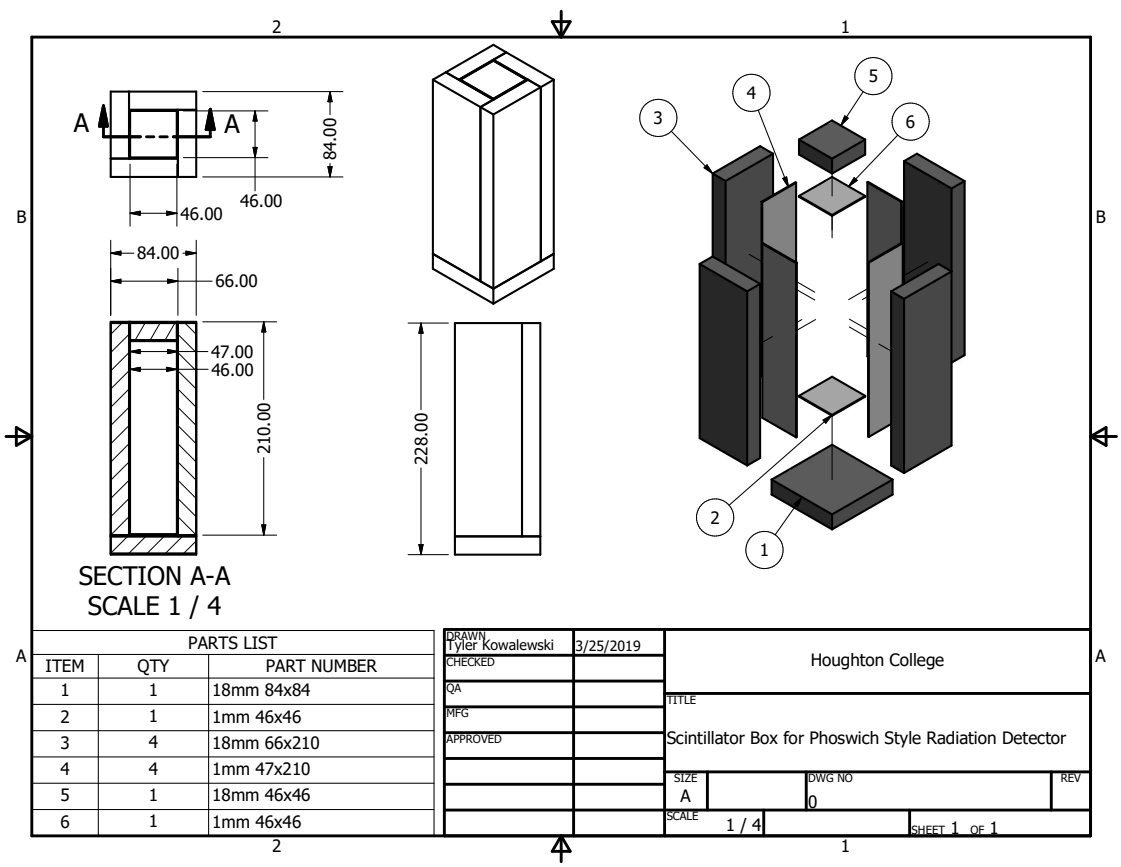

Figure 49. The 4π phoswich detector system. This model will be under construction during summer 2019 and will be used to maximize the number of beta particles are counted during the experiment.

5.3. Future Experiments

Many other preliminary experiments can be conducted using the small-scale set up at Houghton College. These experiments will use either the laser or the fast valve to simulate the rapid release of neutral radioactive gas into the ICF target chamber, where either a turbopump or getter will collect the gas, the ion gauges will monitor the pressure and for some experiments, the detector system will count the decays. The most important reaction products to understand are ^{6}He, ^{8}Li, ^{12}B since these result from the reactions with the highest predicted yield.

Figure 50 shows an idea for a future test involving vaporizing a radioactive source with a laser. In this experiment, a substrate would have a film of radioactive material on it. For example, it could be a graphite substrate with a film of ^{137}Ba from a ^{137}Cs radioisotope generator. A method to create this substrate inside the evacuated chamber or transfer from outside the chamber to the inside is being developed. Assume the substrate covered in ^{137m}Ba is in the center of the target chamber as shown below. The 6 W laser will be pushed up against the vacuum chamber and is incident on the substrate through a viewport. When the laser comes in contact with the substrate, it will begin releasing radioactive gas at different angles. The gas will expand around the chamber. Fast mini ion gauges will monitor the pressure in the chamber on a hundred microsecond scale to confirm that gas has been released from the substrate and hopefully show how the gas moves in the chamber. This gas will then be trapped in the turbopump and "cross" using the same procedure as the ^{41}Ar experiment. ^{137m}Ba decays by gamma emission with a half-life of about 153 s. The emitted gamma rays would be detected using a NaI detector. This experiment can be done using the collection tube approach or the collect it all approach. This method of trapping neutral radioactive gas will be another step closer towards the behavior of the gas after an ICF shot because the laser will be releasing the reaction products.

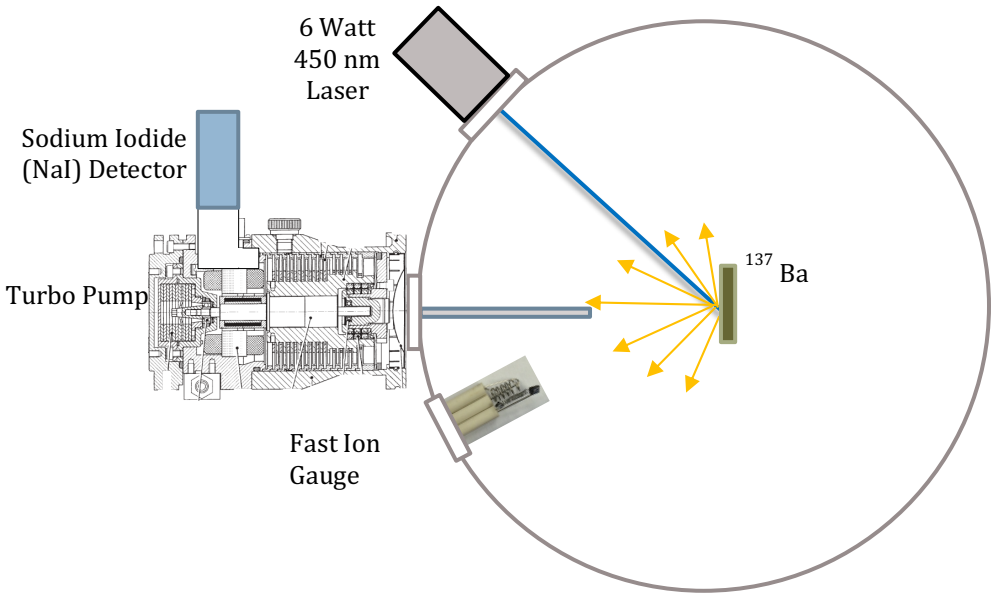

Figure 50. Preliminary laser test with a substrate. A film of ^{137m}Ba created using a ^{137}Cs radioisotope generator will be placed on a substrate at the center of the target chamber. The 6 W laser will be on the substrate through a viewport from outside the chamber. When the laser comes in contact with the substrate, radioactive gas will fly off the substrate at different angles. The gas will then expand and bounce around the chamber. Fast mini ion gauges will be placed in the new lid and around the chamber to monitor the pressure to confirm that gas has been released and hopefully show how the gas moves in the chamber. This gas will then be trapped in the turbopump and "cross" using the same procedure as the ^{41}Ar experiment and the emitted gamma rays from the ^{137}Ba decay would be counted using a NaI detector.

Figure 51 shows another possible experiment in the small scale feasibility study to determine what fraction of radioactive gas can be trapped and detected. This experiment also utilizes the laser and would be more closely related to the behavior of the gas in the ICF target chamber at LLE. This proposed preliminary experiment starts with a microballoon or target capsule, preferably a target that has been rejected for use in an ICF shot at LLE. The chamber would be full of some type of gas (most likely He) while the microballoon or target capsule are suspended in the center. The gas will permeate the walls of the microballoon or capsule creating a target filled with radioactive gas. The laser will again be placed outside the target chamber and will be incident on the target capsule in the center of the target chamber. The laser would vaporize the microballoon/target capsule filled with radioactive gas. Hopefully, the gas will expand isotropically in the chamber. This could be observed and

measured using fast mini ion gauges placed around the chamber in the new lid. This gas can also be trapped using the collection tube or collect it all method and a detector system can be used to identify the gas that was released. This would be the closest to an ICF shot behavior in a small scale experiment that could be done at Houghton College. This type of experiment would indicate how the gas behaves when a target is hit with one laser. Multiple lasers could also be used. A complication with this experiment is determining a good method for inserting the microballoon/target capsule into the target chamber center. Measuring the fraction of the gas/nuclei collected could also be difficult. An approach to determine the amount of gas permeating the walls of the microballoon/target capsule would need to be considered to know the fraction collected.

5.4. Conclusion

This goal of this research is to use ICF as a tool to study fundamental nuclear science. An application of interest for nuclear physics is currently nucleosynthesis models. Measuring the cross sections of low-energy nuclear fusion reactions with sub-second half-life reaction products has never been done before and can have implications for nuclear astrophysics. Specifically, the $^{3}H(t,\gamma)^{6}He$ radiative capture reaction has never been measured before.

A detector system has been built to measure the beta particles from the sub-second half-life reaction products that are produced during the ICF implosion. The reaction products do not have enough energy to escape the plasma so a trapping mechanism must be developed to measure the nuclei. Currently, a small scale feasibility study is being carried out at Houghton College to answer questions about the ICF experiment at LLE.

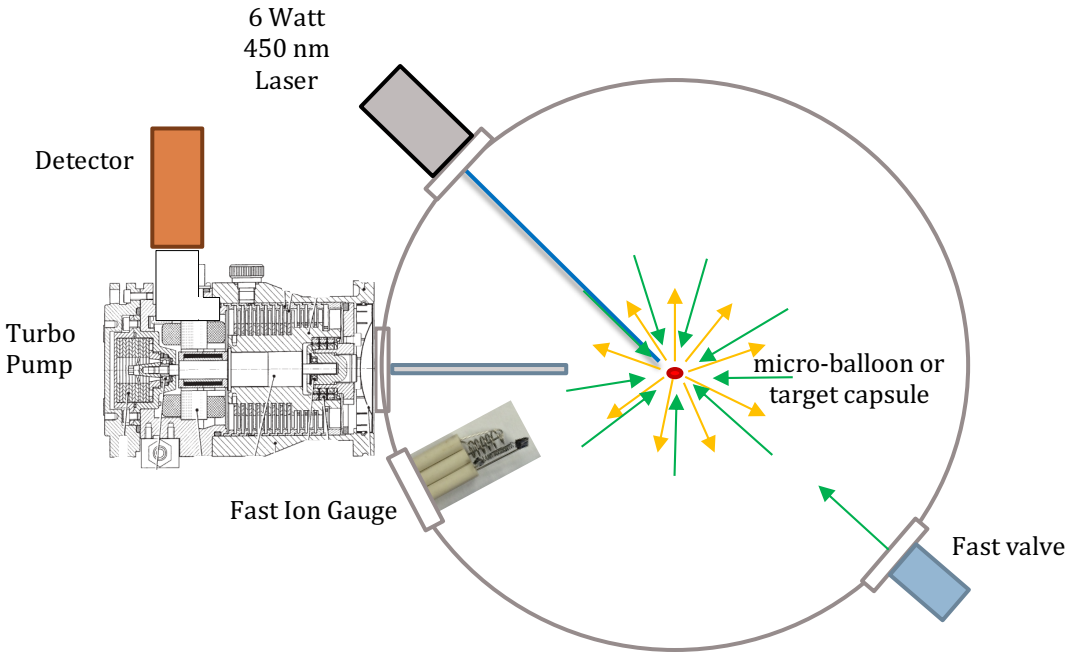

Figure 51. Future experiment: isotropic release of radioactive gas. This figure shows the set up for microballoon/target capsule experiment where a laser is incident on a microballoon/target capsule filled with some type of gas and vaporized. The gas will hopefully expand isotropically. This can be observed via fast mini ion gauges.

Appendix A

FEMTODAQ COMPUTER CODE

Python code used to collect data at SUNY Geneseo 08-01-2017

```
#!/usr/bin/python

# energy_ex.py
# (c) 2016 SkuTek Instrumentation
# Author: D. Hunter
#
# versions:
#       0.1         09/22/16  - initial version based on
histogram_ex.py
#       1.0         10/11/16  DH        - corrected usage
because ARMED is not active high
#       1.1         10/25/16  DH        - updated logic for
status read
#
# Capture energy data from the FemtoDAQ on inputs 0 and 1
# Create a CSV compatible text file with the data
#

import sys,time, datetime
from timeit import default_timer as timer
from FemtoLib import *                          # import
the Digitizer class
import Adafruit_BBIO.GPIO as GPIO

# from DAQfile import DataFile                  # import
the DataFile class

### GPIO parameters
GPIO_B = "GPIO1_29"  # input channel B

### parameters for data capture
OFFSET0 = 90        #offset %
OFFSET1 = -90    #offest %

SIG_POL0 = INVERT   # ADC polarity
SIG_POL1 = NONINV   # ADC polarity
TRIG_POL = RISING   # Trigger polarity

BLR0 = ENABLE                 # baseline restore
BLN_BLOCK0 = 350              # [samples] baseline blocking
period
BLR1 = ENABLE                 # baseline restore
BLN_BLOCK1 = 350              # [samples] baseline blocking
period

PULSE_WIN = 350               # [samples] pulse height
window
SIG_AVG0 = 4                  # [samples] signal averaging
time (QDC length)
SIG_AVG1 = 4                  # [samples] signal averaging
time (QDC length)
PT_DELAY = 0                  # [samples] post trigger
delay


# main routine
if __name__ == '__main__':
        if len(sys.argv) < 5: # need run number and timeout
parameter
          print 'Usage: decay_exp.py run_num t repeats'
          print ' start_run = starting run number'
          print ' num_run = number of runs'
          print ' t = time out value (milliseconds) [1-
65535]'
          print ' repeats = number of times to repeat time
out value for a given run \n'
          print 'Digital I/O:'
          print '  0 = (IN)  External Trigger'
          print '  1 = (IN)  Veto'
          print '  2 = (OUT) Armed'
          print '  3 = (OUT) Logging Busy'
          sys.exit()


        # convert run number and catch any errors
        try:
          start_run  = int(sys.argv[1])
        except:
          print 'Invalid starting run number'
          sys.exit()

        if (start_run < 0):
          print 'Invalid starting run number (must be >=
0)'
          sys.exit()


        # convert number of runs and catch any errors
        try:
          num_run  = int(sys.argv[2])
        except:
          print 'Invalid number of runs'
          sys.exit()

        if (num_run < 1):
          print 'Invalid number of runs (must be > 0)'
          sys.exit()

        # convert timeout and catch any errors
        try:
          TimeOut  = int(sys.argv[3])
        except:
          print 'Invalid timeout value (must be 1-65535)'
          sys.exit()

        if (TimeOut <= 0):
          print 'Invalid timeout value (must be 1-65535)'
          sys.exit()

        try:
          repeats  = int(sys.argv[4])
        except:
          print 'Invalid run number'
          sys.exit()

        if (repeats < 1):
          print 'Invalid run number (must be at least 1)'
          sys.exit()

        ##########################
        #  SET UP THE FEMTODAQ
        ##########################

        digi = Digitizer()     # create a digitizer object
        digi.WaitForReady()    # wait for it to be ready

        # read the firmware
        fwStr = digi.GetFirmwareString()

        # read the ADCtype from the digitizer
        ADCtype = digi.IdentifyADC()
        digi.InitADC()                  # normal mode

        # turn off data and pulse test mode in case they
were on before
        digi.DisableDataTest()
        digi.DisableInternalPulseGenerator()

        digi.SetChannelSignalPolarity(0,SIG_POL0)
        digi.SetChannelSignalPolarity(1,SIG_POL1)

        digi.SetChannelOffsetVoltage(0,OFFSET0)
        digi.SetChannelOffsetVoltage(0,OFFSET1)

        if BLR0:
          digi.EnableChannelBaselineRestore(0)
        else:
          digi.DisableChannelBaselineRestore(0)

        if BLR1:
          digi.EnableChannelBaselineRestore(1)
        else:
          digi.DisableChannelBaselineRestore(1)

        digi.SetChannelBaselineBlocking(0,BLN_BLOCK0)
        digi.SetChannelBaselineBlocking(1,BLN_BLOCK1)
```

```
        # set the signal averaging time for each channel
        digi.SetChannelSignalAveragingTime(0,SIG_AVG0)
        digi.SetChannelSignalAveragingTime(1,SIG_AVG1)

        # set the post trigger delay
        digi.SetPostTriggerDelay(PT_DELAY)

        # set the pulse energy window
        digi.SetPulseEnergyWindow(PULSE_WIN)

        digi.EnableExternalTrigger()

        digi.SetEnergyLogTimeout(TimeOut)
        digi.EnableEnergyLogging()

        digi.Initialize(False)# Initialize w/o ADC init


        GPIO.setup(GPIO_B,GPIO.IN)  #set GPIO B to be an
input to read in faraday cup

        ####################################
        #Loop through runs
        ####################################

        for run in range(start_run, start_run+num_run):

          ## first make sure that faraday cup is out for 5
seconds

          print 'Please remove Faraday cup.\n'
          count_beam_on = 0
          #start = timer()
          while (count_beam_on < 1000):
                    if (GPIO.input(GPIO_B)==True) :
                              count_beam_on = count_beam_on
+ 1
                              #print count_beam_on
                    else:
                              count_beam_on = 0

          #end = timer()
          #print 'time (ms) = %10.5f\n' % ((end-
start)*1000)

          print 'BEAM ON for 5 seconds.\n'
          time.sleep(6)
          print 'Please insert the Faraday cup.\n'

          GPIO.wait_for_edge(GPIO_B, GPIO.FALLING)

          # open output file
          outputfilename =
'run_'+str(run).rjust(4,'0')+'.dat'
          f = open(outputfilename, 'w')

          print >>f, '6He Decay Experiment Acquisition'
          print>>f, 'Digitizer firmware revision:', fwStr
          print>>f, 'Initializing ADC',ADCtype

          print  'Run '+str(run)+' started at: '+
datetime.datetime.now().strftime("%I:%M:%S%p on %B %d, %Y")
          print>>f,   'Run '+str(run)+' started at: '+
datetime.datetime.now().strftime("%I:%M:%S%p on %B %d, %Y")

          events = 0
          start = time.time()           #start time (sec)

          for x in range(0, repeats):

                    loop_start = time.time()      #
iteration start (sec)

                    # start a new capture
                    digi.StartCapture()

                    # poll until timeout or data ready
                    bailOut = 656       # exit if > 65535
milliseconds

                    i = 0
                    while (i < bailOut):
                              status =
digi.GetEnergyLogStatus()

                              # if data ready or timeout
and no data
                              if ((status & 0x0100) ==
0x0100) or ((status & 0x00A0) == 0x00A0):
                                        break
                              time.sleep(0.1)
                              sys.stdout.write('.')
                              sys.stdout.flush()
                              i = i + 1

                    loop_stop = time.time()       #
iteration start (sec)

                    ts = digi.GetEnergyLogTimeStamp()
                    dt = digi.GetEnergyLogDeadTime()
                    ec = digi.GetEnergyLogCount()
                    events = events + ec

                    # collect all of the values
                    data_temp = digi.GetEnergyLog()
                    for index,item in enumerate(data_temp):
                              (tt,aa1,aa2)=item
                              ts = tt   # get correct time
stamp for last entry, GetEnergyLogTimeStamp does not work?
                              tt = tt+(loop_start-
start)*100000000
                              data_temp[index]=(tt,aa1,aa2)

                    if (x==0):
                              data = []
                              data.extend(data_temp)
                    else:
                              data.extend(data_temp)

                    print '\n\nClock Data Collection time =
%10.6f seconds\n' % (loop_stop-start)
                    print 'Status      : 0x%04X' % (status)
                    print 'Time Stamp  : %d' % (ts)
                    print 'Dead Time   : %d' % (dt)
                    try:
                              print '             : %.2f%%'
% (100*(float(dt)/float(ts)))
                    except:
                              print '             : NaN'

                    print 'Event Count : %d \n' % (ec)
                    print 'Total Events : %d \n' % (events)

          stop = time.time()


          # write useful info to terminal
          print "\n\n++++++++++++++++++++++++++++++++"
          print  'Run ended at: ' +
datetime.datetime.now().strftime("%I:%M:%S%p on %B %d, %Y")
          print  'Clock Data Collection time = %10.6f
seconds\n' % (stop-start)
          print 'Total Events : %d \n' % (events)


          # write out the data to a file
          print>>f, "\n\n++++++++++++++++++++++++++++++++"
          print>>f,  'Run ended at: ' +
datetime.datetime.now().strftime("%I:%M:%S%p on %B %d, %Y")
          print>>f,  'Clock Data Collection time = %10.6f
seconds\n' % (stop-start)
          print>>f, 'Total Events : %d \n' % (events)


          # write to output file
          for s,a,b in data:
                    #(s,a,b) = d
                    print>>f, '%d   %d   %d' % (s,a,b)

          print >>f, '6He Decay Experiment Acquisition'
          f.close()

        status = digi.GetEnergyLogStatus()
        print 'Final Status: 0x%04X' % (status)

        # turn off pulse energy logging
        digi.DisableEnergyLogging()

        digi.close()          # release the SPI lines
        print 'Done'
```

analyze.C file: C code used to analyze data collected 08-01-2017

```
#include <iostream>

//
==========================================================
==========================
// Subroutine to read data from run file, fill histograms
and ntuple
//
==========================================================
==========================

void read_file(TString fname, Int_t *cuts, TH1F *h0, TH1F
*h1, TH2F *h01, TH1F *ht, TNtuple *ntuple, float offset) {

char cline[256];
        // input line buffer

// data from Femtodaq
Int_t adc0,adc1;
long timestamp, start;
float m, b;
float dE_low1, dE_low1_E, dE_low2,dE_low2_E;

//printf("Opening input file: %s   ", fname.Data());
ifstream in;
in.open(fname.Data());

// Read in the first 12 comment lines
for (int i=1; i<12; i++) {
        in.getline(cline,256);
        //printf("%s",cline);
        //cout<<"line"<<i<<": "<<cline<<endl;

        }


// number of data lines read in from each file
Int_t nlines = 0;

// Read in data and fill histograms and ntuple
do {
        in >> timestamp>>adc0>>adc1;
        //printf("in fail = %d\n",in.fail());

        if (in.fail()) break;
        //timestamp = (decay_func->GetRandom()+0.2)*1000.;
// test function

   if (nlines==0) start = timestamp;

        //if (nlines < 5) printf("%d  time=%ld  adc0=%d
adc1=%d \n",in.good(),timestamp,adc0,adc1);
        //printf("%d %d  time=%ld  adc0=%d adc1=%d
\n",nlines, in.good(),timestamp,adc0,adc1);

        if((float)((timestamp-start)/1.0e8)-offset >= 0) {
          h0->Fill(adc0);     //  hist dE
          h1->Fill(adc1);     //  hist E
          h01->Fill(adc1,adc0);         // dE vs E
          if ((float)((timestamp-start)/1.0e8)-offset <
0.11) printf("t<0.11s: %s  \n", fname.Data());
          }

        dE_low1 = cuts[0];
        dE_low2 = cuts[1];
        E_low = cuts[3];
        E_high = cuts[4];

        if (adc0<cuts[2] && adc1>cuts[3] && adc1<cuts[4])
        {
          m = (float)(dE_low2-dE_low1)/(E_high-E_low);
          b = dE_low1 - m*E_low;
          if (adc0>m*adc1+b   )         ht->Fill(
(float)((timestamp-start)/1.0e8)-offset );
          }

        ntuple->Fill(timestamp,adc0,adc1);

        nlines++;

   } while(!in.eof());

printf(" found %d points\n",nlines);

//printf("start=%ld  \n",start);
//printf("time=%ld  adc0=%d adc1=%d
\n",timestamp,adc0,adc1);

in.close();
}


//
==========================================================
==========================
// Main
//
==========================================================
==========================

void analyze(TString fname="test") {
//  read in and analyzed data from decay_exp.py
//  created: 07/2016 Mark Yuly
//  modified: 01/19/2017 Mark Yuly    read in data saved by
new FemtoDAQ FPGA program

// ========== USER SETTABLE VALUES
==============================
// length of run in seconds
Int_t run_length = 10;

// size of time bin (ms)
Int_t time_bin_size = 100;

// cut on dE-E to make the time histogram
Int_t dE_low1 =1250;  // dE low cut is a line, define two
points on line
Int_t dE_low2 =1375;
Int_t dE_high = 2100;
Int_t E_low = 370;
Int_t E_high = 1675;
Int_t cuts[5]={dE_low1, dE_low2, dE_high,E_low,E_high};


// scale factor for calibration
float scalex =260;
float scaley = 600;
int off_x= 350;
int off_y=1200;

//
==========================================================
=======


TString run_file;             // list of run file names to
process
int num_list;                           // number of files
to process
float offset;                           // offset for each
run
int in_run_num;               // run number to input
char buffer[100];             // temporary buffer

char cline[256];
        // input line buffer
char str[30];
        // char string buffer

// calibration data for energy deposited in each detector
float T[17]={
0.35,0.4,0.45,0.5,0.55,0.6,0.7,0.8,0.9,1,1.25,1.5,1.75,2,2.
5,3,3.5};
float
dE_CSDA[17]={0.306,0.256,0.236,0.224,0.215,0.209,0.201,0.19
6,0.192,0.190,0.187,0.186,0.186,0.186,0.187,0.189,0.192};
float
E_CSDA[17]={0.044,0.144,0.214,0.276,0.335,0.391,0.499,0.604
,0.708,0.810,1.063,1.314,1.564,1.814,2.313,2.811,3.308};
float
dE_proj[17]={0.350,0.259,0.239,0.228,0.221,0.216,0.211,0.20
7,0.205,0.204,0.202,0.200,0.200,0.199,0.199,0.199,0.199};
float E_proj[17]
={0.000,0.141,0.211,0.272,0.329,0.384,0.489,0.593,0.695,0.7
96,1.048,1.300,1.550,1.801,2.301,2.801,3.301};
int print_e[17]={ 0,1,0,0,0,1,0,0,1,0,1,1,1,1,1,1,1};


// number of time bins
Int_t num_time_bin = run_length*1000./time_bin_size ;
printf("Number of time bins %d\n",num_time_bin);

// create the histograms
TString root_name = fname;
root_name.Append(".root");
TFile *f = new TFile(root_name,"RECREATE");
```

```
TH1F *h0 = new TH1F("h0","ADC0_spectrum",4000,0,3999);
h0->SetFillColor(0);
TH1F *h1 = new TH1F("h1","ADC1_spectrum",4000,0,3999);
h1->SetFillColor(0);
TH2F *h01 = new TH2F("h01","ADC0 vs
ADC1",4000,0,3999,4000,0,3999);
h01->SetFillColor(0);
TH1F *ht = new TH1F("ht","counts vs
time",num_time_bin,0.,run_length);
ht->SetFillColor(0);

// create the root tree for output root file
TNtuple *ntuple = new TNtuple("ntuple","data from ascii
file","timestamp,adc0,adc1");



//Either open a single run file, or loop through a list of
run files
if (fname(0,3)=="run") {                // single run file
        //printf("Opening run run file: %s\n",
fname.Data());
        offset = 0;
        read_file(fname, cuts, h0, h1, h01, ht, ntuple,
offset);
        printf(" File opened and read successfully.\n");
        }
else {
        //printf("Opening run list file: %s\n",
fname.Data());
        ifstream in_list;
        in_list.open(fname.Data());

        // number of data lines read in from each file
   numlist = 0;

        // Read in the file names and offsets
        do {
        in_list >> offset>>in_run_num;
        sprintf(buffer,"run_%04d.dat",in_run_num);
        run_file=buffer;
        //printf("[%s]",run_file.Data());

          //if (numlist < 50) printf("%d  %s  %4.2f
\n",in_list.good(),run_file.Data(),offset);
          read_file(run_file, cuts, h0, h1, h01, ht,
ntuple, offset);
          numlist++;
        } while (!in_list.eof());

        printf(" Found %d runs in list\n",numlist);
        }

// Show histograms of dE E and 2D
TCanvas *c1 = new
TCanvas("c1",fname.Data(),200,10,800,600);
c1->SetFillColor(0);

TPad *pad1 = new
TPad("pad1","ADC0",0.03,0.62,0.50,0.92,21);
pad1->SetFillColor(0);
TPad *pad2 = new
TPad("pad2","ADC1",0.51,0.62,0.98,0.92,21);
pad2->SetFillColor(0);
TPad *pad3 = new TPad("pad3","ADC0 vs
ADC1",0.03,0.02,0.97,0.57,21);
pad3->SetFillColor(0);
pad1->Draw();
pad2->Draw();
pad3->Draw();

pad1->SetBottomMargin(0.15);
pad1->SetLeftMargin(0.14);
pad2->SetBottomMargin(0.15);
pad2->SetLeftMargin(0.14);

h0->GetXaxis()->SetTitle("dE (ADC0)");
h0->GetXaxis()->SetLabelSize(0.06);
h0->GetXaxis()->SetTitleSize(0.06);
h0->GetYaxis()->SetTitle("Number of counts");
h0->GetYaxis()->SetLabelSize(0.06);
h0->GetYaxis()->SetTitleSize(0.06);
h0->GetYaxis()->SetTitleOffset(1.1);

h1->GetXaxis()->SetTitle("E (ADC1)");
h1->GetXaxis()->SetLabelSize(0.06);
h1->GetXaxis()->SetTitleSize(0.06);
h1->GetYaxis()->SetTitle("Number of counts");
h1->GetYaxis()->SetLabelSize(0.06);
h1->GetYaxis()->SetTitleSize(0.06);
h1->GetYaxis()->SetTitleOffset(0.8);
```

```
h01 -> SetYTitle("dE (ADC0)");
h01->GetYaxis()->SetTitleOffset(0.9);
h01 -> SetXTitle("E (ADC1)");
h01->GetYaxis()->SetRange(1000, 2200);
h01->GetXaxis()->SetRangeUser(300, 2000.);

pad1->cd();
h0->Draw();
pad2->cd();
h1->Draw();
pad3->cd();
h01->Draw();
pad3->Draw();
c1->Update();



for (Int_t i=0; i<17; i++) {
        if (print_e[i]==1){
          TMarker* mk = new
TMarker(E_proj[i]*scalex+off_x,dE_proj[i]*scaley+off_y,20);
          //printf("%4.2f     %5.3f  %5.3f \n",T[i],
E_proj[i] ,dE_proj[i] );
          mk->SetMarkerColor(kRed);
          h01->GetListOfFunctions()->Add(mk);
          }
        }

for (Int_t i=0; i<17; i++) {
        if (print_e[i]==1){
          //cout<<T[i]<<endl;
          TText *xlabel = new TText();
          xlabel -> SetTextFont(60);
          xlabel -> SetTextColor(kRed);
          xlabel -> SetTextSize(0.05);
          xlabel -> SetTextAlign(12);
          xlabel -> SetTextAngle(0);
          sprintf(str, "%4.2g", T[i] );
          xlabel -> DrawText(E_proj[i]*scalex-
0+off_x,dE_proj[i]*scaley+50+off_y, str);
          }

        }

TText *xlabel = new TText();
xlabel -> SetTextFont(60);
xlabel -> SetTextColor(kRed);
xlabel -> SetTextSize(0.05);
xlabel -> SetTextAlign(12);
xlabel -> SetTextAngle(0);
xlabel ->
DrawText(E_proj[16]*scalex+300,dE_proj[16]*scaley+200,
"MeV");

TLine *line1 = new TLine(E_low,dE_low1,E_high,dE_low2);
line1->SetLineColor(kGreen);
line1->Draw();

TLine *line2 = new TLine(E_low,dE_low1,E_low,dE_high);
line2->SetLineColor(kGreen);
line2->Draw();

TLine *line3 = new TLine(E_low,dE_high,E_high,dE_high);
line3->SetLineColor(kGreen);
line3->Draw();

TLine *line4 = new TLine(E_high,dE_low2,E_high,dE_high);
line4->SetLineColor(kGreen);
line4->Draw();

/*for (Int_t ei=E_low; ei<E_high; ei=ei+100) {
        float m = (float)(dE_low2-dE_low1)/(E_high-E_low);
        float b = dE_low1 - m*E_low;
        TMarker* mk1 = new TMarker(ei,m*ei+b,20);
        mk1->SetMarkerColor(kGreen);
        h01->GetListOfFunctions()->Add(mk1);
        }*/

//Show histogram vs time and fit histogram
TCanvas *c2 = new
TCanvas("c2",fname.Data(),200,10,800,600);
c2->Divide(1,3);

c2->cd(1);
gPad->SetBottomMargin(0.15);
ht->GetYaxis()->SetTitle("Number of counts");
ht->GetXaxis()->SetTitle("time (s)");
gStyle->SetErrorX(0.0001);
ht->SetLineColor(kBlack);
ht->SetMarkerStyle(20);
ht->SetFillColor(kGreen);
```

```
ht->GetXaxis()->SetLabelSize(0.06);
ht->GetXaxis()->SetTitleSize(0.06);
ht->GetYaxis()->SetLabelSize(0.06);
ht->GetYaxis()->SetTitleSize(0.06);
ht->GetYaxis()->SetTitleOffset(0.5);

ht->Draw("E1");
gPad->Draw();


// exponential decay + background fit function
TF1 *decay_func = new TF1("decay_func","[0]*exp(-
[1]*x)+[2]+[3]*x",0.,run_length);

decay_func->SetParameter(0,25);
decay_func->SetParameter(1,.859);
decay_func->SetParameter(2,0);
decay_func->SetParameter(3,0);

//Do the fits and graph

//int num_fit_bin = run_length*1000./time_bin_size;
int num_fit_bin = num_time_bin;
float x[num_fit_bin], ex[num_fit_bin];
float p0[num_fit_bin], p0e[num_fit_bin];
float p1[num_fit_bin], p1e[num_fit_bin];
float p2[num_fit_bin], p2e[num_fit_bin];
float p3[num_fit_bin], p3e[num_fit_bin];
float thalf[num_fit_bin],ethalf[num_fit_bin];

float chisq[num_fit_bin];
int ndof[num_fit_bin];
float chidof[num_fit_bin];

for (int i=0;i<num_fit_bin;i++) {
        chisq[i]=100000000.;
        ndof[i]=1;
}

float fit_min = 0;
float fit_max = 2.;

for(int i=0; i<num_fit_bin; i++) {
//      x[i]=i*time_bin_size/1000.;
        x[i]=i*time_bin_size/1000.;
        ex[i]=0.;
        if (x[i]>=fit_min &&x[i]<=fit_max) {
        ht->Fit("decay_func","QN","",x[i],10.);
        p0[i] = decay_func->GetParameter(0);
        p0e[i] = decay_func->GetParError(0);
        p1[i] = decay_func->GetParameter(1);
        p1e[i] = decay_func->GetParError(1);
        p2[i] = decay_func->GetParameter(2);
        p2e[i] = decay_func->GetParError(2);
        p3[i] = decay_func->GetParameter(3);
        p3e[i] = decay_func->GetParError(3);

        chisq[i]=decay_func->GetChisquare();
        ndof[i]=decay_func->GetNDF();
        chidof[i]=chisq[i]/ndof[i];

        thalf[i]=log(2.)/p1[i];
        ethalf[i]=pow((log(2.)/p1[i]),2) * p1e[i];

        printf("%d  x=%4.2f  %f %4.2f  %5.4f+/-%5.4f   %4.2f
%4.2f  %5.4f+/-
%5.4f\n",i,x[i],chidof[i],p0[i],p1[i],p1e[i],p2[i],p3[i],th
alf[i],ethalf[i]);
        }

        }

float best=100000.;
int ibest;
for(int i=0; i<num_fit_bin; i++) {
        if ( chidof[i] < best && x[i]>=fit_min &&
x[i]<=fit_max) {
        ibest = i;
        best = chidof[i];
        }
}

printf("\nBEST: %d x=%4.2f  %4.2f+/-%4.2f   %5.4f+/-%5.4f
%4.2f+/-%4.2f   %4.2f+/-%4.2f
\n",ibest,x[ibest],p0[ibest],p0e[ibest],

        p1[ibest],p1e[ibest],p2[ibest],p2e[ibest],p3[ibest],
p3e[ibest]);

printf("CHISQ/DEF: %4.2f  thalf=%5.4f+/-%5.4f
\n",chidof[ibest],thalf[ibest],ethalf[ibest]);

printf("\nt=0.1 fit: %d x=%4.2f  %4.2f+/-%4.2f   %5.4f+/-
%5.4f   %4.2f+/-%4.2f   %4.2f+/-%4.2f
\n",1,x[1],p0[1],p0e[1],
          p1[1],p1e[1],p2[1],p2e[1],p3[1],p3e[1]);

printf("CHISQ/DEF: %4.2f  thalf=%5.4f+/-%5.4f
\n",chidof[1],thalf[1],ethalf[1]);

TF1 * ff1= new TF1();
decay_func->Copy(*ff1);
ff1-
>SetParameters(p0[ibest],p1[ibest],p2[ibest],p3[ibest]);
ff1->SetLineColor(kGreen);
ff1->Draw("SAME");

TF1 * ff2= new TF1();
decay_func->Copy(*ff2);
ff2->SetParameters(p0[1],p1[1],p2[1],p3[1]);
ff2->SetLineColor(kRed);
ff2->Draw("SAME");

c2->cd(2);
gPad->SetBottomMargin(0.15);
TGraph *gr1 = new TGraph(num_fit_bin,x,chidof);
gr1->GetXaxis()->SetLimits(fit_min, fit_max);
gr1->SetMinimum(0);
gr1->SetMaximum(30);
gr1->SetLineColor(kBlack);
gr1->SetMarkerStyle(20);
gr1->SetFillColor(kGreen);
//gr->SetTitle("a simple graph");
gr1->GetXaxis()->SetTitle("fit starting time (s)");
gr1->GetYaxis()->SetTitle("chisq/dof");
gr1->GetXaxis()->SetLabelSize(0.06);
gr1->GetXaxis()->SetTitleSize(0.06);
gr1->GetYaxis()->SetLabelSize(0.06);
gr1->GetYaxis()->SetTitleSize(0.06);
gr1->GetYaxis()->SetTitleOffset(0.5);
gr1->Draw();

c2->cd(3);
gPad->SetBottomMargin(0.15);
TGraphErrors *gr = new
TGraphErrors(num_fit_bin,x,thalf,ex,ethalf);
gr->GetXaxis()->SetLimits(fit_min, fit_max);
gr->SetMinimum(0);
gr->SetMaximum(2.);
gr->SetLineColor(kBlack);
gr->SetMarkerStyle(20);
gr->SetFillColor(kGreen);
//gr->SetTitle("a simple graph");
gr->GetXaxis()->SetTitle("fit starting time (s)");
gr->GetYaxis()->SetTitle("half life (s)");
gr->GetXaxis()->SetLabelSize(0.06);
gr->GetXaxis()->SetTitleSize(0.06);
gr->GetYaxis()->SetLabelSize(0.06);
gr->GetYaxis()->SetTitleSize(0.06);
gr->GetYaxis()->SetTitleOffset(0.5);
gr->Draw();

float xx[2],yy[2];
xx[0]=-2;xx[1]=10.;yy[0]=0.807;yy[1]=0.807;
TGraph *gr2 = new TGraph(2,xx,yy);
gr2->SetLineColor(kRed);
gr2->Draw("SAME");
c2->Update();



// write the histogram and ntuples to root file
f->Write();
}
```

Appendix B

VOLTAGE LEVEL TRANSLATOR CIRCUIT FOR THE $^{9}BE(N,\alpha)^{6}HE$ EXPERIMENT ELECTRONICS

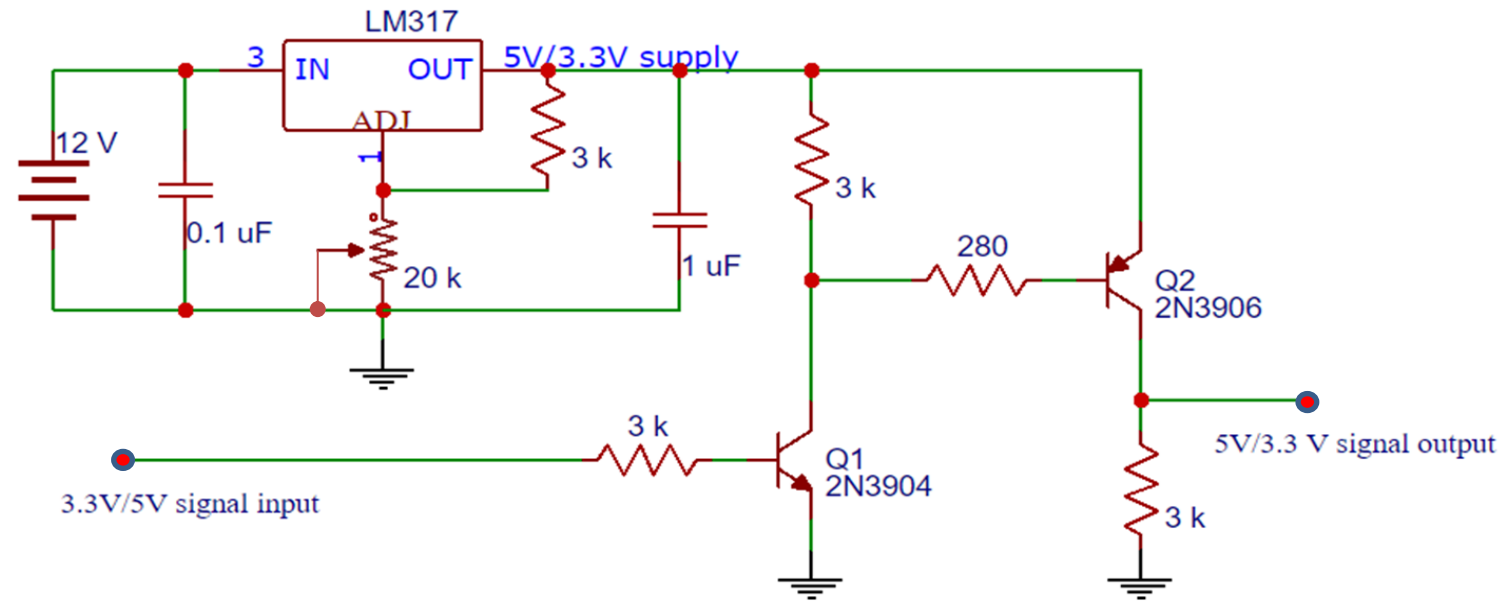

Appendix C

LATCH CIRCUIT

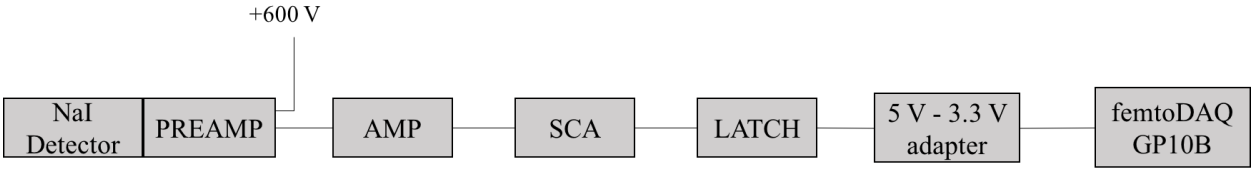

Appendix D

ARDUINO CODE FOR THE FAST VALVE

```
const int button_pin = 13; //Pin you want to read the button signal
from
const int gate_pin = 4; //Pin you want to output to MOSFET gate
const int wait_time = 1000; //How long after the button push you want
the valve to be open for

void setup() {
  Serial.begin(115200);
  pinMode(button_pin,INPUT);
  Serial.print("Button Pin (13) set to Input...");
  pinMode(gate_pin,OUTPUT);
  Serial.print("Button Pin (13) set to Input...");

}

void loop() {
  if (digitalRead(button_pin)== HIGH) {
    delay(250);                       //wait quater of a second for
full push (prevents holding button down for slighty too long from
effecting pulse)
    digitalWrite(gate_pin,HIGH);      //Open the valve
    delay(wait_time);                 //wait for wait_time
    digitalWrite(gate_pin,LOW);       //closes the valve
    delay(1000);
  } else {digitalWrite(gate_pin,LOW);}  //close the valve if the
button isnt pushed
}
```

References

[1] R. Woods, J.L. McKibben, and R.L. Henkel, Nucl. Instrum. Methods **122**, 81 (1974).

[2] United States Government Accountability Office, Report to the Committee on Armed Services, U.S. Senate, Report GAO-15-272, 2015.

[3] Loomis et al., Los Alamos National Laboratory Report LA-UR-05-0775, 2005.

[4] S. Brandenburg *et al.*, in *Cyclotrons and Their Applications 2001*, proceedings of the 16th International Conference on Cyclotrons and Applications, edited by F. Marti (American Institute of Physics, 2001), p. 463.

[5] G. W. Hitt et al., Nucl. Instrum. Methods **A 566**, 264 (2006).

[6] OMEGA EP System Operations Manual: Chapter 2, **S-AD-M-006**, 1-24 (2006).

[7] L.H. Gresh, R.L. McCrory, J.M. Soures, *Inertial Confinement Fusion: An Introduction*, (University of Rochester, Laboratory for Laser Energetics, 2008).

[8] Boehly, T.R. *et al.*, Opt. Commun. **133**, 495-506 (1997).

[9] Waxer, L.J. *et al.*, Opt. Photonics News **16**, 30-36 (2005).

[10] J-L Miquel *et al.*, J. Phys.: Conf. Ser. **688** 012067 (2016).

[11] D. T. Casey *et al.*, Phys. Rev. Lett. **109**, 025003 (2012).

[12] Wilkinson et al., Phys. Rev. **C 31**, 2036 (1985).

[13] National Nuclear Data Center, information extracted from the Chart of Nuclides database, http://www.nndc.bnl.gov/chart/.

[14] J. Melendez and I. Ramirez, Astrophys. J. **615**, L33 (2004).

[15] M. Asplund *et al.*, Astrophys. J. **644**, 229 (2006).

[16] V.V.Zerkina, B.Pritychenkob, NIM **A888**, 31 (2018).

[17] V.G. Kiptily, F. E. Cecil, and S. S. Medley. Plasma Physics and Controlled Fusion **48**, R59 (2006).

[18] J.A. Frenje *et. al.,* Phys. Lett. **107**, 122502 (2011).

[19] D.B. Sayre *et. al.,* Phys. Lett. **111**, 052501 (2013).

[20] M. A. Stoyer, C. A. Velsko, B. K. Spears, D. G. Hicks, G. B. Hudson, T. C. Sangster, and C. G. Freeman, Rev. Sci. Instrum. **83**, 023505 (2012).

[21] I. Kurchatov, E. Teller, Bulletin of the Atomic Scientists. **12**, 269-272 (1956).

[22] A.J. Koning, S. Hilaire and M.C. Duijvestijn in *Proceedings of the International Conference on Nuclear Data for Science and Technology. 2008,* p. 211-214.

[23] D.R. Tilley, H.M. Hofmann, C.M. Cheves, J.H. Kelley, J.L. Godwin, C.G. Sheu, G.M. Hale and H.R. Weller, Nuclear Physics **A708** (2002).

[24] T. Weber and T. Intrator, Review of Scientific Instruments **85**, (2014).

[25] W. Skulski, A. Ruben and S. BenZvi, IEEE Transactions on Nuclear Science, **64**, 1677-1682 (2017).

[26] S. Padalino, K. Palmisano, in Proceedings of APS Division of Plasma Physics Meeting, 2019 (unpublished).

[27] B. Pritychenko, E. Betak, M.A. Kellett, B. Singh, J. Totans, NIM **A640**, 213 (2011).